Alma Mater Studiorum - Università di Bologna

DOTTORATO DI RICERCA IN

CHIMICA

Ciclo 35

Settore Concorsuale: 03/C1 - CHIMICA ORGANICA

Settore Scientifico Disciplinare: CHIM/06 - CHIMICA ORGANICA

KINETIC AND MECHANISTIC STUDIES ON PEROXIDATION AND STABILIZATION OF LIPIDS WITH INDUSTRIAL AND BIOLOGICAL RELEVANCE

Presentata da: Fabio Mollica

Coordinatore Dottorato

Luca Prodi

Supervisore

Riccardo Amorati

Co-supervisore

Luca Valgimigli

Esame finale anno 2023

ABSTRACT

Lipid peroxidation is a complex mechanism that causes the degradation of lipid material of both industrial and biological significance. During processing, it is known that thermal stress produces oxidation and polymerization of oils, with the consequent formation of various oxygenated compounds such as hydroperoxides, peracids, epoxides, ketones and polymeric compounds which alter the chemical-physical properties of the oil and cause the formation of incrustations and solid deposits. Additionally, biological lipids with both structural and bioactive roles are prone to peroxidation, which can cause substantial damage to the plasma membrane by changing its permeability and functionality and have pathogenic effects including cancer and long-term degenerative disorders. In order to create innovative strategies to slow down the deterioration of lipids, it is crucial to improve our understanding of oxidation reactions and kinetics.

To this purpose, Chapter II of this thesis focuses on the kinetic study of the oxidation reactions that take place during the thermal processing of bio-oils for industrial application. Through a new method, based on the optically detected profile of the O_2 concentration in the headspace during the isotherms at 130°C, it was possible to evaluate the kinetic parameters of oxidation of various lipid materials. This allowed us to distinguish between the different lipid materials based on their intrinsic properties (molecular structure, acidity, and the presence of intrinsic antioxidants or metals). The effect of 18 antioxidants from the major families of natural and synthetic phenols were studied using the same methodology in order to acquire crucial data for enhancing the antioxidant activity of phenols based on structure-activity at high temperatures. According to EPR spectroscopy, the antioxidant's (A•) phenoxyl radical's stability and inhibitory activity are inversely correlated, showing that the antioxidant may actually accelerate the chain reaction rather than break it. Finally, it has been described how the antioxidant activity of α-tocopherol, revealed to be scarce in our conditions, can be improved in the presence of γ-terpinene, through a synergistic action. Experiments have demonstrated how γ-terpinene generates hydroperoxyl radicals (HOO•), which are responsible for the reduction of the tocopheroxyl radical by transfer of an H atom, extending its antioxidant efficacy.

Chapter III describes the synthesis and study of the antioxidant activity of polydopamine nanoparticles, in order to clarify the unclear mechanism of action of this material. The reaction

of polydopamine nanoparticles with biologically relevant ROO• radicals in water at pH 7.4 was measured and the results compared with those obtained with the popular DPPH• and ABTS•+ assays. Furthermore, its antioxidant activity has been increased by binding to a dialkyl nitroxide, which is highly active against ROO• in water.

Finally, in Chapter IV it was reported how the γ-terpinene strongly inhibits the peroxidation of unsaturated lipids in heterogeneous model systems (micelles and liposomes) by forming HOO• radicals which diffuse outside the lipid nucleus, blocking the propagation of the chain radical. Furthermore, γ-terpinene shows a very potent protective activity against ferroptosis (a type of iron-dependent programmed cell death characterized by the accumulation of lipid peroxides at lethal doses) being effective in the nanomolar range in the human neuroblastoma cell model (SH-SY5Y).

Statement of Originality

I hereby certify that the work described in this thesis is the original work of the author, with exceptions for work performed by collaborators noted in the preface to each chapter. The work in this thesis draws upon a great deal of published research. Any published (or unpublished) work by others is cited and fully acknowledged within the references.

Fabio Mollica

INDEX

CHAPTER IV: PRO-AROMATIC NATURAL TERPENES AS UNUSUAL ANTIOXIDANTS WITH POTENT FERROPTOSIS INHIBITION ACTIVITY

CHAPTER I
BACKGROUND AND SIGNIFICANCE

1.1 Introduction

Over 50 years of research on both practical and theoretical aspects of lipid oxidation have developed the current knowledge of lipid oxidation kinetics, processes, mechanisms and products. Earth's oxygen-rich environment, while necessary to sustain life as we know it, is not without consequences. In fact, oxygen is responsible for the degradation of virtually all petroleum products, from lubricants and polymers to raw materials and specialty chemicals. Lipids are often used in high temperature preparations, and it is known that under such conditions, thermal stress causes oxidation and polymerization, with the formation of volatile, non-volatile and polymeric compounds which affect characteristic physical properties of the oil, leading to the formation of clogs and solid deposits with a huge economic impact.[1,2] Furthermore, the autoxidation process also occurs in biological contexts. Many of the polyunsaturated fatty acids and sterols essential for life are among the most sensitive hydrocarbons. Lipid oxidation products have been associated with a several of pathophysiological conditions, and their accumulation has been linked to neurodegenerative diseases and cancer.[3–5] In this chapter, the mechanism of autoxidation will be clarified, taking into account the mechanisms responsible for the formation of by-products.

1.2 Autoxidation

Any discussion of lipid oxidation must begin by considering the classical free-radical chain reaction, described in its simplest form in *Scheme 1.1*. The general mechanism of hydrocarbon autoxidation was first proposed by Charles E. Frank[6] in 1950 and later developed by Dr. Keith Ingold,[7] and involved three main steps: initiation, propagation, and termination.

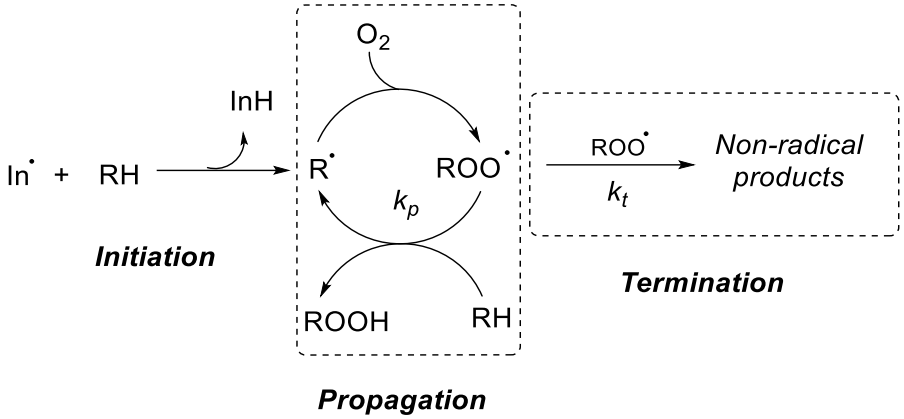

Scheme 1.1 *Chain reaction of autoxidation for a substrate (RH)*

Ab initio lipid alkyl radicals are formed when initiators (In•) such as metals, preformed free radicals, light and heat react with substrate (RH) by electron transfer or H-atom abstraction (HAT) which yields a carbon centered radical (R•). In the propagation step, the alkyl radical reacts rapidly with oxygen to form the alkyl peroxyl radical (ROO•), which in turn reacts with another substrate to give a hydroperoxide (ROOH) and a new alkyl radical. The newly formed carbon free radicals will re-join with oxygen and continue the propagation process. This chain process continues until the termination step where two radical species react with each other to form stable species.[8]

1.2.1 Mechanism

Initiation

$$ROOH \rightarrow RO^{\bullet} + HO^{\bullet} \qquad \text{Eq 1.1a}$$

$$M^{n+} + ROOH \rightarrow M^{(n+1)+} + RO^{\bullet} + HO^{-} \qquad \text{Eq 1.1b}$$

$$In\text{-}In \xrightarrow{k_d} 2In^{\bullet} \qquad \text{Eq 1.1c}$$

$$RO^{\bullet}/HO^{\bullet}/In^{\bullet} + RH \xrightarrow{R_i} R^{\bullet} + InH \quad \text{Eq 1.2}$$

Propagation

$$R^{\bullet} + O_2 \xrightarrow{k_1} ROO^{\bullet} \quad \text{Eq 1.3}$$

$$ROO^{\bullet} + RH \xrightarrow{k_p} ROOH + R\bullet \quad \text{Eq 1.4}$$

Termination

$$2ROO^{\bullet} \xrightarrow{k_t} ROO\text{-}OOR \quad \text{Eq 1.5}$$

$$ROO\text{-}OOR \rightarrow RCHO + RCOH + O_2 \quad \text{Eq. 1.6}$$

As mentioned above, autoxidation is the prototype of the free radical chain reaction. Moreover, as it can be initiated by - and produce - hydroperoxides, when hydroperoxide participate in the initiation step, it can be considered an autocatalytic process. Spontaneous homolysis of the O-O bond in peroxides (*Eq 1.1a*), or its one-electron reduction (*Eq. 1.1b*), for example by Fe^{2+}, produces highly reactive alkoxy and/or hydroxyl radicals. Because of the complex chemistry of involved (*i.e.* Fe^{2+} and ROOH concentrations are not constant), the rate of initiation R_i is unpredictable. Instead, when a controlled rate of initiation is desired, thermal decomposition of an azo-initiator is preferred, since the homolytic decomposition of azo-initiators (*Eq. 1.1c*) depends only on the temperature, and if the azo-initiators are used in large excess, R_i is constant during the entire course of the autoxidation. The use of azo-initiators is ideal for studying the autoxidation process in model systems, thus avoiding autocatalysis phenomena. In the presence of an azo-initiator, the radical formation rate is given by *Eq. 1.7*:

$$R_i = 2ek_d[In\text{-}In] \qquad \text{Eq 1.7}$$

where k_d represents the unimolecular decomposition rate constant of the azo-derivative, while *e* represents the efficiency of the reaction, *i.e.* the quantity of radicals that leave the cage of the solvent and trigger autoxidation. Commonly, R_i can be easily determined by measuring the length of the inhibition period (τ) of a reference antioxidant, whose stoichiometric coefficient *n* (*i.e*. the number of radicals trapped) is known. These parameters are related to each other by the following relationship (*Eq 1.8*):

$$R_i = \frac{n[AH]}{\tau} \qquad \text{Eq 1.8}$$

In this phase, called the induction period, all the radicals generated by the initiator are trapped by the antioxidant: radical production speed and induction period are inversely correlated.

The subsequent extraction of a labile hydrogen atom from the hydrocarbon substrate, or the addition to double bonds initiate the chain reaction (*Eq. 1.2*). Under normal conditions (*i.e*. in the presence of oxygen), the alkyl radical formed in this way is preferentially converted to a peroxyl radical, although it could give rise to other reactions, such as two alkyl radicals reacting with each other, although unlikely. Indeed, they react faster with oxygen (k_1 is typical around 10^9 $M^{-1}s^{-1}$ in organic solvents at 300 K)[9] than with lipids and their redox potential is low enough to be inefficient oxidizers. Furthermore, the possible addition reaction of the carbon-centered radical to the double bond, which becomes dominant in an environment with low oxygen pressure or under vacuum, cannot be excluded.[10]

Anyway, peroxyl radicals initially formed at any site on a fatty acid perform a H-atom abstraction from a substrate (or addition to a double bond) generating an alkyl radical, propagating the chain. The number of substrate molecules (RH) involved in the reaction for each initiating radical is referred as the chain length. This value can be easily determined from the ratio between the rate of oxygen consumption and the rate of formation of radicals, R_i (*Eq 1.9*).

$$x = \frac{-d[O_2]/dt}{R_i} \qquad \text{Eq 1.9}$$

The rate-limiting propagation step involves H-atom transfer (HAT) from the hydrocarbon substrate to a peroxyl radical, characterized by the key propagation rate constant, k_p (eq. 1.4). The *Figure 1.1* shows the k_p values of known lipid substrates. As shown, fatty acids with a higher number of unsaturation usually have a high k_p. This is due to the presence of methylene groups between double bonds with low C-H bond energy, which represent the specific positions for H-atom abstraction (*vida infra*).

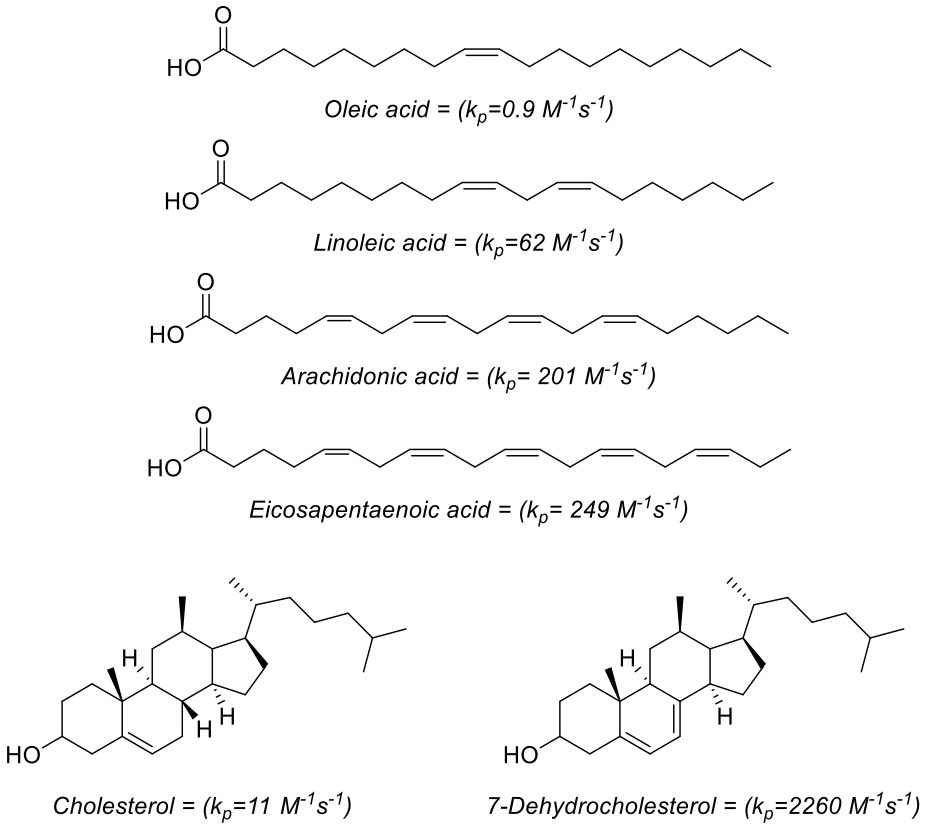

Figure 1.1 *Structures of representative lipids and their associated propagation rate constants at 30 °C.*[11,12]

Propagation competes with termination of the radical chain reaction (*Eq. 1.5*). In this step the radical species combine with each other in various ways to give non-radical products. Three types of combination's reaction can occur: between the peroxyl radicals, between the carbon centered radicals, or the crossed one between a peroxyl and an alkyl. However, since alkyl radicals react with a diffusion-controlled rate constant with

dissolved oxygen, the combination of the peroxyls is the more likely reaction. The value of the rate constant (k_t) usually increases along the series: tertiary peroxyl < secondary ≈ primary. Tertiary peroxyls have a lower recombination rate constant due to the fact that the decomposition of the adduct to four oxygen atoms does not necessarily lead to the disappearance of the radicals. (*Eq. 1.10*).

$$2ROO^{\bullet} \rightarrow ROO\text{-}OOR \rightarrow RO^{\bullet} + O_2 + RO^{\bullet} \qquad \text{Eq. 1.10}$$

Russell[13] has proposed an explanation for the increase in speed of combination of secondary and primary versus tertiary peroxyls. The reaction would take place through a cyclic transition state during which one of the hydrogens is transferred to give ketones, alcohols and oxygen as molecular products, without producing new reactive species (*Eq. 1.6*).

1.2.2 Kinetics

The rate of autoxidation is presented in *Eq. 1.21* which is obtained by solving the kinetic equations describing the different steps (*see Eq. 1.11, 1.12, 1.13*) and applying the steady state approximation.

$$-\frac{d[O_2]}{dt} = k_1[R^{\bullet}][O_2] \qquad \text{Eq 1.11}$$

$$\frac{d[R^{\bullet}]}{dt} = Ri + k_p[ROO^{\bullet}][RH] - k_1[R^{\bullet}][O_2] \qquad \text{Eq 1.12}$$

$$\frac{d[ROO^{\bullet}]}{dt} = k_1[R^{\bullet}][O_2] - k_p[ROO^{\bullet}][RH] - 2k_t[ROO^{\bullet}]^2 \qquad \text{Eq 1.13}$$

Using the steady state approximation for transient species we have:

$$\frac{d[R^{\bullet}]}{dt} = 0 \qquad \text{Eq. 1.14}$$

$$Ri + k_p[ROO^\bullet][RH] - k_1[R^\bullet][O_2] = 0 \qquad \text{Eq. 1.15}$$

$$\frac{d[ROO^\bullet]}{dt} = 0 \qquad \text{Eq 1.16}$$

$$k_1[R^\bullet][O_2] - k_p[ROO^\bullet][RH] - 2k_t[ROO^\bullet]^2 = 0 \qquad \text{Eq 1.17}$$

By combining equations 1.15 and 1.17 one obtains:

$$R_i = 2k_t[ROO^\bullet]^2 \qquad \text{Eq 1.18}$$

$$[ROO^\bullet] = \sqrt{\frac{Ri}{2k_t}} \qquad \text{Eq. 1.19}$$

Substituting equation 1.15 into 1.19 we have:

$$k_1[R^\bullet][O_2] = R_i + k_p[RH]\sqrt{\frac{Ri}{2k_t}} \qquad \text{Eq.1.20}$$

By replacing 1.20 with 1.11 the oxygen consumption rate is obtained:

$$-\frac{d[O_2]}{dt} = \frac{k_p}{\sqrt{2k_t}}[RH]\sqrt{R_i} + R_i \qquad \text{Eq.1.21}$$

If the chain is then sufficiently long (> 30) it is possible to neglect the oxygen consumption by the inhibitor (R_i) compared to the consumption by the substrate.

1.2.3 Initiation in biological systems

Reactive species such as hydroxyl radicals, superoxides and peroxyl radicals present in biological systems have the ability to initiate lipid oxidation events in vivo. Superoxide ($O_2^{\bullet-}$) is a key reactive oxygen species and its production occurs, for example, as a by-product of the one-electron redox chemistry of coenzyme Q10

(ubiquinol) in the mitochondria as a result of cellular respiration. Superoxide itself is not harmful, but it can lead to other more reactive radicals through several pathways presented in *Scheme 1.2*. The superoxide can be protonated to form the hydroperoxyl radical reversibly (pK_a 4,8 in water[14]), while the reaction between two hydroperoxyl radicals is controlled by diffusion; therefore, hydrogen peroxide can be formed from superoxide spontaneously or enzymatically (SOD). Hydrogen peroxide undergoes a one-electron reduction (Fenton reaction) to produce a highly reactive hydroxyl radical; or, hydroxyl radicals can also be produced by the reaction of hydrogen peroxide and chlorine catalyzed by myeloperoxidase (MPO), forming hypochlorous acid as an intermediate. HOCl undergoes electron transfer followed by homolytic cleavage thereby forming highly reactive hydroxyl radicals and chloride ions as byproducts. Initiator radicals can also form when superoxide combines with a nitric oxide radical to form peroxynitrite. Peroxynitrite is a powerful oxidizing and nitrating agent which can also react with CO_2 to form nitrogen dioxide and a carbonate radical. Alternatively, peroxynitrite can be protonated (pKa 6.8)[15] and homolyzed to form nitrogen dioxide and a hydroxyl radical.

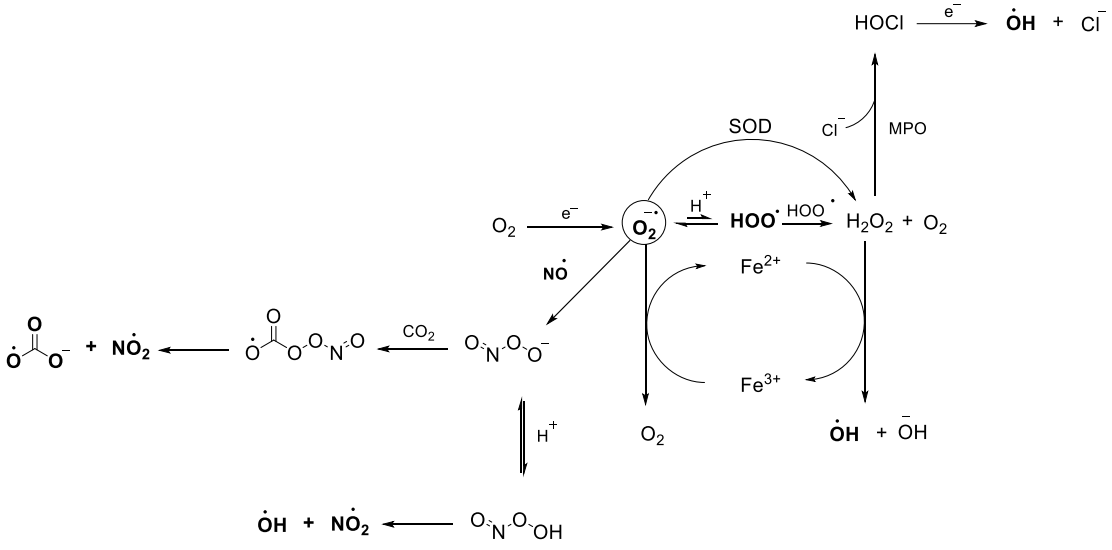

Scheme 1.2 *Production of reactive oxygen (and nitrogen) species in vivo.*

Due to the strong OH bond in water (enthalpy of bond dissociation, BDE, of almost 120 kcal), the hydroxyl radical is highly reactive and is, together with the other reactive oxygen (and nitrogen) species, capable of react directly with biological targets (e.g. by damaging DNA or proteins) or initiate free radical chain reactions such as lipid autoxidation as in lipid bilayer membranes or lipoproteins.

ROS are not the only initiators of lipid oxidation in vivo. Hydroperoxides can also be generated by enzyme systems such as lipoxygenase[16] and cyclooxygenase,[17] or through the oxidation of lipids by singlet oxygen ($^1O_2$).

$$^0S \xrightarrow{h\nu} {}^1S \xrightarrow{^3O_2} {}^3S \xrightarrow{^1O_2} {}^0S + {}^1O_2 \qquad \text{Eq.1.22}$$

The ground state of molecular oxygen is the triplet state ($^3O_2$), singlet oxygen can be generated when a photosensitizer (^0S) undergoes activation by light to the first excited state (^1S), followed by intersystem crossing to form a triplet state (^3S); the latter is able to convert triplet oxygen to singlet oxygen (*Eq. 1.23*).[18] Singlet oxygen reacts with the double bond of unsaturated fatty acids in a different way, to give an "*ene*" addition mechanism (*Scheme 1.3*).[19]

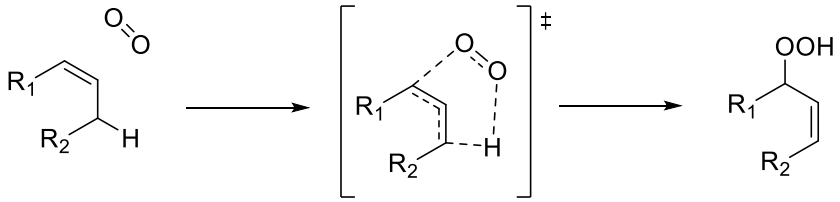

Scheme 1.3 *Reaction of singlet oxygen and an alkene, to yield a hydroperoxide.*

Photosensitizers present in human skin (*e.g.* porphyrins and flavins) can convert $^3O_2$ to $^1O_2$ because of UV exposure. Furthermore, this kind of reaction is characteristic of foods rich in lipids, where there are natural or artificial pigments that generate singlet oxygen of $^1O_2$, which lead to the formation of oxidized lipids.

1.2.4 Inhibition

Autoxidation is inhibited in the presence of antioxidants, which may be classified as preventative or chain-breaking, depending upon their mechanism of action.[20]

These antioxidants are defined as "preventive" as they prevent the initiation of the oxidative process and are therefore capable of inhibiting or counteracting the formation of free radicals. Their action is mainly carried out with the decomposition of hydroperoxides and peroxides and with the chelation of transition metals. An example is SOD (Superoxide Dismutase): it catalyzes the disproportionation of superoxide to form hydrogen peroxide and oxygen (*Scheme 1.4*), and thereby preventing the formation of superoxide-derived initiating radicals. CAT (catalase enzyme) decomposes the hydrogen peroxide produced by the disproportionation reaction and transforms it into water and molecular oxygen (*Scheme 1.4*).[21]

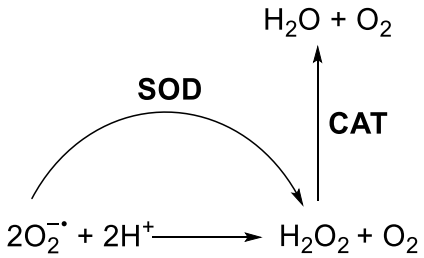

Scheme 1.4 *SOD and CAT operation scheme.*

Other important preventive antioxidants are glutathione peroxidase (GPx), metal chelators,[22] UV absorbers (e.g. melanin) and $^1O_2$ quenchers, all of which, in some way, prevent radical formation or scavenge reactive oxygen species that can act as initiators.

Chain-breaking antioxidants differ from preventives in the different mechanism of action. They block one or more steps of the propagation stage by trapping the free radicals that form during the oxidation reaction (*Scheme 1.5*). The fundamental characteristics of chain-breaking antioxidants are two: they react faster with the chain propagating radicals than the oxidizable substrate; and they give rise to stable radicals which in turn do not propagate the oxidative chains.

Propagation: $ROO^{\bullet} + RH \xrightarrow{k_p} ROOH + R\bullet$

Inhibition: $ROO^{\bullet} + AH \xrightarrow{k_{inh}} ROOH + A\bullet$

Scheme 1.5*: Fates of peroxyl radicals: propagation vs. inhibition.*

Therefore, an effective chain-breaking antioxidant has $k_{inh} >>> k_p$. It is therefore evident that what makes a good antioxidant is its kinetic characteristics, *i.e.* the ability to compete with peroxyl for the oxidizable substrate, which in turn depends on the enthalpy of dissociation of the O-H bond, the BDE. Phenolic antioxidants, for example, work by blocking the peroxyl free radicals of the autoxidative chain through the hydrogen transfer of the OH bond, thus forming the corresponding hydroperoxide and a phenoxy radical. The BDE of the ROO-H bond in hydroperoxides is about 90 kcal/mol. Therefore, to undergo hydrogen extraction by the peroxyl radical, a chain-breaking antioxidant must have a BDE of the A-H bond, lower than this value. Indeed, phenols exhibiting lower BDE(OH) are generally better antioxidants. Since in unsubstituted phenol the BDE of the OH bond is equal to 88 kcal/mol, for a phenol to have good antioxidant capacities, it will be necessary to introduce substituents, to lower the energy of the O-H bond. Electron donating (ED) substituents, especially in the ortho and para positions conjugated to the phenolic OH, weaken this bond and increase the rate of hydrogen transfer to the extraction radical. This strategy represents the most followed guideline in the rational design of new phenolic antioxidants.[23–25]

Another important aspect, the radical A• derived from the antioxidant should not propagate the chain reaction, for example by subtracting a labile H atom to generate an alkyl radical. The mechanism of phenolic antioxidants is well known, in which the phenoxy radical derived from the antioxidant is persistent enough to trap a second peroxyl radical, to form a non-radical product.[26] This is demonstrated in *Scheme 1.6* for α-tocopherol.[27] The number of radicals that an antioxidant manages to trap is called the "stoichiometric coefficient" and indicated with *n*.

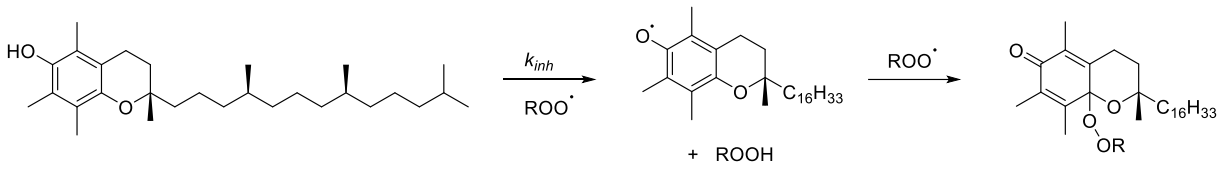

Scheme 1.6 *Radical-trapping antioxidant activity of a-tocopherol.*

The kinetics of autoxidation in the presence of a chain-breaking antioxidant can be represented by the rate equation Eq. 1.23:

$$-\frac{d[O_2]}{dt} = \frac{k_p[RH]R_i}{nk_{inh}[AH]} + R_i \qquad \text{Eq.1.23}$$

which is obtained by solving the kinetic equation describing the different steps, including termination's reactions that occur in the presence of antioxidant:

$$ROO^{\bullet} + AH \xrightarrow{k_{inh}} A^{\bullet} + ROOH \qquad \text{Eq.1.24}$$

$$ROO^{\bullet} + A^{\bullet} \xrightarrow{k_3} A^{\bullet} + ROOH \qquad \text{Eq.1.25}$$

$$-\frac{d[O_2]}{dt} = k_1[R^{\bullet}][O_2] \qquad \text{Eq.1.26}$$

$$\frac{d[R^{\bullet}]}{dt} = Ri + k_p[ROO^{\bullet}][RH] - k_1[R^{\bullet}][O_2] \qquad \text{Eq.1.27}$$

$$\frac{d[ROO^{\bullet}]}{dt} = k_1[R^{\bullet}][O_2] - k_p[ROO^{\bullet}][RH] - 2k_t[ROO^{\bullet}]^2 + k_{inh}[ROO^{\bullet}][AH] + k_3[ROO^{\bullet}][A^{\bullet}] \qquad \text{Eq.1.28}$$

$$\frac{d[A^{\bullet}]}{dt} = k_{inh}[ROO^{\bullet}][AH] - k_3[ROO^{\bullet}][A^{\bullet}] \qquad \text{Eq.1.29}$$

If applying the steady state approximation, the equations describing the rates of formation of radical species can be set equal to zero, therefore the Eq. 1.27 and the Eq. 1.29 become respectively:

$$k_1[R^\bullet][O_2] = R_i + k_p[ROO^\bullet][RH] \qquad \text{Eq. 1.30}$$

$$k_{inh}[ROO^\bullet][AH] = k_3[ROO^\bullet][A^\bullet] \qquad \text{Eq. 1.31}$$

Substituting these last two expressions in the equation Eq. 1.28 and applying the approximation of the steady state for the $ROO^\bullet$ species we have:

$$2k_t[ROO^\bullet]^2 + k_{inh}[ROO^\bullet][AH] - R_i = 0 \qquad \text{Eq. 1.32}$$

By solving the second-degree equation with respect to [ROO•] and ignoring the negative answer, Eq. 1.33 is obtained:

$$[ROO^\bullet] = \frac{1}{2k_t}\left\{-k_{inh}[AH] + \sqrt{k_{inh}^2[AH]^2 2k_t R_i}\right\} \qquad \text{Eq. 1.33}$$

Substituting equation Eq. 1.30 in Eq. 1.26 it is obtained:

$$-\frac{d[O_2]}{dt} = k_p[ROO^\bullet][RH] + R_i \qquad \text{Eq. 1.34}$$

Substituting equation Eq. 1.33 for $[ROO^\bullet]$ we have:

$$-\frac{d[O_2]}{dt} = \frac{k_p[RH]}{2k_t}\left\{-k_{inh}[AH] + \sqrt{k_{inh}^2[AH]^2 2k_t R_i}\right\} + R_i \qquad \text{Eq. 1.35}$$

The expression Eq. 1.35 is general in nature and represents oxygen consumption both in the absence and in the presence of an induction period. In the latter case it is possible

to derive a simpler equation: in fact, in the presence of a good antioxidant, the recombination of peroxyls is negligible ($2ROO^{\bullet} \rightarrow$ products) because the termination rate with the antioxidant and the corresponding radical ($ROO^{\bullet} + A^{\bullet}$) are far more important. Based on these considerations, Eq. 1.32 becomes:

$$2k_{inh}[ROO^{\bullet}][AH] - R_i = 0 \qquad \text{Eq. 1.36}$$

from which we obtain:

$$[ROO^{\bullet}] = \frac{R_i}{2k_{inh}[AH]} \qquad \text{Eq. 1.37}$$

Substituting equation Eq. 1.37 in Eq. 1.34, the consumption of oxygen in the closed section will be given by:

$$-\frac{d[O_2]}{dt} = \frac{k_p[RH]R_i}{nk_{inh}[AH]} + R_i \qquad \text{Eq. 1.38}$$

If the chain is long enough, the term R_i can be neglected, and the following equation is obtained:

$$-\frac{d[O_2]}{dt} = \frac{k_p[RH]R_i}{nk_{inh}[AH]} \qquad \text{Eq. 1.39}$$

The formula for determining the R_i knowing the induction period is instead obtained from the following equations. If considering the decay of the inhibitor:

$$-\frac{d[AH]}{dt} = k_{inh}[AH]\,[ROO^{\bullet}] \qquad \text{Eq. 1.40}$$

in Eq. 1.40 we replace Eq. 1.37, and we obtain:

$$-\frac{d[AH]}{dt} = \frac{R_i}{2} \qquad \text{Eq. 1.41}$$

By integrating the differential equation, we have:

$$-\int_0^t d[AH] = \frac{R_i}{2}\int_0^t dt \qquad \text{Eq. 1.42}$$

$$[AH]_0 - [AH]_t = \frac{R_i}{2}t \qquad \text{Eq. 1.43}$$

At time t = τ, what is when all the inhibitor has been consumed, you get:

$$[AH]_0 = \frac{R_i}{2}\tau \qquad \text{Eq. 1.44}$$

Or:

$$R_i = \frac{2[AH]}{\tau} \qquad \text{Eq. 1.45}$$

The numerical term that appears in the numerator is the stoichiometric coefficient, that is, the number of peroxyls inactivated by each inhibitor molecule: it is equal to 2 because at the beginning of the calculations it was assumed that all A• radicals trap a peroxyl. With this formula it is therefore possible, from the initiation rate R_i, to obtain the induction time τ or vice versa.

1.3 Lipidic Peroxidation

1.3.1 What makes a hydrocarbon oxidizable?

As mentioned above, the abstraction of the H-atom from a substrate by a peroxyl radical controls the propagation step, so the strength of the C-H bond break (Bond Dissociation Energy, BDE) should determine the propagation's rate (k_p). Peroxyl radicals operate a HAT in specific positions of unsaturated lipids; it occurs

preferentially in allyl hydrogen (-CH_2 near the double bond) with weaker C-H bond energies than alkyl or bis-allyl hydrogen which has even lower C-H bond energies, since it is located between two double bonds and is doubly activated. *Fig.1.2*)

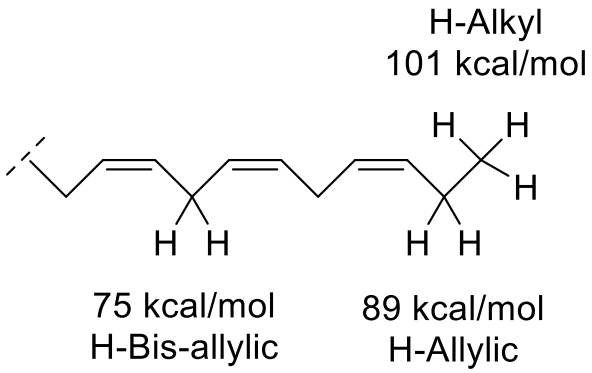

Figure 1.2 *BDE related to the C-H bond of the respective alkyl, allyl, bis-allyl bonds.*

Therefore, the order of reactivity is H-bis-allylic > H-allylic >> H -alkyl. It is intuitive that the difference in the k_p values for oleic and linoleic acid (*Fig. 1.1*) is due to the presence of one more H-bis-allylic in the linoleic acid than only H-allylic in the oleic acid. Hence, the magnitude of the propagation rate constants is generally corelated to the strength of their weakest C-H bonds, with some exceptions, but in general, there are three factors that govern the HAT rate of the hydrogen atom from peroxyls:

- Availability of low H-bond energy sources in solvent and lipids, which provide targets. Chain propagation is facilitated in neat lipids where the lipid allyl groups are the only source of hydrogens, at high lipid concentrations where fatty acid chains come in closer contact, in aprotic solvents that do not compete with lipids as targets and in higher polyunsaturated fatty acids with multiple bis-allylic hydrogens.
- Viscosity of the medium, which modulates accessibility[28]. HAT increases in low viscosity media but is impeded in viscous solvents[29].
- Temperature, which provides thermal energy to reduce bond dissociation energy. [30] However, any increases in HAT at elevated temperatures compete against reaction rates that are also increasing for other pathways and the final balance is not always predictable.

1.3.2 Distribution of primary products

What happens after the initial HAT is an interesting dilemma. According to current knowledge, the free electron distributes itself across a resonance-stabilized double bond system upon hydrogen abstraction from allyl hydrogens. Since HAT occurs on both sides of a double bond, each isolated double bond has two resonance systems, with the electron concentrated on the two distal carbons. For polyunsaturated fatty acids, the resonance systems allows a distribution of the spin on three positions, thus stabilizing even more the radical. In both systems the concentration of the electron density on the central carbon makes the outer carbons relatively deficient in electrons (indicated with arrows in *Figure 1.3*) and susceptible to the addition of oxygen. These locations are important to recognize because they provide markers for the formation of hydroperoxides and derived by-products.[31]

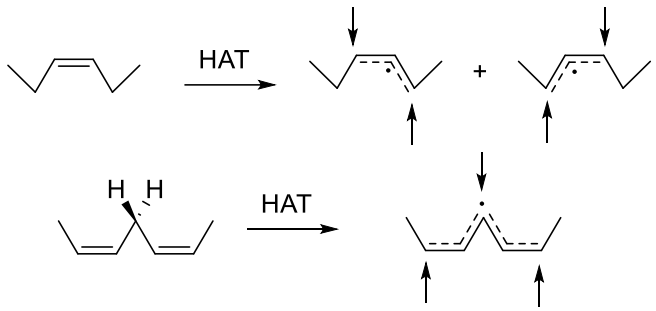

Figure 1.3 *Resonance structures after HAT and relative positions susceptible to the addition of oxygen.*

The lipid unsaturation promotes the autoxidation rate, and at the same time increases the complexity of the distribution of the products that are formed following the addition of O_2. In fact, several factors are involved such as conditions (conjugation of the double bond, polarity of the solvent, viscosity of the solvent, temperature) but also the propensity of oxygen to attack reversibly the alkyl radical. The peroxyl radicals can undergo to a β-fragmentation mechanism, whose rate constant is k_β. Basically the

process involves removing the peroxyl oxygen, bond rotation and/or migrating the free radical within the fatty acid resonance.

Oleic acid (and its esters), with a single unsaturation comprising C9 and C10, autoxidizes to give six primary hydroperoxide products (*Scheme 1.7*). HAT from one of the allylic positions, followed by the addition of oxygen at both ends of the formed allylic radicals gives four possible kinetic products (8-cis-OOH, 9-trans-OOH, 10-trans-OOH, 11-cis-OOH). The reversible addition of oxygen allows the formation of the trans-alkene thermodynamic products (8-trans-OOH, 11-trans-OOH). Porter et al. have identified an asymmetric distribution of the six oleate autoxidation products with a mixture of cis (minor products) and trans alkenes (major products).[32]

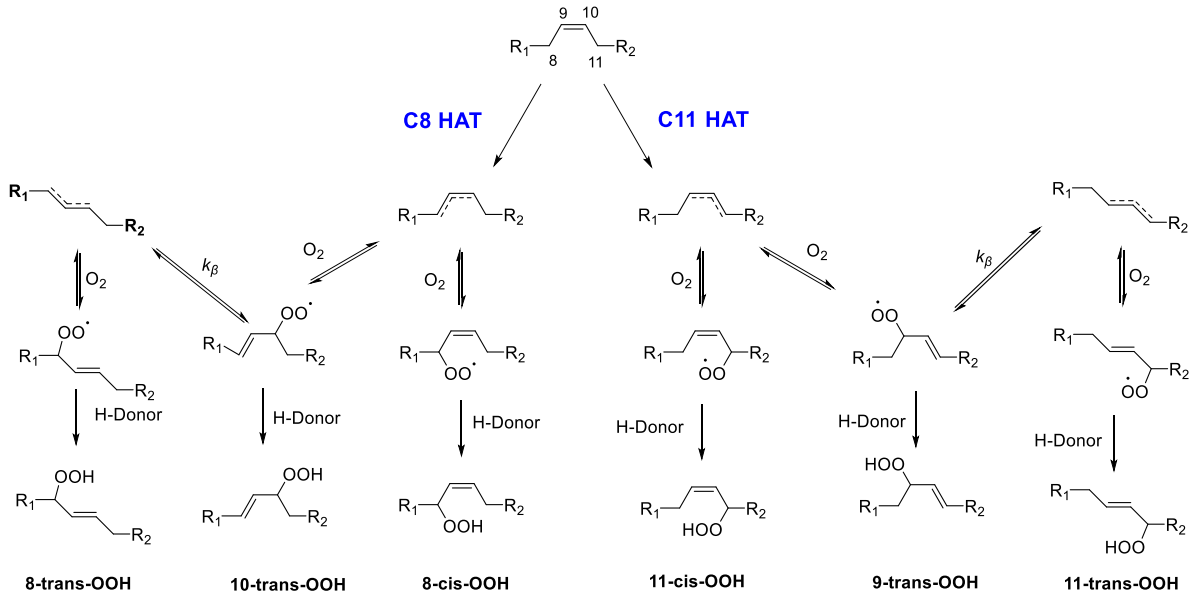

Scheme 1.7 *Product formation in the autoxidation of esters of oleate.*

Linoleic acid (or its ester) which is doubly unsaturated has a slightly more complex product distribution (*Scheme 1.8*). HAT from the bis-allyl position produces a delocalized pentadienyl radical to which oxygen can add at any of three positions which carry an unpaired electron spin density (C9, C11 and C13). Addition at positions C9 and C13 produces conjugated products with *cis, trans* configurations of the two double bonds, in contrast to the *cis, cis* configurations of the non-conjugated double bonds

formed by addition to C11. Indeed, 11-hydroperoxide can be trapped only in the presence of a hydrogen atom donor able to compete with the rapid β-fragmentation of the 11-peroxyl radical (k_β = 1.9×10^6 s^{-1}). The reversible addition of oxygen is also a competitive factor, as with slower k_β in 9- and 13-peroxyl radicals (k_β = 690 s^{-1}). Thus, the initially formed *cis, trans* products can rearrange themselves to give (thermodynamic) *trans, trans* products.[33,34]

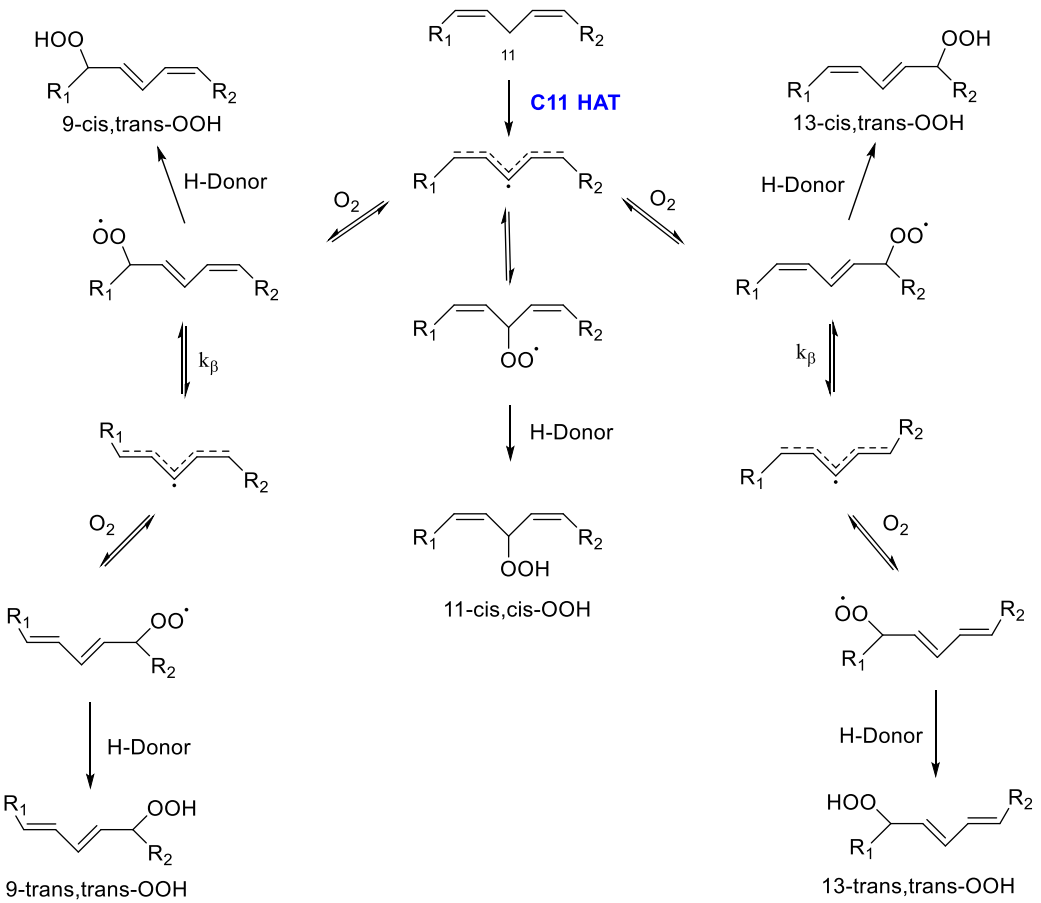

Scheme 1.8 *Product formation in the autoxidation of esters of linoleate.*

1.3.3 The peroxyl radical addition

A second reaction, that becomes competitive when hydrogen abstraction is slow, is the addition of peroxyl radical to the double bonds to form an *ortho*-peroxide alkyl radical, which in the case of oleate is unstable and further reacts to generate an epoxide and an alkoxyl radical. In the case of other substrates, such as styrene, in which the

ortho-peroxide alkyl radical is stabilized by resonance, the alkyl radical can react with O_2 forming polymeric products. Thus triggers a true branching reaction since new propagating radicals (alkoxyl) with higher reactivity are generated from the initial peroxyl radical (*Scheme 1.9*).

While in literature this reaction is well known in the hydrocarbon autoxidation, it is essentially ignored in the field of lipid peroxidation. Indeed, these competing pathways depend on the nature of the substrate and the conditions. For example, natural sterols, including the monounsaturated lipid *cholesterol,* [35] have been reported to undergo both HAT and peroxyl radical addition; in contrast there are relatively few reports of peroxyl radical addition to fatty acids, which implies that the HAT of polyunsaturated lipids constituting membranes is much faster than addition.

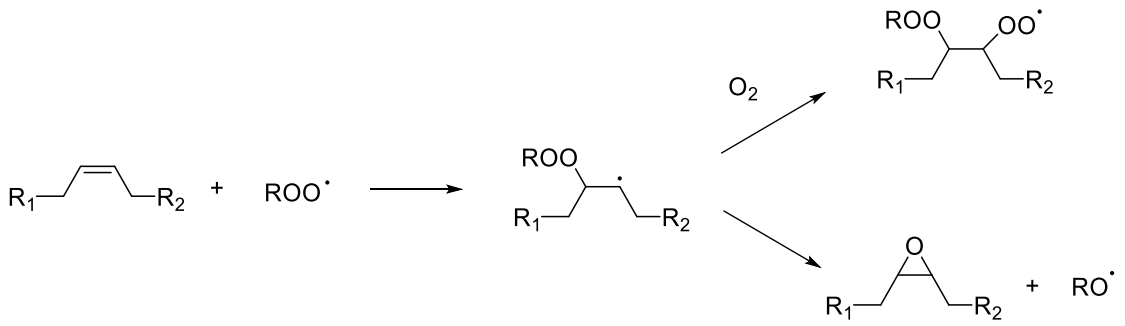

Scheme 1.9 *Addition of peroxyl radical to the double bonds*

However, this reaction is very important when it comes to lipids for industrial use, especially when they require heat treatment. Although little is known, peroxyl addition appears to become more important with heat.[36] Neff et al.[37] showed that the dimer linkages in methyl linoleate were mostly C-O-O-C at lower temperatures but shifted to C-C and C-O-C with increasing temperatures. Moreover, metals catalyze addition reactions of peroxyl radicals, with interesting implications for food systems.[38]

1.3.4 The fate of hydroperoxides

When decomposition factors are present, hydroperoxides are subject to low energy O-O bond decomposition reaction (BDE = 25-38 kcal/mol) and O-H bond cleavage,

(re)generating reactive radicals. For example, metals such as iron catalyze heterolytic generating one radical and one ion per event. Metals are highly effective catalysts because they are always present in food and biological systems (*Scheme 1.10*).

$$ROOH + Fe^{n+} \rightarrow RO^{\bullet} + {}^{-}OH + Fe^{(n+1)+}$$

$$ROOH + Fe^{(n+1)+} \rightarrow ROO^{\bullet} + H^{+} + Fe^{n+}$$

Scheme 1.10 *Decomposition of peroxide by transition metals*

It should not be underestimated the homolytic decomposition by heat and UV light, which splits the O-O bond providing alkoxy and hydroxyl radicals. These are much more reactive and much more oxidising species than peroxyl radicals, supplying a wider spectrum of secondary reactions and greatly accelerating oxidation and destabilization of the system. (*Scheme 1.11)*

$$ROOH \xrightarrow{h\nu/\Delta} RO^{\bullet} + \quad {}^{\bullet}OH$$

Scheme 1.11 *Decomposition of peroxide by light or heat*

At high enough concentrations, hydroperoxides react with each other, undergoing disproportionation and regenerating reactive radicals again **(***Scheme 1.13)*. Bimolecular decomposition has the same effect as heat and UV light: generation of two reactive radicals from a relatively stable ROOH. With faster reactions alkoxyl radical dominates kinetically, but peroxyl radical still produces secondary chains. The net result should be a dramatic increase in new chain initiation, detectable in accelerated oxygen consumption rates.

$$2ROOH \rightarrow ROO^{\bullet} + H_2O + RO^{\bullet}$$

Scheme 1.13 *Bimolecular decomposition of peroxides*

Over the years, several chemical mechanisms have been proposed that lead to the cleavage of a carbon-carbon bond in the fatty acid chain. One of these is the Hock rearrangement of a hydroperoxide *Scheme 1.14*. Protonation of the hydroperoxide produces a good leaving group and rearrangement of a C-C to C-O bond. The final product is unstable, and hydrolysis occurs.

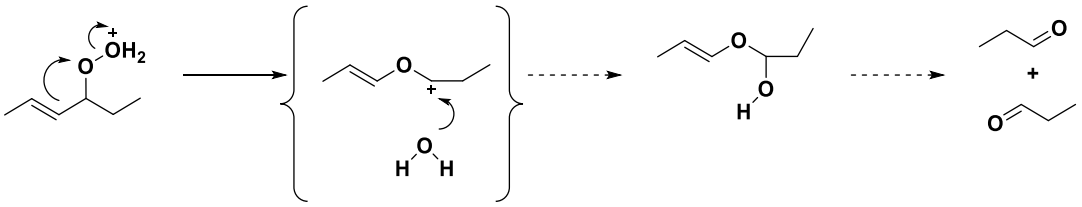

Scheme 1.14 *Hock's rearrangement mechanism*

1.3.5 Secondary products

The main consequence of the decomposition of hydroperoxides is the generation of two new radical species with a greater oxidizing power than the original peroxyl radical (ROO•, E° = 1 V): alkoxy radicals (RO•) and hydroxyl radicals (•OH) (E° = 1.6 and 2.32 V against NHE, respectively)[39,40] which are more reactive and less selective in their attack on lipids and other molecular constituents. In fact, alkoxy radicals are able to abstract the H-atom from positions with higher bond energies than peroxyl radicals (allylic and bis-allylic hydrogens) and with a higher rate ($k \sim 10^7 - 10^8$ M^{-1} s^{-1}).[41] Furthermore, they can give rearrangement, addition and scission reactions, to form reactive intermediates (such as aldehyde) can form adducts with DNA, proteins and other nucleophilic reactions that have been implicated in a number of degenerative conditions, including aging, cancer, atherosclerosis, macular degeneration, Alzheimer's and Parkinson's disease.

Various mechanisms can contribute to ketone formation (*Scheme 1.15*), including H-atom abstraction from the carbon bearing the hydroperoxide and expulsion of a hydroxyl radical. Peroxidic O-O bonds can also be cleaved by homolysis or one electron reduction (*e.g.* with Fe^{2+}) leading to carbonyls and chain scission products.

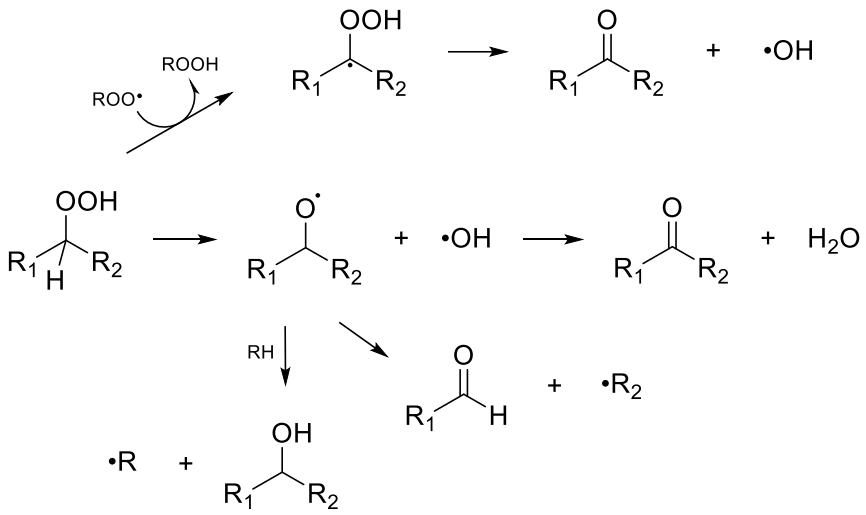

Scheme 1.15 *Fates of primary products of lipid autoxidation. A) Alcohol, ketone or aldehyde formation from a hydroperoxide*

1.4 Conclusion

Over the past 30 years, there has been a significant advancement in our chemical understanding of lipid peroxidation; it is now possible to examine the structure of a given fatty acid and anticipate the rate at which it autoxidizes as well as which products will occur under various circumstances. We are also aware of the characteristics that an antioxidant must have in order to work effectively. However, there are still many unanswered questions, *e.g.* how do fatty acids react at high temperatures in the presence/absence of antioxidants? Are there new materials that boost the stability of a lipid substrate? Do essential oils have a cellular protective effect and are they able to prevent lipid peroxidation through novel inhibitory mechanisms? In this thesis we will attempt to answer these questions, bearing in mind that even a single piece of information can aid future research.

References

1. Tavakoli, J. *et al.* Improving the Frying Performance and Oxidative Stability of Refined Soybean Oil by Tocotrienol-Rich Unsaponifiable Matters of Kolkhoung (Pistacia *khinjuk*) Hull Oil. *J Am Oil Chem Soc* **95**, 619–628 (2018).
2. Farhoosh, R. & Nyström, L. Antioxidant potency of gallic acid, methyl gallate and their combinations in sunflower oil triacylglycerols at high temperature. *Food Chem* **244**, 29–35 (2018).
3. Niki, E. Lipid peroxidation: Physiological levels and dual biological effects. *Free Radic Biol Med* **47**, 469–484 (2009).
4. Yin, H., Xu, L. & Porter, N. A. Free Radical Lipid Peroxidation: Mechanisms and Analysis. *Chem Rev* **111**, 5944–5972 (2011).
5. Xu, L. & Porter, N. A. Free radical oxidation of cholesterol and its precursors: Implications in cholesterol biosynthesis disorders. *Free Radic Res* **49**, 835–849 (2015).
6. Frank, C. E. Hydrocarbon Autoxidation. *Chem Rev* **46**, 155–169 (1950).
7. Ingold, K. U. Peroxy radicals. *Acc Chem Res* **2**, 1–9 (1969).
8. Amorati, R., Baschieri, A. & Valgimigli, L. Measuring Antioxidant Activity in Bioorganic Samples by the Differential Oxygen Uptake Apparatus: Recent Advances. *J Chem* **2017**, 1–12 (2017).
9. Maillard, B., Ingold, K. U. & Scaiano, J. C. Rate constants for the reactions of free radicals with oxygen in solution. *J Am Chem Soc* **105**, 5095–5099 (1983).
10. Labuza, T. P. & Dugan, L. R. Kinetics of lipid oxidation in foods. *C R C Critical Reviews in Food Technology* **2**, 355–405 (1971).
11. Xu, L., Davis, T. A. & Porter, N. A. Rate Constants for Peroxidation of Polyunsaturated Fatty Acids and Sterols in Solution and in Liposomes. *J Am Chem Soc* **131**, 13037–13044 (2009).
12. Howard, J. A. & Ingold, K. U. Absolute rate constants for hydrocarbon autoxidation. VI. Alkyl aromatic and olefinic hydrocarbons. *Can J Chem* **45**, 793–802 (1967).

13. Traylor, T. G. & Russell, C. A. Mechanisms of Autoxidation. Terminating Radicals in Cumene Autoxidation. *J Am Chem Soc* **87**, 3698–3706 (1965).
14. Bielski, B. H. J., Cabelli, D. E., Arudi, R. L. & Ross, A. B. Reactivity of HO_2/O_2^- Radicals in Aqueous Solution. *J Phys Chem Ref Data* **14**, 1041–1100 (1985).
15. Pryor, W. A. & Squadrito, G. L. The chemistry of peroxynitrite: a product from the reaction of nitric oxide with superoxide. *American Journal of Physiology-Lung Cellular and Molecular Physiology* **268**, L699–L722 (1995).
16. Haeggström, J. Z. & Funk, C. D. Lipoxygenase and Leukotriene Pathways: Biochemistry, Biology, and Roles in Disease. *Chem Rev* **111**, 5866–5898 (2011).
17. Rouzer, C. A. & Marnett, L. J. Endocannabinoid Oxygenation by Cyclooxygenases, Lipoxygenases, and Cytochromes P450: Cross-Talk between the Eicosanoid and Endocannabinoid Signaling Pathways. *Chem Rev* **111**, 5899–5921 (2011).
18. Kanner, J., German, J. B., Kinsella, J. E. & Hultin, H. O. Initiation of lipid peroxidation in biological systems. *C R C Critical Reviews in Food Science and Nutrition* **25**, 317–364 (1987).
19. Singleton, D. A. *et al.* Mechanism of Ene Reactions of Singlet Oxygen. A Two-Step No-Intermediate Mechanism. *J Am Chem Soc* **125**, 1319–1328 (2003).
20. Amorati, R., Baschieri, A. & Valgimigli, L. Measuring Antioxidant Activity in Bioorganic Samples by the Differential Oxygen Uptake Apparatus: Recent Advances. *J Chem* **2017**, 1–12 (2017).
21. Greenwald, R. A. Superoxide dismutase and catalase as therapeutic agents for human diseases a critical review. *Free Radic Biol Med* **8**, 201–209 (1990).
22. Valgimigli, L. & Pratt, D. A. Antioxidants in Chemistry and Biology. in *Encyclopedia of Radicals in Chemistry, Biology and Materials* (John Wiley & Sons, Ltd, 2012). doi:10.1002/9781119953678.rad055.
23. Brigati, G., Lucarini, M., Mugnaini, V. & Pedulli, G. F. Determination of the Substituent Effect on the O−H Bond Dissociation Enthalpies of Phenolic Antioxidants by the EPR Radical Equilibration Technique. *J Org Chem* **67**, 4828–4832 (2002).

24. Lucarini, M., Mugnaini, V., Pedulli, G. F. & Guerra, M. Hydrogen-Bonding Effects on the Properties of Phenoxyl Radicals. An EPR, Kinetic, and Computational Study. *J Am Chem Soc* **125**, 8318–8329 (2003).
25. Lucarini, M., Pedulli, G. F. & Cipollone, M. Bond Dissociation Enthalpy of .alpha.-Tocopherol and Other Phenolic Antioxidants. *J Org Chem* **59**, 5063–5070 (1994).
26. Lucarini, M., Mugnaini, V., Pedulli, G. F. & Guerra, M. Hydrogen-Bonding Effects on the Properties of Phenoxyl Radicals. An EPR, Kinetic, and Computational Study. *J Am Chem Soc* **125**, 8318–8329 (2003).
27. Traber, M. G. & Atkinson, J. Vitamin E, antioxidant and nothing more. *Free Radic Biol Med* **43**, 4–15 (2007).
28. Walling, Cheves. & Padwa, Albert. Positive Halogen Compounds. VI. Effects of Structure and Medium on the β-Scission of Alkoxy Radicals. *J Am Chem Soc* **85**, 1593–1597 (1963).
29. Porter, N. A., Caldwell, S. E. & Mills, K. A. Mechanisms of free radical oxidation of unsaturated lipids. *Lipids* **30**, 277–290 (1995).
30. Ingold, K. U. Peroxy radicals. *Acc Chem Res* **2**, 1–9 (1969).
31. E.N. Frankel. *Lipid Oxidation*. (Oily Press, 2005).
32. Porter, N. A., Mills, K. A. & Carter, R. L. A Mechanistic Study of Oleate Autoxidation: Competing Peroxyl H-Atom Abstraction and Rearrangement. *J Am Chem Soc* **116**, 6690–6696 (1994).
33. Tallman, K. A., Roschek, B. & Porter, N. A. Factors Influencing the Autoxidation of Fatty Acids: Effect of Olefin Geometry of the Nonconjugated Diene. *J Am Chem Soc* **126**, 9240–9247 (2004).
34. Tallman, K. A., Pratt, D. A. & Porter, N. A. Kinetic Products of Linoleate Peroxidation: Rapid β-Fragmentation of Nonconjugated Peroxyls. *J Am Chem Soc* **123**, 11827–11828 (2001).
35. Zielinski, Z. A. M. & Pratt, D. A. H-Atom Abstraction vs Addition: Accounting for the Diverse Product Distribution in the Autoxidation of Cholesterol and Its Esters. *J Am Chem Soc* **141**, 3037–3051 (2019).

36. Mounts, T. L., McWeeny, D. J., Evans, C. D. & Dutton, H. J. Decomposition of linoleate hydroperoxides: Precursors of oxidative dimers. *Chem Phys Lipids* **4**, 197–202 (1970).
37. Neff, W. E., Frankel, E. N. & Fujimoto, K. Autoxidative dimerization of methyl linolenate and its monohydroperoxides, hydroperoxy epidioxides and dihydroperoxides. *J Am Oil Chem Soc* **65**, 616–623 (1988).
38. Kochi, J. K. Addition of peroxides to conjugated olefins catalyzed by copper salts. *J. Am. Chem. Soc.* **84**, 2785–2793 (1962).
39. Koppenol, W. H. Oxyradical reactions: from bond-dissociation energies to reduction potentials. *FEBS Lett* **264**, 165–167 (1990).
40. Wood, P. M. The potential diagram for oxygen at pH 7. *Biochemical Journal* **253**, 287–289 (1988).
41. Erben-Russ, Michael., Michel, Christa., Bors, Wolf. & Saran, Manfred. Absolute rate constants of alkoxyl radical reactions in aqueous solution. *J Phys Chem* **91**, 2362–2365 (1987).

CHAPTER II
OXIDATION AND STABILIZATION OF BIO-OILS AT HIGH-TEMPERATURE

2.1 Preface

Bio-oils used for various industrial purposes, such as the production of biodiesel, undergo extensive oxidation and degradation during transformation processes. Therefore, it is extremely important to predict their high-temperature stability, as well as to develop new techniques able to counteract lipid peroxidation. This chapter reports the kinetic studies carried out on bio-oils following treatment at 130°C. Through a new procedure, based on the optically detected profile of the O_2 concentration in the headspace during the isotherms at 130 °C, it was possible to evaluate the oxidation kinetic parameters of several bio-oil raw materials, including used cooking oils, mono-, di- and triglycerides of natural origin, free fatty acids, transesterified oils. The same method was then used to carry out a kinetic study of O_2 consumption during the spontaneous peroxidation of stripped sunflower oil at 130 °C in the presence of 18 antioxidants belonging to the main families of natural and synthetic phenols, including α-tocopherol, alkylphenols (BHT, BHA), hydroquinones (TBHD), catechols (quercetin, catechin) and gallates, in order to obtain important information to optimize the antioxidant activity of phenols based on the structure-activity relationships at high temperatures. Finally, the synergistic antioxidant activity of γ-terpinene with α-tocopherol, its synthetic analogue 2,2,5,7,8-pentamethyl-6-chromanol (PMHC), BHT, TBHQ and catechol was studied by measuring the O_2 consumption and the formation of hydroperoxides in stripped sunflower oil at 130°C, demonstrating that this terpene is a promising natural antioxidant for high temperature food applications. Part of this chapter is presented as it was published in *Antioxidants* (Mollica, F.; Lucarini, M.; Passerini, C.; Carati, C.; Pavoni, S.; Bonoldi, L.; Amorati, R. *Antioxidants* 2020, 9, 399 and Mollica, F.; Bonoldi, L.; Amorati, R. *Antioxidants,* 2022, 11, 2142.) and *ACS Food*

Science & Technology (Mollica, F.; Gelabert, I.; Amorati, R. *ACS Food Sci. Technol.* 2022, 2, 1, 180–186)

2.2 Introduction

Replacing fossil-derived energy sources with renewable feedstock is important to cope with the gradual depletion of non-renewable fossil fuels, pollution, and excessive CO_2 emissions.[1] The conversion of waste and used cooking vegetable oils to renewable diesel is sought as a profitable source of biofuels, because it is less energy demanding than processes involving different feedstock. Up-conversion, however, requires the storage and manipulation of feedstocks at relatively high temperatures, which is a well-known condition that increases degradation processes.[2] In fact, degradation of natural oils at high temperature is a problem occurring in many technological applications, ranging from food deep-frying[3,4] to biodiesel processing.[5] Thermal stress causes oxidation and polymerization of oils, with the formation of volatile, non-volatile, and polymeric compounds that affect the oil chemical-physical characteristics and lead to the formation of fouling and solid deposits. The extent of this process depends on many parameters, the most important being the oil composition, temperature, and accessibility of oxygen.[6] When O_2 is present in the system, oxidation is the most relevant oil degradation mechanism, consisting of a free-radical mediated autoxidation, which leads to the formation of hydroperoxides and other oxygenated compounds. In turn, hydroperoxides undergo homolytic cleavage and increase the decomposition by generating new radicals.[7] The extent of autoxidation is dependent on oil composition, as the susceptibility of fatty acids toward oxidation increases in the order: saturated < monounsaturated < polyunsaturated.[7] It is further promoted by the presence of metals.[7] Oil stability is instead increased by the presence of antioxidants which may be naturally present in the oil or can be added on purpose. Natural tocopherols, which are commonly present in seed oils, have poor performances compared to synthetic antioxidants such as BHT, gallate esters, and butylated hydroquinones.[5] In addition, unsaponifiable oil

components, including phytosterols and oryzanol, have been found to increase oil stability presumably by a mechanism not related to radical trapping.[6]

The chemical mechanism of oil autoxidation is a radical chain shown *in Scheme 2.1a*[8] and was described in detail in Chapter I. Summing up, initiation processes generate alkyl radicals (R•) that react with O_2 at a diffusion-controlled rate yielding alkyl hydroperoxides (ROO•). Initiation occurs through various processes including the decomposition of traces of hydroperoxides, possibly catalyzed by transition metals, or by the direct reaction of activated C-H bonds with O_2.[9] Peroxyl radicals then propagate the oxidative chain by different pathways *(Scheme 2.1c)*. Chain breaking antioxidants act by trapping peroxyl radicals through the reactions depicted in *Scheme 2.1b*. Following this general oxidation scheme, the duration of the inhibition period of an antioxidant (τ) is proportional to its concentration and inversely proportional to the initiation rate ($\tau \sim [AH]/R_i$).[9–11]

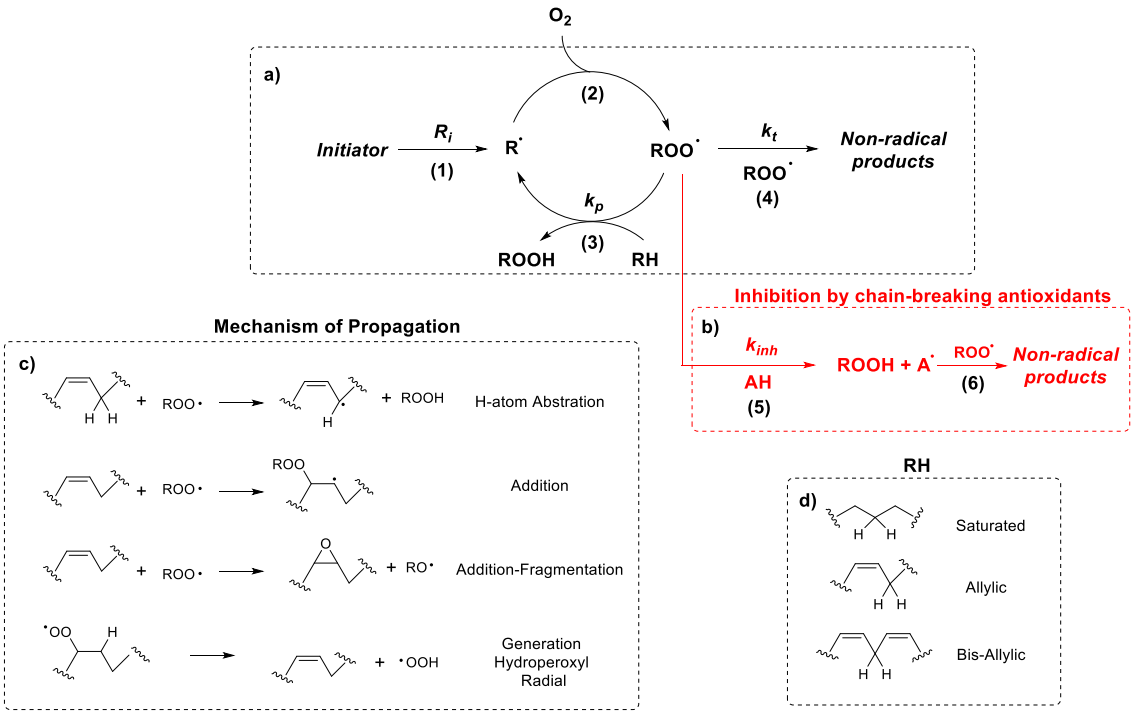

Scheme 2.1. *a) Mechanism of autoxidation of natural fatty acids; b) Mechanism of inhibition by chain-breaking antioxidant; c) The main mechanism of propagation by peroxyl radicals; d) oxidizable portion of fatty acids.*

In general, the study of the oxidation of lipid substrates in the industrial (but also academic fields) is carried out by measuring various parameters, such as iodine number, anisidine value, peroxide value, and Oxidative Stability Index (OSI). However, being methods based on by-products, they can give partial information, as well as being experimentally challenging. For this reason, to improve our understanding of the oxidative reactions of lipids at high temperatures, we have developed an innovative method based on the study of the O_2 consumption by a substrate, optically detected during the isotherms at 130°C. The study of O_2 uptake is among the best methods to follow autoxidation reactions, because there is little interference from other processes, and allows to obtain important kinetic parameters describing the behavior of the substrate under such conditions. *Figure 2.1* shows the apparatus used for these studies. Oxygen consumption was measured in a round bottom flask surmounted by a short glass condenser, over which the optical oxygen meter and the thermometer were introduced through a silicone rubber septum which seals the system. The operating principle is based on luminescence quenching of a sensor dye. The dye is excited with red light, and the properties of the resulting luminescence are measured in the near infrared. The presence of molecular oxygen quenches the luminescence, changing its intensity and lifetime fully reversibly. The probe provides the direct measure of O_2 concentration and shows virtually no interferences to other gases. The probe was a Robust Oxygen Probe manufactured by *Pyroscience* GmbH (Aachen, Germany), coupled to a FireStingO_2 control unit having a thermometer probe for continuous temperature correction. The probe provides the direct measure of O_2 concentration, and the glass condenser maintains the probe tip at about 30 °C and this equipment is suited for measuring O_2 uptake up to 180 °C. The data obtained from the apparatus are subsequently processed to obtain graphs of oxygen consumption as a function of time.

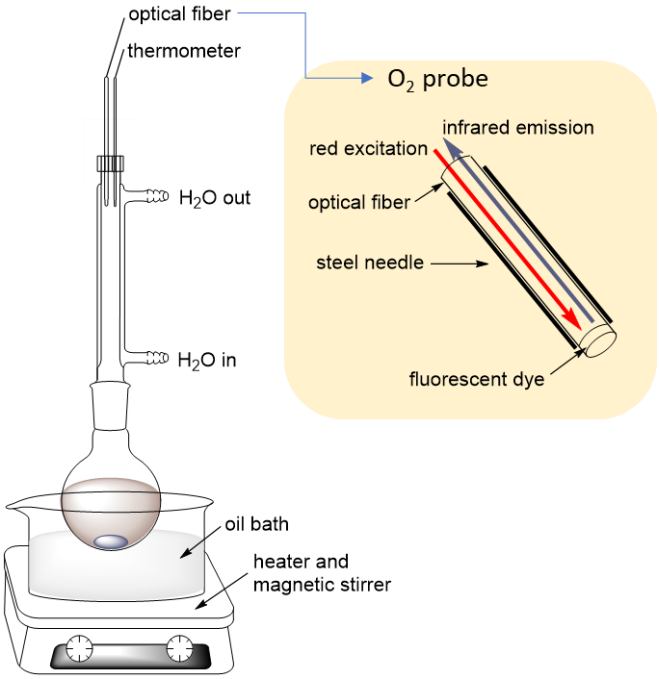

Figure 2.1 *Apparatus for measuring oxygen consumption and scheme of the optical O_2 probe.*

2.3 Determination of kinetic parameters in high temperature autoxidation

As mentioned above, the oxidation stability can be measured by different parameters, such as iodine value, anisidine value, peroxide value, and Oxidative Stability Index (OSI). The iodine value is related to the concentration of double bonds in the pristine oil, which is more oxidizable if it has a higher unsaturation level, while peroxide and anisidine values are related to the oxidation degree.[12] Generally speaking, oxidation proceeds through the formation of primary and secondary oxidation products, *i.e.*, first peroxide and conjugated dienes, and then carbonyls and acids.[13] The peroxide value is related to the concentration of hydroperoxides and therefore highlights the dimension of the first oxidation step, while the anisidine value (*AOCS Official Method Cd 18-90*) is related to the concentration of aldehydes and ketones, and accounts for the dimension of the secondary oxidation process. These analytical methods for the quantitative determination of specific products are very accurate; however, they are experimentally demanding, and may present the limit of partial information. In addition, they are

focused on the oxidation level, but not directly on the kinetics of the oxidation process. The OSI method (*AOCS Cd12b-92*) is performed by passing purified air through a sample that is kept under high temperature (70–110 ◦C), promoting a rapid degradation of the triglycerides with formation of volatile organic acids, conveyed by the air stream into a conductivity cell full of water where the acids are solubilized. These acids, once dissolved in the water solution, dissociate into ions, thus changing the conductivity of the water. The time requested to induce the rapid rise in conductivity (hours) is the OSI time.[12,14] This method is largely applied for the characterization of oxidation stability of oils and fats, and particularly in the case of biodiesel of various origins in both academic studies and industrial applications.[15,16]

Having a separate evaluation of factors underlying oil autoxidation (that are initiation, propagation, and inhibition) would be of fundamental importance to understand and control this unwanted process. For this reason, to improve our knowledge of oil oxidative reactions at high temperatures, we studied the full profile of O_2 uptake of several samples of oils during isotherms at 130 °C by an optical O_2 probe (*see paragraph 2.1*). The study of O_2 uptake is among the best methods to follow autoxidation reactions, because there is little interference with other processes.[10,11,17–19] For instance, hydroperoxides and aldehydes are known to be degraded by radical and non-radical reactions, therefore their level is not always related to the substrate oxidation.[5,7] In addition to the duration of the inhibited period, this experimental setup allowed measuring the O_2 consumption rates before and after the onset of the fast oxidation regime, *i.e.* three independent parameters describing oil oxidation, and shedding some light on the separate factors impacting on it. We also performed these kinetic measurements in the presence of a fixed amount of the antioxidant propyl gallate, as an expedient to have a semiquantitative evaluation of the magnitude of the initiation rate R_i.

	Description	R_{inh} *nmol/s*	τ 10^3 *s*	R_{st} *nmol/s*	τ-τ_{PG} 10^3 *s*	*Fe Ppm*	H^+ *mg KOH/g*	$OSI^{[b]}$ *h*	$SA^{[c]}$	$MO^{[c]}$	$DI^{[c]}$ $(TRI)^{[c]}$
Type A											
BIO26	*Refined Used Cooking oil (T)*	*0*	*<1*	*100*	*3*	*3*	*8.55*	*1*	*19.05*	*52.72*	*27.10 (1.13)*
BIO44	*Used Cooking Oil (T)*	*0*	*<1*	*94*	*15.5*	*4.3*	*8.62*	*0*	*26.30*	*50.60*	*21.20 (1.90)*
BIO57	*Oil Distillation pitch (T)*	*0*	*<1*	*38*	*0*	***1472***	***33.79***	*0.7*	*60.05*	*35.86*	*0.68 (3.41)*
BIO65	*Vegetable oil fraction(T)*	*0*	*<1*	*54*	*60*	*3.7*	*31.07*	*0.83*	*42.59*	*46.82*	*10.59 (0)*
BIO84	*Safflower oil (T)*	*0*	*<1*	*120*	*3.2*	*<0.5*	*0.96*	*2.01*	*18.30*	*17.16*	*64.54 (0)*
BIO85	*Linseed oil (T)*	*0*	*<1*	*180*	*2.2*	*<0.5*	*1.20*	*0.10*	*14.00*	*22.00*	*16.00 (48)*
BIO130	*Tall oil (1) (A)* [d]	*0*	*<1*	*100*	*0*	***31.3***	***159.63***	*0.1*	*52.40*	*27.80*	*16.90 (2.90)*
BIO131	*Tall oil (2) (A)* [d]	*0*	*<1*	*86*	*0*	***67.9***	***155.14***	*0.1*	*51.10*	*28.90*	*17.40 (2.60)*
BIO132	*Tall oil (3) (A)* [d]	*0*	*<1*	*90*	*0*	***35.01***	***155.43***	*0.1*	*52.20*	*28.00*	*17.10 (2.70)*
BIO145	*Tall oil fatty acid (A)*	*0*	*<1*	*128*	*0*	*0.6*	***193.27***	*0.1*	*30.60*	*30.94*	*36.10 (2.36)*
Type B											
BIO19	*Palm oil (T)*	*1.5*	*70*	*48*	*80*	*5.5*	*8.48*	*30.50*	*55.06*	*36.22*	*8.56*
BIO22	*Soybean oil (T)*	*8.9*	*10*	*120*	*8*	*0.5*	*2.24*	*6.38*	*25.17*	*21.76*	*49.70*
BIO23	*Fractioned Seed rape oil (M,D,T)*	*36*	*5.5*	*49*	*65*	*9.1*	*1.39*	*0.1*	*48.56*	*37.49*	*13.24 (0.70)*
BIO38	*Corn oil (T)*	*6.0*	*12.0*	*110*	*6.0*	*<0.5*	*0.11*	*9.40*	*19.65*	*27.20*	*52.50 (0.65)*
BIO54	*Animal fat (T)*	*2.2*	*17.0*	*38*	*320*	*1.1*	*8.62*	*7.28*	*51.63*	*42.63*	*5.22 (0.52)*
BIO61	*Empty fruit bunch (T)*	*0.88*	*120*	*40*	*180*	*7.8*	*33.76*	*9.12*	*54.32*	*37.12*	*8.44 (0.12)*
BIO62	*Carinata oil (T)*	*11*	*4.5*	*94*	*9.5*	*0.8*	*0.10*	*5.53*	*33.00*	*40.50*	*20.75 (5.75)*

BIO68	*Castor oil (D,T)*	*0.28*	*260*	*76*	*165*	*2.1*	*0.32*	*44.69*	*8.17*	*87.58*	*4.25 (0)*
BIO73	*RBD Palm oil (T)*	*8.25*	*6*	*48*	*46*	*<0.5*	*0.21*	*na*	*56.8*	*34.4*	*8.8 (0)*
BIO86	*Jojoba oil (T)*	*0.24*	*45*	*60*	*255*	*<0.5*	*0.47*	*43.06*	*5.81*	*93.55*	*0.64 (0)*
BIO87	*Cotton oil (T)*	*21*	*2.5*	*100*	*1.5*	*<0.5*	*0.10*	*4.18*	*31.70*	*19.25*	*49.05 (0)*
BIO109	*Canapa oil (T)*	*18.0*	*2.5*	*90*	*19.5*	*2.4*	*27.61*	*2.20*	*44.20*	*14.10*	*34.90 (6.70)*
BIO113	*Palm kernel oil (T)*	*5.4*	*3.5*	*27*	*297.5*	*1*	*3.94*	*10.68*	*87.59*	*10.93*	*1.47 (0)*
BIO128	*Animal fat (ME)*	*23.0*	*44*	*60*	*25*	*<0.5*	*3.12*	*na*	*40.2*	*46.40*	*11.80 (1.70)*
BIO146	*Tobacco oil (T)*	*23*	*3.2*	*140*	*4.6*	*1.36*	*7.32*	*0.10*	*12.72*	*11.57*	*74.34 (1.36)*
BIO171	*Fatty acids (ME)*	*36*	*2.5*	*85*	*3.5*	*4.21*	*4.96*	*0.80*	*53.70*	*36.10*	*10.20 (0)*
BIO185	*Palm oil mill effluent (A)*	*11*	*7.5*	*93*	*6.5*	***126***	***132.02***	*0.95*	*23.89*	*45.46*	*30.65 (0)*
BIO210	*Fatty acids (ME)*	*8.3*	*12*	*72*	*0.6*	*0.8*	*0.18*	*8.69*	*43.9*	*41.8*	*14.3 (0)*
Type C											
BIO77	*C10SE1 (BE)* [e]	*43*	*1*	*17*	*0*	*3.7*	*4.57*	*0.2*	*92*	*8*	*0 (0)*
BIO69	*C10SE1 (BE)* [e]	*54*	*2.5*	*18*	*0*	***14.3***	*4.57*	*0.2*	*92*	*8*	*0 (0)*

Table 2.1. *Oil composition, iron content, acidity, oxidation stability index and parameters for oil oxidation at 130 °C: t = duration of the induction time; R_{inh} = initial O_2 consumption rate; R_{st} = steady O_2 consumption rate; $\tau PG - \tau$ = propyl gallate effect on induction time.*

[a] Legend: T, triglycerides; D, diglycerides; M, monoglycerides; A, free fatty acids; ME, methyl ester; BE, butyl ester. [b] Oxidative stability index. [c] SA, saturated; MO, monounsaturated; DI, diunsaturated; TRI, triunsaturated fatty acids, in mol%. [d] Different batches. [e] C_{10} saturated fatty acids esters, samples stored in different conditions. Samples with high acidity or iron content (see discussion) are marked in bold.

2.3.1 Results

Analysis of the O_2 Consumption Plots

The oils considered in the present study included triglycerides; mixtures of mono-, di-, and triglycerides in different proportions; free fatty acids; transesterified oils; waste oils; and oils deriving from wood processing, to reflect the diversity of bio-based matrixes used to produce biodiesel (*see Table 2.1*). Based on the shapes of the oxygen consumption plots, measured in the headspace of a stirred reaction vessel at 130 °C, oils were divided into three families: (A) linear O_2 consumption from the beginning of the experiment (Type A oils); (B) initial slow O_2 consumption (Type B oils); and (C) initial fast O_2 consumption (Type C oils). The symbols used to indicate these periods are τ = duration of the induction period (*IP)*; R_{inh} = initial rate; and R_{st} = steady rate (see *Figure 2.2*). The results of O_2 consumption experiments are reported in *Table 2.1*.

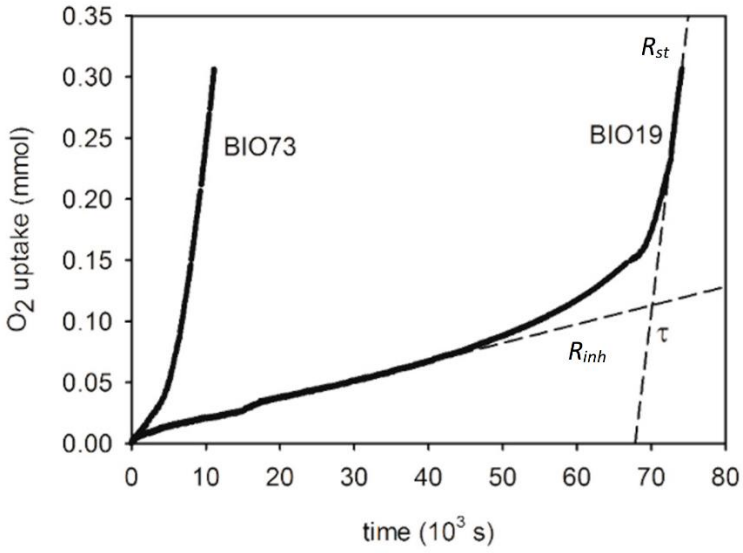

Figure 2.2 *O_2 uptake measured during the oxidation at 130 C of raw (BIO19) and purified (BIO73) palm oil.*

Inhibition Period (Type B oils)

Oils belonging to Type B showed an induction period before the onset of fast O_2 consumption, which can be attributed to the presence of intrinsic antioxidants in the oils. For example, the two samples BIO19 and BIO73 are constituted by raw and

purified palm oil, respectively. In *Figure 2.2*, it is shown that the inhibition period of BIO19 is much longer than that of BIO73, despite the former contains higher levels of iron, a well-known oxidation catalyst. We explain this with the removal of endogenous antioxidants during the purification treatment. Interestingly, the slopes of O_2 uptake after the end of the induction time R_{st} of the two oils are almost coincident, indicating that R_{st} reflects the composition of triglycerides while other minor differences (see *Table 2.1*) are not relevant. The length of the induction periods of Type B oils are reported in *Table 2.1* and *Figure 2.3a*. The length of the induction period (τ) was related to the Oil Stability Index (OSI), which represents the induction time at 110 °C measured by the Rancimat apparatus.

If comparing the two set of values (*Figure 2.3b*), it can be noted that τ is in general shorter than OSI, reasonably as the effect of the higher temperature that leads to greater production of radicals and hence to faster consumption of the antioxidants. In most cases, the two parameters show similar stability ranking of the oils. Some exceptions in the general agreement could be due to the different experimental setup, or to specific chemical effects involving the chain-carrying radicals.

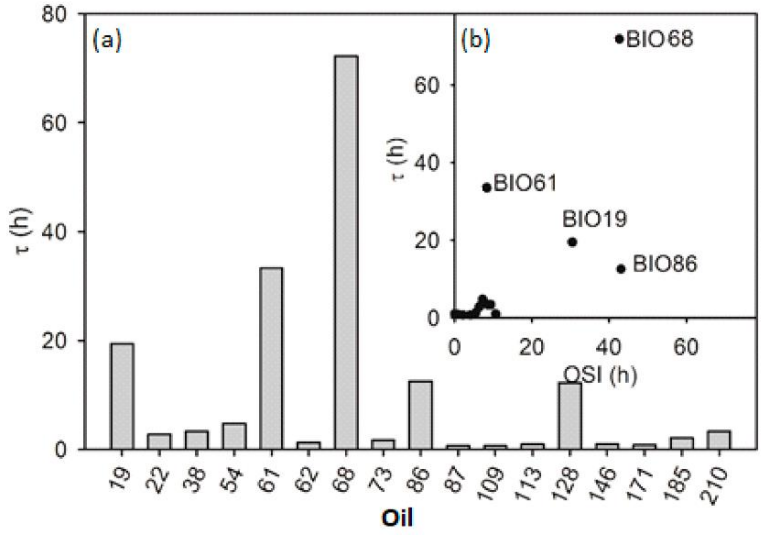

Figure 2.3 *(a) Induction period of Type B oils. (b) The inset reports the relationship between OSI values and τ, showing that τ is in general smaller than OSI, except for BIO61 and BIO68.*

Steady Oxygen Consumption (Rst) in Type A-C Oils

A steady oxygen consumption is shown by Type A oils soon after the beginning of the oxidation, while in the case of Type B and C oils, it is reached after an initial inhibited or accelerated period. The steady oxygen consumption measured for all oils, reported in *Figure 2.4*, showed a marked variation among the oils, ranging from 17 nmol/s of a fully saturated oil (BIO77) to 180 nmol/s of linseed oil (BIO85). To understand in detail the determining factors of oil oxidation, R_{st} dependence on oil characteristics was analyzed by multiple linear regression. This procedure showed that the main determinant of R_{st} was the percent concentration of mono (MO)-, di (DI)-, and tri (TRI)-unsaturated fatty acids eq. 2.1 (r^2 = 0.78); however, the best results were obtained when also the oil acidity (H^+, expressed as mg KOH/g) was considered, as shown in eq. 2.2) (r^2 = 0.92).

$$R_{st}\ (nmol/s) = 20.1 + (0.570\ MO\%) + (1.54\ DI\%) + (2.65\ TRI\%) \qquad \text{Eq 2.1}$$

$$R_{st}\ (\text{nmol/s}) = 9.82 + (0.634\ \text{MO\%}) + (1.63\ \text{DI\%}) + (2.65\ \text{TRI\%}) + (0.154\ \text{H+}) \qquad \text{Eq 2.2}$$

Inclusion of the iron content or peroxide value caused a worsening of the regression coefficient. While the dependence of R_{st} on oil unsaturation is not unexpected, the role of acid is less clear and will be the object of further studies.

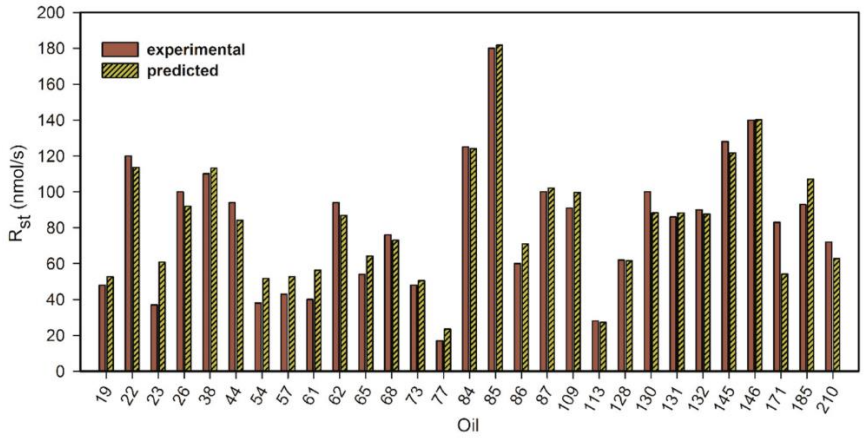

Figure 2.4 *Overview of experimental R_{st} of oils at 130 °C and comparison with the values predicted by the multiple linear regression shown in Eq. 2.2.*

Standard Addition of Propyl Gallate

To get further information on oil behavior, we performed the oil oxidation with the addition of 500 mg/L of propyl gallate (PG), a widely used antioxidant for oil stabilization, to every sample. The aim of these experiments was to classify oils by measuring the duration of the inhibition period given by a constant amount of the same antioxidant (PG), while the activity of naturally occurring antioxidants is in general different. The effect of PG ($\tau PG - \tau$) was obtained from the difference between the inhibition in the presence (τPG) and in the absence of PG (τ), as shown in *Figure 2.5a*.

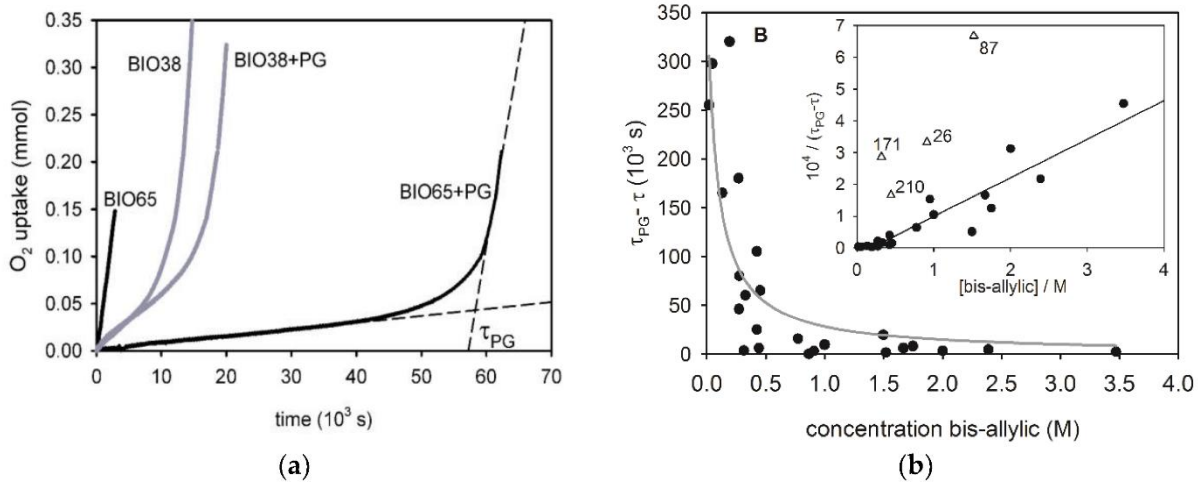

Figure 2.5 *(a) Effect of propyl gallate (PG, 500 ppm) on the oxidation of two different oils; and (b) relationship between the PG effect (τPG-τ) and oil composition. Oils showing no PG effect because of high iron or acidity contents were not included. The inset shows the linear relationship between 1/(τPG-τ) and the concentration of bis-allylic groups, white triangles indicate outliers (see text).*

It can be noted that the slope of O_2 uptake at the end of the induction period (*i.e.*, R_{st}) with or without PG are essentially the same, confirming that, when the concentration of antioxidants expires, the oxidation process of the bulk oil is the same (for instance, R_{st} was 54 and 50 nmol/s for BIO65 and BIO65+PG, respectively). The results collected in *Table 2.1* clearly show that the effect of PG is nearly zero in oils having a high iron content (see, for instance, BIO57 and BIO130 - 132), or high acidity (see BIO145). If

comparing for instance the palm oils samples (BIO19, BIO73, and BIO185), having comparable fatty acid composition, the first two showed a high PG effect (80×10^3 s and 46×10^3 s, respectively), whereas BIO185, having a large acidity and iron content, displayed a relatively small PG effect (6.5×10^3 s). The effect of PG on oil oxidation was then analyzed by various regression methods, excluding those oils having high iron and acidity content, marked in bold in *Table 2.1*. The best fitting, reported in Eq. 2.3, is an inverse dependence on the concentration of bis-allylic groups in the sample (*Figure 2.5b)*, while other parameters such as the peroxide or acidity levels, had no significant role.

$$\tau PG - \tau \;=\; 3.0\,x\,10^4/(0.080 \;+\; [bis-allylic]) \qquad \text{Eq 2.3}$$

This agrees with previous reports showing that the effect of antioxidants is low in oils having a high unsaturation degree.[20] If plotting the same data as $1/(\tau PG - \tau)$ vs. [bis-allylic], a fairly straight relationship (see Eq. 2.4, $r^2 = 0.87$) is found with a few outliers, reasonably due to the interaction of PG with impurities.[21–23] This plot is shown in the inset of *Figure 2.5b* and the outliers are indicated by a triangle.

$$1/(\tau PG - \tau) \;=\; 1.2\,x\,10^{-4}\,x\,[bis-allylic] \;-\; 2.2\,x\,10^{-5} \qquad \text{Eq 2.4}$$

The physical meaning of these relationships is explained in section *2.3.2* based on the kinetic equations describing oil oxidation.

Initial Fast O_2 Consumption (Type C Oils)

In the case of two oils, BIO69 and BIO77, the oil oxidation started with a high rate of O_2 uptake for a short time, which then decreased to reach a constant value. By inspecting the results reported in *Table 2.1*, the final O_2 consumption rate (*i.e.*, R_{st}) for Type C oils were the lowest among all oils. This can be explained by considering that BIO69 and BIO77 are almost completely composed of saturated fats, so that R_{st} is low, while the presence of traces of more oxidizable material is responsible for the initial oxidation burst. The addition of PG caused a slow-down of O_2 consumption in the case of BIO77 (from 17 to 10 nmol/s) with no inhibition period, probably because the low

R_i of this oil renders τPG exceedingly long. In the case of BIO69, PG had no effect presumably because the high iron level found in this oil.

2.3.2 Discussion

These equations provide some useful indications that can help to rationalize the results obtained (*for details see Chapter I*).

$$\textit{Steady state, slope} = -\frac{d[O_2]}{dt} = R_{st} = \frac{k_p}{\sqrt{2k_t}}[RH]\sqrt{R_i} + R_i \qquad \text{Eq 2.6}$$

$$\textit{Inhibition period, slope} = -\frac{d[O_2]}{dt} = R_{inh} = \frac{k_p[RH]R_i}{nk_{inh}[AH]} + R_i \qquad \text{Eq 2.7}$$

$$\textit{Inhibition period, duration } \tau = \frac{n[AH]}{R_i} \qquad \text{Eq 2.8}$$

Equation 2.6 describes the rate of oxygen consumption during the autoxidation of a generic oxidizable substrate RH in the absence of antioxidants (R_{st}), where k_p and k_t are the propagation and termination rate constants, respectively, and R_i is the initiation rate. This equation is valid if O_2 concentration is large enough to transform all carbon-centered radicals (R•) into alkylperoxyl ones (ROO•), so that other reactions of R• can be neglected, and if generation of new radical due to hydroperoxides (ROOH) homolysis can be excluded. This is the case in our experimental conditions. In fact, if ROOH generated radicals, the rate of O_2 consumption would increase with time [8,11], which we did not experimentally observe. We found instead a constant O_2 consumption rate (R_{st}) in absence of antioxidants, indicating that ROOH do not significantly participate in the initiation process, and that the initiation rate (R_i) is approximately constant throughout the experiment. However, some degree of peroxide decomposition during the autoxidation cannot be excluded, because the O_2 consumption depends on the square root of R_i, so small increases in R_i would cause only small changes on Rst. Therefore, peroxide dissociation can be neglected, the rate of initiation R_i does not change during the reaction, and the rate of oil oxidation depends on the concentration

of the oxidizable groups that in turn is related to the facility of oxidation of fatty acids (*i.e.*, on $k_p/\sqrt{2k_t}$). Unfortunately, we have not been able to rationalize the effect of the acidity of the oil, which however can influence kp, kt or both.

In the presence of an antioxidant (AH) the oxygen consumption rate (R_{inh}) at the beginning of the induction period is described by Equation 2.7, where k_{inh} is the rate constant for the reaction of peroxyl radicals with the antioxidant and *n* is the number of radicals trapped by each antioxidant molecule.[8] The duration of the inhibition period (τ) is proportional to the concentration of the antioxidant and inversely proportional to the initiation rate (Equation 2.8). [8,11,24]

The presence of an inhibition period is clear experimental evidence of the presence of a naturally occurring antioxidant in the oil. It finishes when the antioxidant is consumed. The inhibition period is characterized by its duration and by the slope ($-d[O2]_{inh}/dt$) that is associated to the effectiveness of the antioxidant in the inhibition of the O_2 consumption. The slope and duration of oxygen consumption during the inhibition period are described by Equations 2.7 and 2.8. From Equation 2.7, $-d[O2]_{inh}/dt = R_{inh}$ depends on the concentration of the oxidizable groups, the nature of the oil (k_p), the antioxidant (*n* and k_{inh}) and the rate of initiation (R_i).

The duration of the inhibited period (Eq. 2.8) depends not only on the type and concentration of antioxidants present in the oil but also it is inversely proportional to the rate of initiation R_i. For this reason, the addition of a known fixed quantity of a specific antioxidant provides an estimate of the R_i value of the oil, as we did with the addition of propyl gallate (PG). As the *n* value for PG at 130 °C is not known, we could obtain only the R_i/n ratio. Interestingly, when excluding oils with high acidity, iron content, and a few other outliers in which PG exerted little or no inhibiting activity, there is a good inverse correlation between $\tau PG - \tau$ and the concentration of bis-allylic groups in the oils with y-intercept close to zero. Therefore, it can be inferred that R_i is directly proportional to the concentration of bis-allylic groups. This result confirms the hypothesis that the initiation of oil oxidation at 130 °C is mainly due to the direct reaction of activated C-H bonds with O_2.

2.3.3 Materials and Methods

Materials. HPLC grade 1,2-dichlorobenzene and PG (propyl gallate) (>98%) were from Sigma-Aldrich (Milan, Italy) and 1-octanol (99%) was from Alfa Aesar (Erlenbachweg, Germany). They were used as received. Oils were provided by Eni S.p.A. Research Center (San Donato Milanese, Italy) and were stored in a refrigerator in the dark. Peroxide levels were ≤ 23.5 mEq O_2/kg and are reported in the Table 2.1. Sampling of viscous or solid oils was done after stirring at 60 °C for a short time.

Oil Characterization. Average composition was analyzed by NMR. The samples were diluted 30% v/v in deuterated chloroform ($CDCl_3$) and ^1H and ^{13}C NMR spectra recorded on a 500 MHz Varian V500 spectrometer (Varian Inc., Palo Alto, CA, USA) [25]. Iron (and other elemental content) was determined by ICP-OES (ICAP 6500 DV Thermo Scientific, Waltham, MA, USA), following the UOP 389 reference method, consisting of sample preparation by ashing and acidic digestion of ashes. Quantitative determinations were duplicated.

The acid value was measured following ASTM D664, Method B for biodiesel and blends using the automated titrator model Titrando 905 (Metrohm, Herisau, Switzerland) equipped with the pH sensing electrode model Solvotrode easyClean (Metrohm, Herisau, Switzerland) The results are expressed as mg KOH required to neutralize 1.0 g of the biodiesel sample.[26]

Oxidative Stability Index. Oxidative stability indices (OSI) were expressed as induction periods in hours and determined according to the EN15751 standard on a Rancimat apparatus (Metrohm, Herisau, Switzerland).[27,28]

Measure of Oxygen Consumption. Oxygen consumption was measured in a 10 mL round bottom flask surmounted by a short glass condenser, over which the optical oxygen meter and the thermometer were introduced through a silicone rubber septum (see Figure 2.2). Samples consisted of 1 mL of oil dissolved in 7 mL 1,2-dichlorobenzene (boiling point = 180 °C) vigorously stirred by an olive-shaped stir bar and heated to the required temperature by a silicone oil bath. The dilution degree was optimized by preliminary experiments to avoid that O_2 transfer from air to the sample is rate limiting. When approximately 75% O_2 was consumed, the O_2 uptake rate

gradually slows down. To measure the oxygen consumption rate in the fast regime with the maximum accuracy, after the complete consumption of O_2, fresh air was introduced, the apparatus was sealed again, and the acquisition of kinetic data. This procedure was repeated until the maximum O_2 consumption rate was constant. The traces of O_2 consumption measured at the initial part of the reaction (that is, excluding the parts in which the reaction was slowed down by an insufficient O_2 concentration) were joined in a unique plot, and the slope evaluated. The procedure of joining the O_2 consumption plots after discarding the final part introduces uncertainty regarding the duration of the inhibited period only if the data break occurs before the end of the inhibition period (τ). In our experiments, the inhibited period was contained in the first experiment, and thus the subsequent opening–closing did not modify τ length. The O_2 concentration was collected every 10 s, and the readings were recorded by a computer by using the probe manufacturer acquisition software. The measure had a dead time of about 1000 s required for thermal equilibration of the sample and for O2 diffusion inside the condenser. To have selective information on the initiation rate R_i, the kinetics were repeated on the fresh oils added with PG dissolved in 1-octanol to yield a final concentration of 500 ppm. All the oxidation reactions were repeated twice and the errors, defined as the distance between the mean and the experimental values, were below 10%. Multiple linear regression analysis was performed by SigmaPlot software (version 11.0, Systat Software Inc., San Jose, CA, USA).

2.4 Kinetic Analysis of High-Temperature Sunflower Oil Peroxidation Inhibited by the Major Families of Phenolic Antioxidants

Phenols represent the most important class of natural and artificial antioxidants, and therefore it is not surprising that many recent studies are based on the manipulation and optimization of their characteristics. For example, in the emerging field of nano-antioxidants,[29,30] natural phenolic polymers like lignin[31] and melanin-like materials[32,33] are among the most promising radical-trapping platforms. Besides, many natural-based waste products currently investigated as a source of antioxidants are particularly rich in phenols, like for instance, cashew-nutshell liquid,[34] or olive mill wastewater.[35]

Knowledge of the factors that determine the efficacy of phenolic antioxidants is of fundamental importance to guide the research toward significant advancements. While several experimental and theoretical studies performed in the past decades have clarified the chemical-physical basis of the antioxidant activity of phenols,[36,37] the prediction of the efficacy in real systems remains challenging. The behavior of phenols as antioxidants for oils at high temperatures is particularly important because these conditions are found not only in many technological applications such as cooking and oil processing but also in accelerated stability tests such as Rancimat (OSI).[38] Previous studies reported the effect of phenols as stabilizers toward oil (or fatty acids methyl esters, FAME) peroxidation at high temperatures, but rarely they are performed by comparing a significant number of different phenols and, to the best of our knowledge, never report a chemical explanation of the results. For example, Dodos et al. compared the activity of ten phenolic antioxidants in the stability at 110 °C of FAME from soybean oil (rich in linoleic acid) by using Rancimat equipment and found the longest induction period (*IP*) in the case of tert-butyl hydroquinone (TBHQ), while monophenols like BHT and BHA did not show significant effects.[39] R. Becker and A. Knorr, in a study of the oxidation of rapeseed oil at 130 °C, showed that, among several investigated phenols, 2,5-di-tert-butyl-hydroquinone had the best activity in terms of IP.[40] However, the reason for this activity ranking remained unclear.

This section reports the study on the antioxidant activity of 18 phenols, chosen among the main families of natural and synthetic phenols, with the aim of deriving a structure/activity relationship and understanding the mechanism of inhibition of lipid peroxidation. We used method described above consisting of real-time measuring of the O_2 consumption in the headspace of a purified oil sample, vigorously stirred at 130 °C. This approach minimizes the loss of the antioxidant by evaporation and allows determining not only the *IP (or* τ*)* but also the slope of the O_2 consumption during the *IP* ($-d[O2]_{inh}/dt = R_{inh}$). While *IP* is a measure of the lifetime of the antioxidants in the selected environment, R_{inh} correlates with the rate of reaction of the antioxidant with free radicals, *i.e.*, its efficacy in slowing down oxidation. The collected results are analyzed by considering the accepted mechanisms underlying lipid peroxidation. With the help of electron paramagnetic resonance (EPR) spectroscopy, we were able to detect, in specific cases, the presence of stable radicals, affording a plausible explanation of the efficacy order. Our results, besides confirming the previously unexplained high activity of hydroquinones, provide a predictive rationalization based on the behavior of the radicals derived from phenols under peroxidation conditions.

2.4.1 Results

Autoxidation Experiments

Stripped high-linoleic sunflower oil (SSO), in the absence of antioxidants, showed an initial linear O_2 consumption, followed by a decrease in the oxidation rate with the decline of O_2 concentration in the headspace (*Figure 2.6, trace a*). In the presence of the antioxidants, the autoxidation onset of SSO was retarded for a variable period of time (induction period, *IP*), after which the O_2 consumption was faster. The minimum slope of O2 consumption during the inhibited or retarded period (inhibited rate, R_{inh}) and the duration of the inhibition *IP* were taken as indicators of the efficacy of the antioxidants. In *Figure 2.6*, some typical O_2 consumption curves and the derivation of R_{inh} and *IP* are reported.

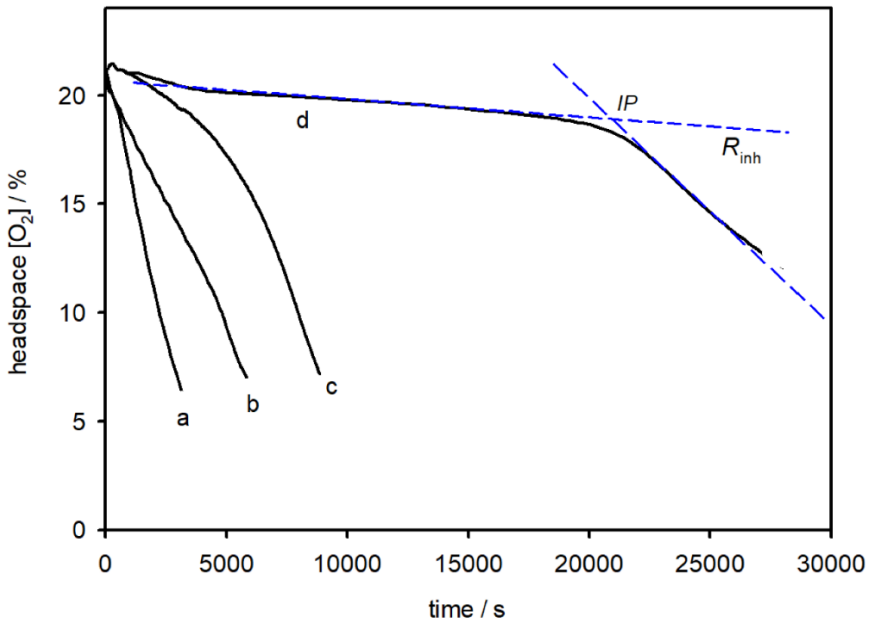

Figure 2.6 *O_2 consumption during the autoxidation of SSO at 130 °C without antioxidants (a) or in the presence of 0.1% (w/w) of α-tocopherol (b), BHT (c) and TBHQ (d).*

By following this procedure, we analyzed several natural and synthetic phenolic antioxidants all at the identical concentration of 0.1% *w/w*, and the results are reported in *Fugure 2.7*. The antioxidants were divided into three families depending on the number of OH groups and their relative position because, as will be evident in the discussion of the results, this feature influences the fate of the radical of the antioxidant and the overall antioxidant efficacy. Monophenols, characterized by the presence of only one phenolic OH group, include α-tocopherol (**7**) and its synthetic analog **8**, two ortho-methoxy phenols (**5** and **6**) having a structural relationship with natural compounds like sinapic acid and eugenol, the well-known antioxidant additives BHT (**3**) and BHA (**2**), and other alkylated or methoxylated phenols used for comparison purposes (**1** and **4**). Hydroquinones are characterized by the presence of two OH groups in para position, and a variable number of alkyl substituents. They include unsubstituted hydroquinone (**9**), tert-butyl hydroquinone (TBHQ, **10**), and 2,5-di-tert-butyl hydroquinone (**11**). The corresponding oxidized para-quinones (**12–14**) were also investigated to ascertain the influence of these compounds on the radical chain, as it was reported that they may act as alkyl (R•)[41] or HOO• radical traps.[42]

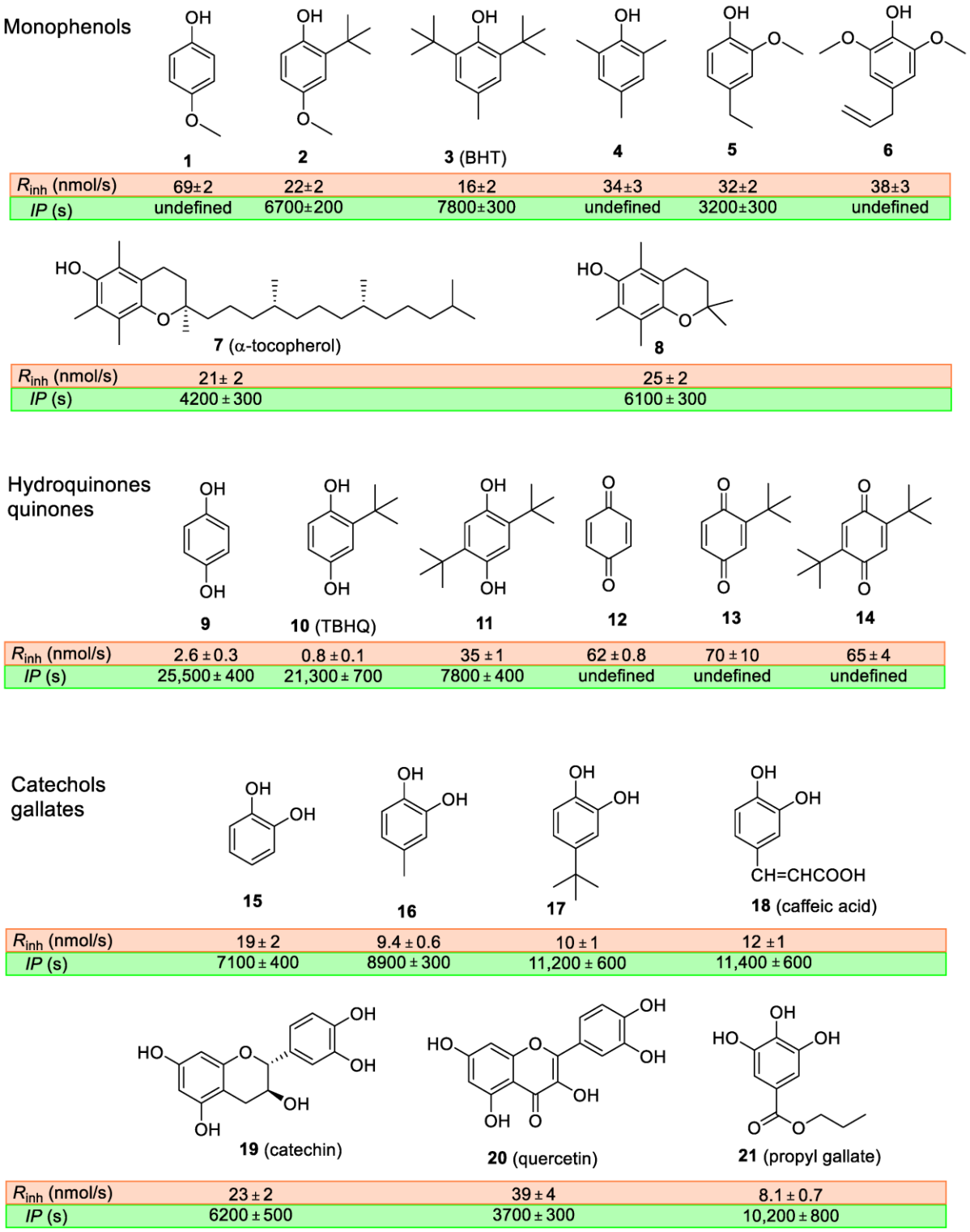

Figure 2.7 *Antioxidant effect of the mono-phenols: oxygen consumption rate in the inhibited period (R_{inh}) and duration of the inhibited period IP. The slope without antioxidants was 70 ± 8 nmol/s. Undefined IP indicates that no induction period is present.*

The last group is represented by catechols, having at least two OH groups in ortho position. They include the natural antioxidants caffeic acid (**18**), catechin (**19**), and quercetin (**20**) as well as unsubstituted catechol (**15**) and the alkylated catechols **16** and **17**, while gallates are represented by the antioxidant additive propyl gallate (**21**). Except for 4-methoxyphenol (**1**) and of benzoquinones **12–14**, all the investigated compounds had some retarding effect on SSO peroxidation. However, the only antioxidants that were able to afford a strong inhibition for a long time were the hydroquinones **9** and **10**. In fact, they were able to reduce 30 and 100 times the slope of O_2 consumption, respectively, while the *IP* was about 2.5 x 10^4 *s*, that is, considerably longer than that of the best non-hydroquinone antioxidants like propyl gallate. If considered on a molar basis, **10** displayed the highest radical trapping stoichiometry, that is the number of radicals trapped by each antioxidant molecule, among all investigated phenols. Because of its exceptional characteristics, the *IP* dependence on the concentration of **10** was investigated in detail, as shown in *Figure 2.8*. The inset in this figure shows that in the concentration range considered, *IP* is linearly dependent on **10** concentrations. In order to test the effect of hydroperoxides on the *IP* of **10**, we studied the effect of **10** (0.02%) in an SSO sample that was previously oxidized without any antioxidant, until reaching a [ROOH] 200 mM, assuming that all consumed O_2 is transformed into ROOH. The results show that the antioxidant effect of **10** almost disappears (compare plot *f* with *b*, *Figure 2.8*), indicating a major effect of peroxide accumulation on *IP*.

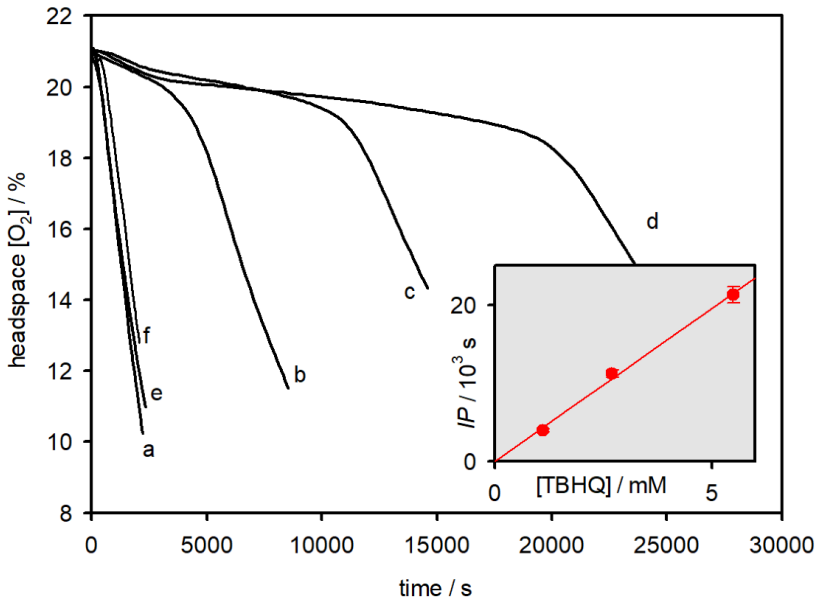

Figure 2.8 *O_2 consumption during the autoxidation of SSO at 130 °C without antioxidants (a) or in the presence of 10: 0.02% (b), 0.05% (c) and 0.1% (d), or 13, 0.1% (e). O_2 consumption of peroxidized SSO in the presence of 10, 0.02% (f). The inset reports the relationship between the 10 concentrations and IP. Some error bars are smaller than the symbol size.*

EPR Experiments

To investigate the relationship between the stability of the radicals and the antioxidant activities of the investigated phenols, we measured the electron paramagnetic resonance (EPR) spectra of **2, 3, 4**, and **10** at 0.1% in SSO under air. Aerated oil samples containing the antioxidants were introduced in the EPR cavity and heated at 40 °C. This temperature was chosen as the best compromise to optimize the signal-to-noise ratio. In the case of α-tocopherol (**7**) and BHT (**3**), the signal arising from their phenoxyl radicals could be clearly detected (*see Figure 2.9a, b*), while in the case of **2** the signal was weak, and in the case of **10** only traces of the radical could be evidenced. The identity of the radicals was ascertained by analyzing the experimental spectra by numerical simulation as shown by the red lines in *Figure 2.9*. This procedure afforded coupling constants (*a*) and *g-factors* that were in good agreement with those reported in the literature for the respective phenoxyl radicals.[43–46] The radical

concentrations (see Figure 2.9) were in the nanomolar range and, considering the experimental error, the radical stability decreased in the order: **3**~**7** > **2** >> **10**.

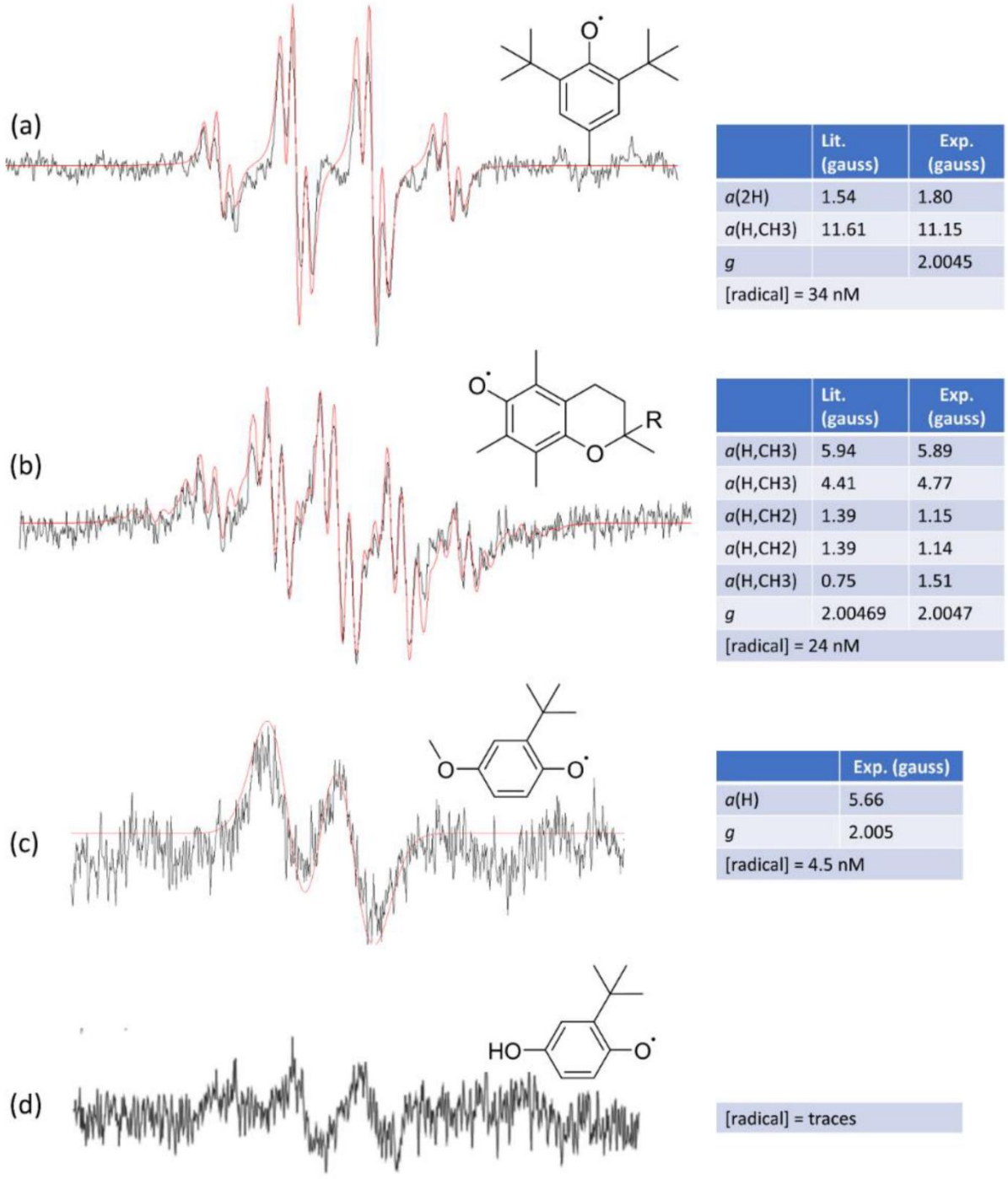

	Lit. (gauss)	Exp. (gauss)
a(2H)	1.54	1.80
a(H,CH3)	11.61	11.15
g		2.0045
[radical] = 34 nM		

	Lit. (gauss)	Exp. (gauss)
a(H,CH3)	5.94	5.89
a(H,CH3)	4.41	4.77
a(H,CH2)	1.39	1.15
a(H,CH2)	1.39	1.14
a(H,CH3)	0.75	1.51
g	2.00469	2.0047
[radical] = 24 nM		

	Exp. (gauss)
a(H)	5.66
g	2.005
[radical] = 4.5 nM	

[radical] = traces

Figure 2.9 *Experimental and simulated (red lines) EPR spectra of SSO after the addition of 0.1% at 40 °C of* ***3*** *(a),* ***7*** *(b),* ***2*** *(c),* ***10*** *(d). The coupling constants (a), the g-factor, and the radical concentrations (estimated error ± 50%) are also reported.*

Stability of Antioxidants

The stability at 130 °C was investigated to understand the role of phenol degradation on the duration of the inhibited period. Selected antioxidants (see Figure 2.10) were dissolved in triacetin, an oxidation-resistant triacylglycerol having no unsaturations, and were placed in the same reactor used in the peroxidation experiments. Then, their concentration was measured by HPLC-DAD analysis at time intervals for 6 h. The hydroquinones **9–11** were considered in order to clarify the excellent antioxidant behavior of 9 and 10 in SSO autoxidation experiments, as opposed to the relatively small efficacy of the dialkylated analog **11**. The monophenol **2** and propyl gallate (**21**) were included for comparison purposes, while **8** was selected to investigate the behavior of α-tocopherol.

We found that in all cases the concentration remained approximately constant, except for the dialkylated hydroquinone **11** and the α-tocopherol analog **8**, whose concentrations, however, decreased only by 20% and 15%, respectively, after 6 h (21.6 × 10^3 *s*). If considering that in the SSO autoxidation experiments their *IP* was 7.7 × 10^3 s and 6.6 × 10^3 *s*, respectively, even in the case of the least stable phenols **8** and **11**, thermal degradation plays a negligible role in the duration of the inhibition. In addition, these experiments also demonstrated that the antioxidant loss by evaporation was negligible even in the case of the low molecular weight phenols **2** and **8**.

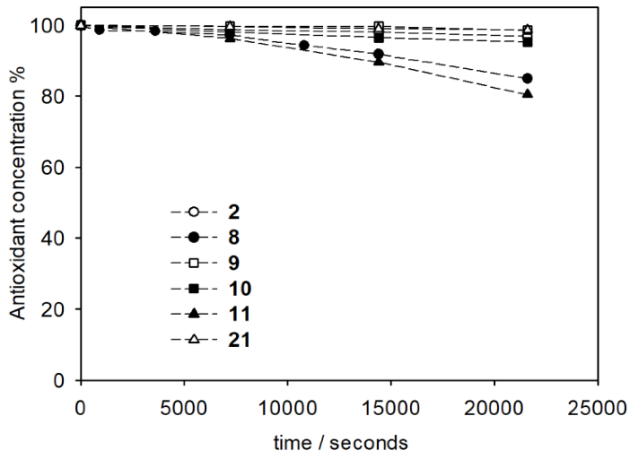

Figure 2.10 *Stability at 130 °C of selected phenols in triacetin under air. Error bars are smaller than the symbol size.*

2.4.2 Discussion

The results collected herein show, in a comprehensive manner, the effect of the major families of phenolic antioxidants on the oxidation of high-linoleic sunflower oil at 130 °C. Despite their structural similarity, phenolic antioxidants display highly variable inhibition capability, as expressed by the reduction of the R_{inh} rate and by the duration of the inhibited period *IP*. Hydroquinones **9** and **10** display the highest inhibition, while other phenols having a very similar structure, such as their methylated analogs **1** and **2**, are much less active. In the case of **10**, which is one of the best antioxidants analyzed here, the *IP* increases linearly with **10** concentrations (inset *Figure 2.8*) suggesting that R_i is constant throughout the duration of the inhibited period of all three experiments shown in *Figure 2.8*, otherwise reduction in the *IP* should have been observed, caused by the increase of hydroperoxides. On the other hand, when **10** is used as an inhibitor of an SSO sample already containing a high level of hydroperoxides, no antioxidant effect is observed, suggesting a major role of ROOH in increasing R_i.

In the case where R_i would be only due to the bulk oil's original composition (*i.e.*, mainly the bis-allylic hydrogen concentration) in all samples, *IP* would be approximately the same throughout the investigated phenols. However, it turned out not to be so: *IP* varied significantly depending on the antioxidant (see values in *Figure 2.7*): antioxidants causing a small reduction of O_2 consumption rate (*i.e.*, those having high R_{inh}) were also characterized by low *IP*. To explain this effect, we hypothesized that in the case of weak antioxidants also, hydroperoxides may contribute to R_i, increasing its value compared to the pristine bulk phase. The O_2 consumed during the inhibited period of weak antioxidants is converted into hydroperoxides, that in turn increase R_i, causing a shortening of *IP*.

$$ROO^{\bullet} + AH \xrightarrow{k_{inh}} ROOH + A^{\bullet} \qquad \text{Eq 2.9}$$

$$ROO^{\bullet} + A^{\bullet} \rightarrow ROOA \qquad \text{Eq 2.10}$$

$$A^{\bullet} + A^{\bullet} \rightarrow AA \qquad \text{eq 2.11}$$

$$A^{\bullet} + RH \rightarrow AH + R^{\bullet} \qquad \text{eq 2.12}$$

Reactions 2.9-2.11 account for the action of phenolic radical-trapping antioxidants, consisting in H-atom donation to the chain-carrying peroxyl radicals ROO•, with a kinetic rate constant k_{inh}, followed by the decay of A• with another radical (reactions 2.10 and 2.11).[28,37] In addition, it must also be considered that, if the decay of the A• radical is not efficient, it can react with the substrate, propagating the oxidative chain via reaction 2.12. This reaction, although regenerating an active antioxidant molecule AH, has, however, the undesired effect of opposing reaction 2.9, thus contributing to the formation of hydroperoxides and increasing R_i.

Overall, this reaction scheme shows that good antioxidants must have a high k_{inh}, value (reaction 2.9) and must decay efficiently to avoid the onset of reaction 2.12.

It is well known that, in order to have high k_{inh}, values, phenols must possess electron-donating (ED) substituents in ortho and para positions with respect to the reactive OH group ED substituents decrease the bond dissociation enthalpy (BDE) of the OH group and thus more easily render the H-atom abstraction by ROO• radicals. The substituent effect is proportional to the ED power of the substituents (OMe = OH > Me = tBu > H) (*Scheme 2.2*) and is modulated by the bulkiness of the substituents and by the presence of intramolecular H-bonds.[47] For example, ortho-methoxy phenols have a low reactivity toward ROO• because the OH group is engaged in a strong H-bond with the OMe substituent. Accordingly, phenols having only one ED substituent (like **1**) or ortho-methoxy substituents (like **5** and **6**), were poor inhibitors of SSO autoxidation.
However, these rules seem not to apply in every case. For instance, **2** and **10** which have the same number of substituents with the same ED ability, show instead quite different antioxidant effects, both in terms of R_{inh} and of *IP*. In addition, α-tocopherol (**7**) and its analog **8** which have the lowest BDE(OH) among the investigated phenols[47] are not the most active ones.

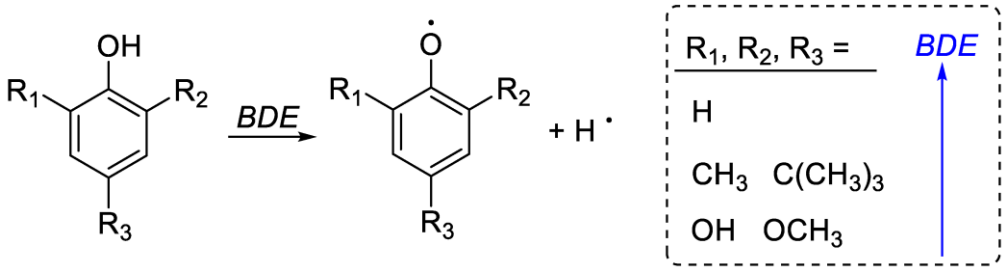

***Scheme 2.2**. Substituent effect on the O-H bond dissociation enthalpy (BDE) of phenols*.

As stability experiments showed that the spontaneous decay of the antioxidants at 130 °C is negligible (*see Figure 2.10*), these differences must be explained by considering the interplay between reactions *2.9-2.12*. EPR experiments were performed to investigate this stability. They showed that the stability of the radicals of the antioxidants increases with the number and bulkiness of the substituents in ortho and para positions to the phenolic OH in the order **3**~**7** > **2**, while the stability of the radical from **10** is extremely low. This result can be explained by the tendency of phenoxyl radicals to decay mainly by radical-radical addition by using the ortho and para positions, as shown in *Scheme 2.3A*.[48] If these positions contain alkyl or methoxy substituents, the decay is slow and possibly reversible. On the other hand, the 4-hydroxylphenoxyl radical formed by **10** (*see Scheme 2.3B*) is very unstable because it decays by H-atom transfer with another radical forming the para-benzoquinone **13** and is therefore unable to propagate the oxidation via reaction 2.12. Interestingly, **13** is the main product that is formed in oxidized soybean oil stabilized by **10**.[49] The instability ranking experimentally observed by EPR follows the antioxidant ranking, proving that persistent radicals can behave detrimentally, because of their contribution to the chain propagation mechanism.

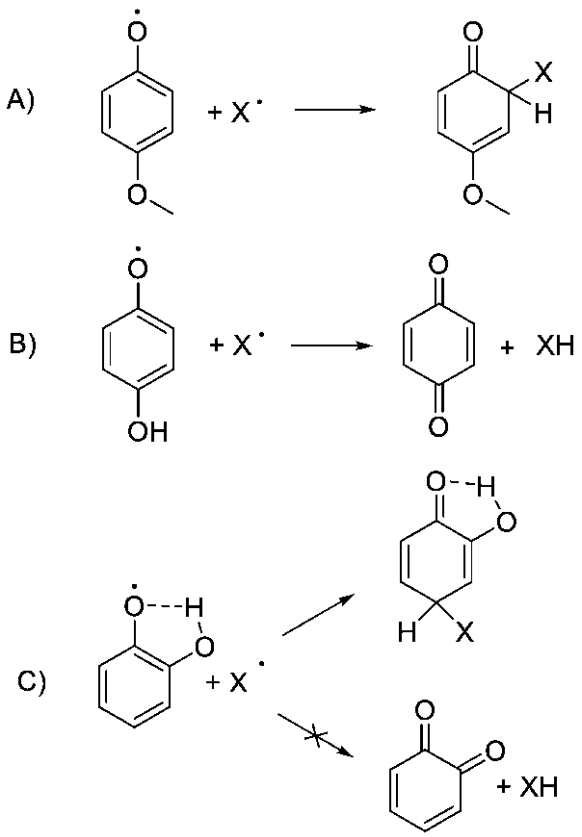

Scheme 2.3 *Decay pathways of the phenoxyl radicals formed by monophenols (A), para-hydroquinones (B), and catechols (C) upon reaction with a generic radical X•.*

In this context, the disappointing behavior of catechol and gallates was unexpected, because also in their case, the phenoxyl radical may potentially decay by forming an ortho-quinone. However, the present results suggest that the OH groups in the phenoxyl radicals from catechols and gallates are not easily transferred to another radical, likely because they are involved in a strong intramolecular H-bond with the -O• group (see *Scheme 2.3C*).[50]

In agreement with this view of reasoning, the plot of *IP* versus R_{inh}, both divided by the molar concentration of the antioxidants to take into account their different molecular weights, shows the presence of a general trend consisting of an inverse relation between *IP* and R_{inh} (*see Figure 2.11*), although the rather scattered data points suggest that other factors contribute to the *IP* vs. R_{inh} relationship.

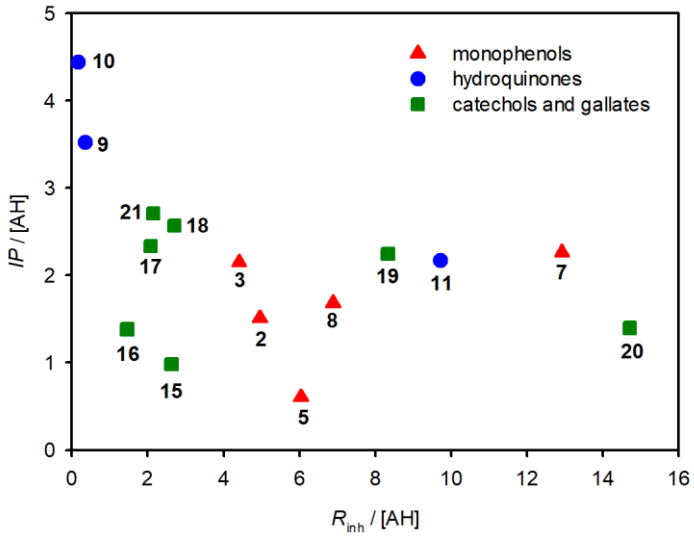

Figure 2.11 *Relation between Rinh and IP divided by the molar antioxidant concentration (in arbitrary units). Antioxidants with undefined IP were omitted.*

It should also be pointed out that the phenomenon of chain propagation by the phenoxyl radicals of the antioxidants A• is not observed at low temperatures when the autoxidation of SSO is accelerated by the decomposition of azo-initiators, probably because the high flux of ROO• radicals ensures an efficient decay of A• for all antioxidants, while the low temperature slows down reaction 2.12.[10] On the other hand, the low *IP* of α-tocopherol compared to γ-tocopherol in soybean and sunflower oils at 100 °C has been in part attributed to reaction 2.12.[51] Moreover, the chain propagation by the α-tocopheroxyl radicals is responsible for the tocopherol-mediated peroxidation in low-density lipoproteins.[52] The low efficacy of the dialkylated hydroquinone **11** is instead to be ascribed to the tendency of the electron-rich semiquinones to react with O_2 forming para-benzoquinones and HOO•, which propagates the oxidative chain (*Scheme 2.4*).[53]

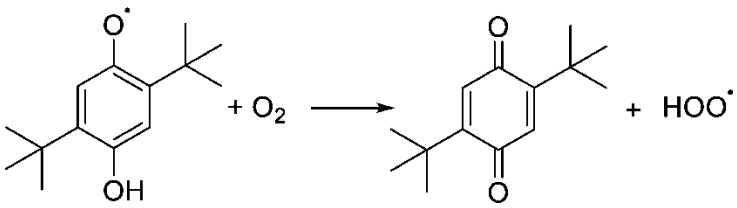

Scheme 2.4 *Chain propagation of dialkylated semiquinone radicals.*

2.4.3 Materials and Methods

Materials. All chemicals and solvents were commercially available (Merk, Sigma-Aldrich, Milan, Italy). Para-methoxyphenol (1), 2-tert-butyl-4-methoxyphenol (2), 2,6-di-tert-butyl- 4-methylphenol (BHT) (3), 2,4,6-trimethylphenol (4), 2-methoxy-4-ethylphenol (5), 2,6-dimethoxy-4-allylphenol (6), (±)-α-Tocopherol (7), 2,2,5,7,8-pentamethyl-6-chromanol (8), para-hydroquinone (9), tert-butylhydroquinone (10), 2,5-di-tert-butylhydroquinone (11), para-benzoquinone (12), tert-butylbenzoquinone (13), 2,5-di-tert-butylbenzoquinone (14), catechol (15), 4-methylcatechol (16), 4-tert-butylcatechol (17), caffeic acid (18), catechin (19), quercetin (20), propyl gallate (21), triacetin were of the highest available purity and were used as received. Antioxidant concentrations are *% w/w*. Solvents were HPLC-grade and were used without further purification. High-linoleic sunflower oil was purchased from a local market. Stripped sunflower oil (SSO) was prepared as previously reported by percolation on basic alumina and by treatment with activated carbon.[54] The SSO composition was determined by 1H-NMR[55]: polyunsaturated chains 59.4 mol %, monounsaturated chains 27.3 mol %, saturated chains 13.3 mol %.

Autoxidation Experiments. Oxygen consumption during the sunflower oil autoxidation was measured by an O_2-sensitive optical probe (Pyroscience GmbH, Aachen, Germany) in a sealed apparatus previously described.[56] Briefly, 2.00 g of oil containing variable amounts of the antioxidants is introduced into a 10 mL round-bottomed flask with a magnetic stir bar connected to a miniaturized water-cooled condenser to keep the temperature of the O_2-sensitive probe below 40 °C (total internal volume 29 mL). The sample is kept under vigorous stirring in a silicone bath at 130 °C. The O_2 probe is calibrated in air before each experiment. The amount of consumed O_2 is calculated from the internal volume of the apparatus. The experiments with peroxidized SSO were performed by oxidizing SSO at 130 °C measuring O_2 uptake. Then the sample was aerated, and a small volume of a concentrated octanol solution of 10 was added.

Analysis of Antioxidant Stability. The experiments were performed under the same conditions as the autoxidation experiments, except for the use of triacetin, which is

resistant to oxidation at 130 °C, in place of SSO. The concentrations of the antioxidants were determined by HPLC separation coupled to a photodiode array (DAD) UV-vis detection and the flow was set to 0.9 mL/min. The column was a Sepachrom C18, 5 µm, 250 mm 4.1 mm. The mobile phase was an isocratic mixture of MeCN/H_2O 60:40 for **9**, **10** and **11**; MeCN/H2O 90:10 for **2**; MeCN/H2O + 3% formic acid 50:50 for **21**; MeCN/MeOH 90:10 for **8**.

EPR Analysis. The determination of the concentration of the radicals of **2**, **3**, **7**, and **10** was performed by an X-band electron paramagnetic resonance (EPR) spectrometer (Elexsys 500, Bruker, Billerica, MA, USA) equipped with a variable temperature dewar placed in the resonant cavity. Suprasil quartz EPR tubes were filled with the pure oil samples (no dilution) up to 4 cm and thermostatted at 40 °C by nitrogen gas flowing in the dewar. The small quantity of oil ensured a homogeneous temperature inside the analyzed sample. Typical instrumental settings were: microwave power = 10 mW, amplitude = 2 G, 64 accumulations. The radical concentration was obtained from the double integration of the EPR signal multiplied by the inverse temperature in Kelvin degrees to correct for the Curie temperature dependence and calibrated with the signal of the strong-pitch standard from Bruker. The spectra were simulated with the software Winsim,[57] freely available from the Public Electron paramagnetic resonance Software Tools (PEST) from NIEHS (National Institute of Environmental Health Sciences). The radicals were identified as the phenoxyl radicals of the investigated antioxidants from the agreement of their spectral parameters (hyperfine coupling constants, *a*, and *g-factors*) with those reported in the literature[58,59] or with those expected from their structure.[60]

2.5 Synergic Antioxidant Effects of the Essential Oil Component γ-Terpinene on High-Temperature Oil Oxidation

In recent years, many research efforts have been directed toward essential oils as a natural alternative to synthetic antioxidants.[61] Essential oils are complex mixtures of volatile compounds obtained mainly by steam-distillation from aromatic and medicinal plants. The antioxidant activity of essential oils rich in phenolic components, such as those extracted from thyme, oregano, and clove, has been explained on the basis of the chemical similarity with phenolic antioxidants.[61] However, other essential oils containing non-phenolic components like limonene, linalool, and citral also behave as antioxidants under specific conditions, because they can interfere with autoxidation radical chain by enhancing the decay of peroxyl radicals.[62] γ-Terpinene, a nonphenolic monoterpene found in several essential oils like citrus, savory, oregano, and others,[63] has been shown to reduce the peroxidation of methyl linoleate and egg yolk phospholipids[64,65] and the peroxidation of low-density lipoproteins.[66] In our ongoing studies toward improved antioxidant strategies, we observed that γ-terpinene had also the ability to prolong the antioxidant activity of α-tocopherol and of caffeic acid in the autoxidation of lipids in homogeneous solution, whereas it had a weak effect on autoxidation rate when used alone.[17,63] Instead of forming an alkylperoxyl radical like most unsaturated hydrocarbons, γ-terpinene generates an hydroperoxyl radical (HOO•)[67] that is able to donate a H-atom to the radical of the antioxidant, reducing it back to the parent phenol (*see Scheme 2.5, reactions A and B*).[63] This peculiar property comes from the pro-aromatic character γ-terpinene, as the release of HOO• by a 1,4-intramolecular H-atom transfer allows its aromatization to para-cymene, another well-documented component of essential oils (*Scheme 2.5A*).[67] While these mechanistic studies enlightened the possibility of an antioxidant synergy between γ-terpinene and phenolic antioxidants, the effectiveness of this process during high temperature oxidation of bulk unsaturated triacylglycerols has not been demonstrated yet.

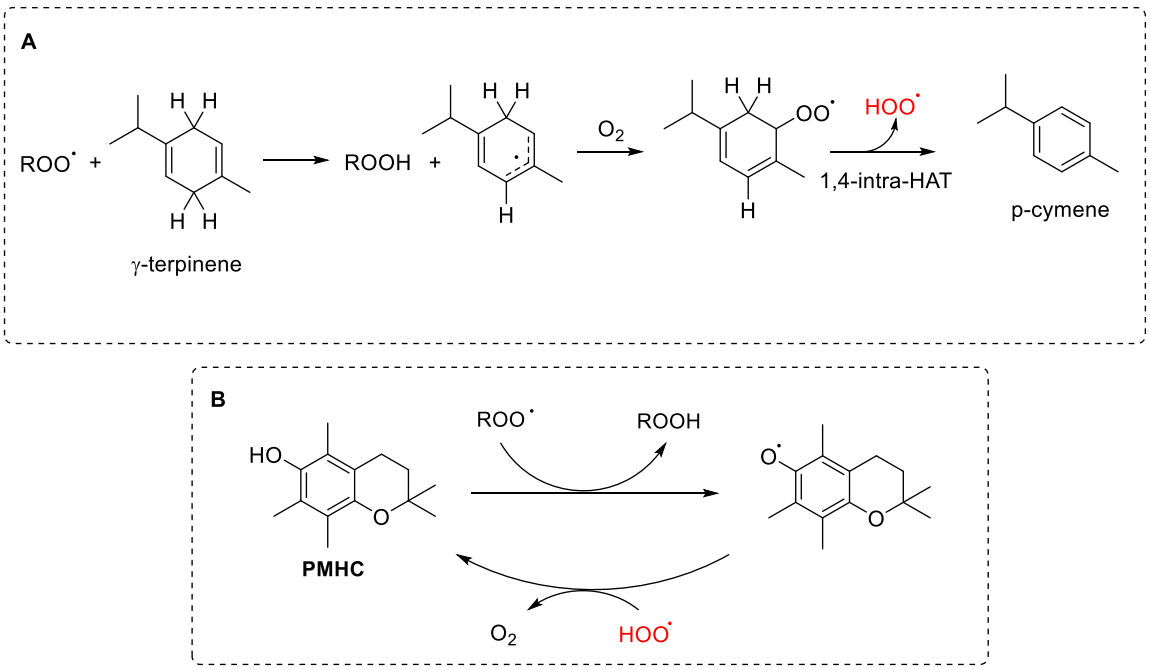

Scheme 2.5 *(A) Oxidation Mechanism of γ-Terpinene. (B) Mechanism of Regeneration of a α-Tocopherol Analogue by HOO• Radicals*

With respect the model system previously investigated, bulk oils are characterized by a high concentration of H-bond accepting groups (the ester links in triglycerides) that are expected to hamper the H-atom transfer from HOO• to the radical of the antioxidant.[17] Moreover, the high temperature may reduce the stability of γ-terpinene, leading to its disappearance before it can display the co-antioxidant activity. Herein, we report the results of our efforts aimed at evaluating the extent of the antioxidant synergy between γ-terpinene and various phenols during the oxidation of sunflower oil at 130 °C. Sunflower oil was chosen because of its widespread use as a food commodity and because, with its high linoleate levels, it is a challenging oxidizable substrate whose oxidation can be reduced only by very active antioxidants.[10] The investigated antioxidants were represented by α-tocopherol, which is naturally present at different levels in most vegetable oils,[68] and by some synthetic phenols used as food additives (TBHQ and BHT) or as a model for natural polyphenols (catechol).[68] To investigate the synergy mechanism, we used also two dialkylnitroxides stable radicals (HO-TEMPO

and AcNH-TEMPO), because it has been demonstrated that these compounds behave as antioxidants when the HOO• radical is present in the system (Scheme 2.6).[69]

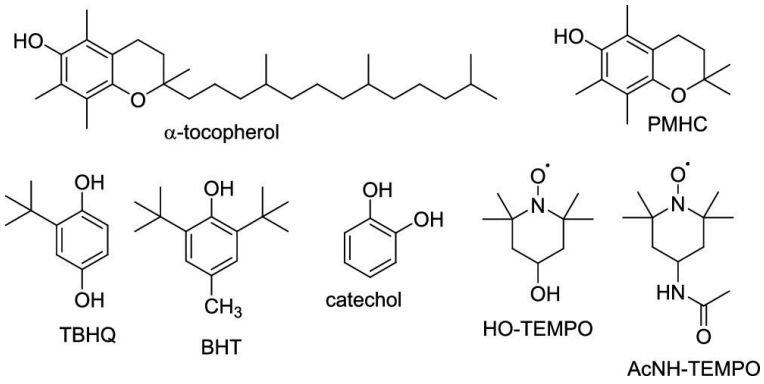

Scheme 2.6 *Investigated Antioxidants*

2.5.1 Results

Synergic Effect of α-Tocopherol and γ-Terpinene on the Oxidation of Sunflower Oil

The effect of γ- terpinene 1% (w/w) on the oxidation of purified (stripped) sunflower oil (SSO) in the presence and in the absence of α-tocopherol is reported in *Figure 2.12A*. The plots can be analyzed quantitatively by measuring various parameters describing oil oxidation: the inhibited (R_{inh}) and non-inhibited (R_{ox}) O_2 consumption rates (in nmol/s) and the length of the induction periods (τ, in seconds) (*see Figure 2.12A*), as reported in *Table 2.2* (entries 3-6). The O_2 consumption during SSO oxidation is linear because the endogenous antioxidants have been removed. When γ-terpinene is added in the absence of α-tocopherol (line b), there is no change in O_2 consumption rate, while the addition of α-tocopherol causes the onset of an inhibited period (line c). Interestingly, when α-tocopherol and γ-terpinene are present together in the sample, an inhibition period is observed (line d) that is longer than that shown by α-tocopherol alone.

Experiments performed at different γ-terpinene concentrations showed a linear dependence between the induction period length (τ) and the concentration of γ-terpinene (*Figure 2.12B*, $R^2 = 0.974$). To confirm these results, we studied the sunflower

oil oxidation by measuring the formation of hydroperoxides. The results, reported in *Figure 2.12C*, showed that freshly prepared SSO is virtually free of hydroperoxides, while after 10000 s at 130 °C (*i.e.*, 2.8 h) their level increases considerably. The addition of α-tocopherol reduces the hydroperoxides formation, and the addition of both α-tocopherol and γ-terpinene decreases ROOH concentration even further, in good agreement with O_2 uptake measures.

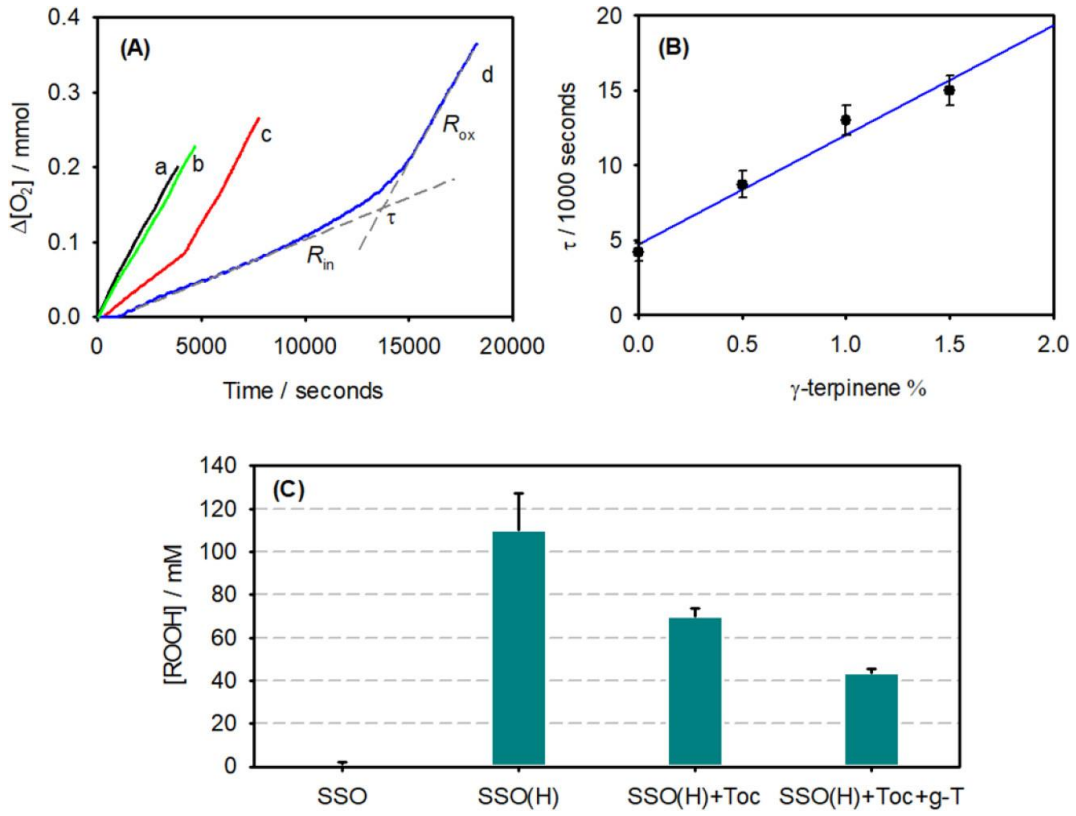

Figure 2.12 *A) Oxygen consumption during the oxidation of stripped sunflower oil (SSO, 2 g) at 130 °C; without any additive (a), with γ-terpinene (1% w/w) (b); with α-tocopherol (0.1%, w/w) (c); with α-tocopherol (0.1%) and γ-terpinene (1%, w/w) (d). B) duration of the induction period of α-tocopherol 0.1% on increasing γ-terpinene concentration. C) concentration of hydroperoxides in stripped sunflower oil before (SSO) and after heating at 130 °C for 10.000 s without antioxidants (SSO(H)), with α-tocopherol 0.1%, w/w (SSO(H)+Toc), and with α-tocopherol 0.1%, w/w and γ-terpinene 1%, w/w (SSO(H)+Toc+g-T).*

***Table 2.2**. Descriptors of Sunflower Oil[a] Autoxidation at 130 °C: Slope of O_2 Consumption during the Inhibited Period (R_{inh}) or in the Absence of the Antioxidant (Rox)[b] and Duration of the Inhibited Period (τ)[c]*

Entry		R_{inh} (nm/s)	R_{ox} (nm/s)	τ (1000 s)
1	SO	17±3	56±5	6.6±0.2
2	SO + g-terpinene 1%	9.3±0.3	67±6	11±1
3	SSO		61±5	
4	SSO + g-terpinene 1%		48±6	
5	SSO + a-tocopherol 0.1%	21±1	54±5	4.2±0.2
6	SSO + a-tocopherol 0.1% + g-terpinene 1%	13±1	48±5	13.2±0.6
7	SSO + PMHC 0.1%	26±3	50±5	6.1±0.5
8	SSO + PMHC 0.1% + g-terpinene 1%	11±1	51±5	10.5±0.5
9	SSO + TBHQ 0.1%	14±1	66±6	28±2
10	SSO + TBHQ 0.1%+ g-terpinene 1%	55±5	60±6	31±2
11	SSO + BHT 0.1%	16±2	49±5	7.1±0.5
12	SSO + BHT 0.1%+ g-terpinene 1%	31±2	48±4	5.1±0.4
13	SSO+ catechol 0.1%	23±2	66±6	7.5±0.6
14	SSO+ catechol 0.1%+ g-terpinene 1%	27±3	45±5	6.2±0.5
15	SSO + HO-TEMPO 0.1%	36±3	60±5	3.7±0.4
16	SSO + HO-TEMPO 0.1%+ g-terpinene 1%	11±1	32±3	15±2
17	SSO + AcNH-TEMPO 0.1%	26 ± 3	45 ± 4	8 ± 1
18	SSO + AcNH-TEMPO 0.1% + γ-terpinene 1%	14 ± 2	21 ± 2	10 ± 1

[a]SO = unpurified sunflower oil, containing intrinsic antioxidants, SSO = stripped sunflower oil.

[b]Slope of O_2 consumption without any antioxidant or after the complete consumption of the antioxidant.

[c]All concentrations are w/w.

Effect of γ-Terpinene on the Oxidation of Not-Purified Sunflower Oil

As can be seen from Figure 2.13A and Table 2.2 (entries 1 and 2), the O_2 consumption at 130 °C of not purified sunflower oil (SO) shows an inhibited period at the beginning of the reaction of about 2 h, which is due to the antioxidants (mainly represented by α-tocopherol) naturally present in the oil.[70] The concentration of the tocopherols in the oil was determined as 490 ± 20 ppm (w/w). When adding γ-terpinene (1%, w/w), the duration of the inhibited period increases to 3.4 h, thus confirming the result obtained with SSO. We also studied SO oxidation by measuring the formation of hydroperoxides. We can see in *Figure 2.13B* that SO, before being heated, has a small amount of hydroperoxides (first bar). The second bar shows that, after heating at 130 °C for 10000 *s*, a significant quantity of hydroperoxides is formed, which decreases if the reaction is performed with the addition of γ-terpinene (third bar). Overall, the results reported in *Figure 2.13B* confirmed the results of the oxygen consumption kinetics.

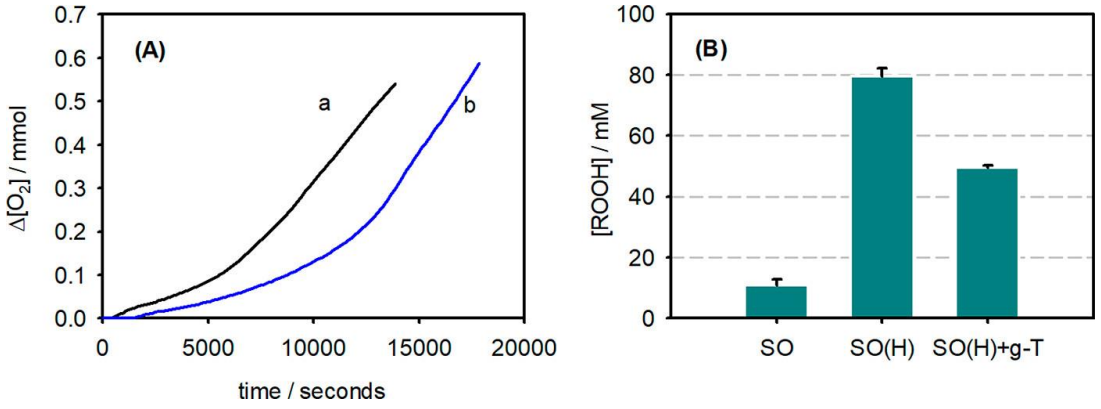

Figure 2.13 *A) oxygen consumption during the oxidation of not-purified sunflower oil (SO, 2 g) at 130 °C; (a) without and (b) with the addition of γ-terpinene (1%, w/w). B) concentration of peroxides in non-purified sunflower oil before (SO) and after heating at 130 °C for 10.000 s without (SO(H)) and with 1% γ-terpinene (SO(H)+g-T)*

Synergy with Phenolic Antioxidants and Mechanistic Studies

The synergic activity of γ-terpinene was also investigated with some commercial phenols. For this purpose, we measured the O_2 consumption profile of SSO oxidation after the addition of 0.1% (*w/w*) of tert-butylhydroquinone (TBHQ), 2,2,5,7,8-

pentamethyl-6-hydroxychromane (PMHC, a structural analogue of α-tocopherol missing the phythyl chain), butylated hydroxytoluene (BHT) and catechol (*see Scheme 2.6*), in the absence and in the presence of γ-terpinene. To demonstrate the formation of HOO• from γ-terpinene, we used also the two nitroxides HO-TEMPO and AcNH-TEMPO, because TEMPO-derived stable radicals behave as antioxidants when the HOO• radical is present in the system.[69] The measured R_{inh} and τ values, reported in *Table 2.2*, show that γ-terpinene increases the antioxidant activity only of PMHC, while in the case of the other phenols, it causes a faster oxidation (R_{inh} increase) and a shorter duration (τ decrease), as shown for BHT in *Figure 2.14A*. However, the nitroxides HO-TEMPO and AcNH-TEMPO that were nearly ineffective when used alone, displayed a large activity improvement after the addition of γ-terpinene (*Figure 2.14B*).

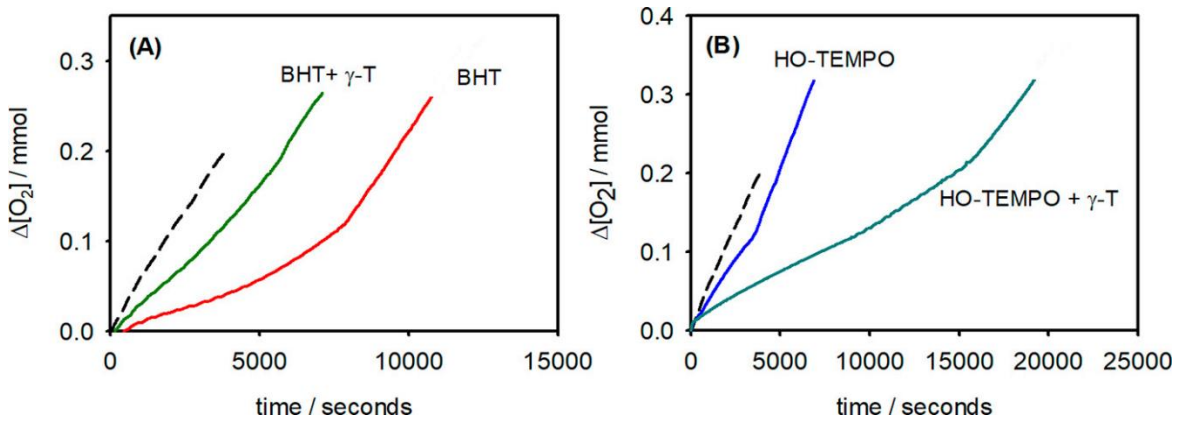

Figure 2.14. Oxygen consumption during the oxidation of stripped sunflower oil (SSO, 2 g) at 130 °C; without any additive (dashed line) or in the presence of an antioxidant, without or with γ-terpinene (γ-T) 1% w/w. A) butylated hydroxy toluene (BHT) 0.1%, w/w; B) 4-hydroxy TEMPO (HO-TEMPO) 0.1%, w/w.

2.5.2 Discussion

As can be inferred by comparing entries 3 and 4 in *Table 2.2*, γ-terpinene alone possesses no ability to reduce the O_2 consumption rate, as previously observed at 30 °C.[63] This agrees with the fact that γ-terpinene is an easily oxidizable hydrocarbon that participates in the oxidative chain. The HOO• radicals, that are produced during γ-terpinene oxidation, abstract a H-atom from allylic and bis-allylic positions of fatty

acids and of other terpene molecules, thus contributing to the propagation of the autoxidation. The nitroxides HO-TEMPO and AcNH-TEMPO have a negligible effect when used alone (see entries 15 and 17 in *Table 2.2*) but become good antioxidants in the presence of γ-terpinene (entries 16 and 18). We and others have previously revealed that TEMPO derivatives are potent but elusive inhibitors of lipid peroxidation. In bulk organic materials, nitroxides are unable to stop lipid peroxidation because they cannot donate a H-atom to propagating ROO• radicals. However, in the presence of acid traces, TEMPO derivatives become antioxidants, because they react with ROO• by a proton-coupled electron transfer mechanism (Scheme 2.7).[24,71] The antioxidant activity of nitroxides is also observed in the presence of HOO• radicals, as they form very efficiently an alkoxyamine (R_2NOH) that is capable of reacting with ROO•.[69] Therefore, these results represent a proof that HOO• radicals are actually produced in the investigated system.

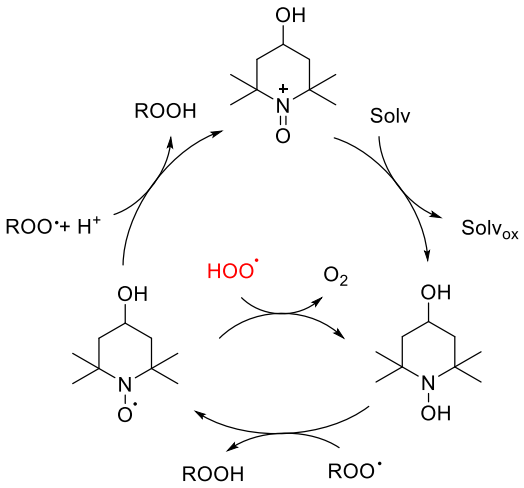

Scheme 2.7 *Antioxidant effect of TEMPO derivatives under different conditions*

As evident from *Table 2.2*, the synergy is observed only with a limited number of antioxidants, which are α-tocopherol and its synthetic derivative PMHC (entries 6 and 8), while it is absent for TBHQ, BHT, and catechol. These results can be compared to those obtained in a model system consisting of chlorobenzene solutions of oxidizable substrates whose oxidation was initiated by the decomposition of an azo-initiator at 30

°C. Under those conditions, α-tocopherol, PMHC, and the catechol derivative caffeic acid phenethyl ester were capable of act synergistically with γ-terpinene.[63]

A reasonable explanation that can unify all these observations is that the reaction of the radical of the antioxidant with HOO• is not fast enough, at 130 °C, to compete with other reaction pathways, that ultimately lead to the irreversible deactivation of the antioxidant.[8] In the case of TBHQ and catechol, their phenoxyl radicals decay quickly to the respective para and ortho benzoquinones by H-atom transfer to a second ROO•, as shown in *Scheme 2.8A* for TBHQ. In the case of BHT, the rate constant of regeneration may be reduced by the steric crowding due to the two tert-butyl groups (*Scheme 2.8B*). The reason why γ-terpinene causes a decrease of the antioxidant activity of TBHQ and BHT is at the moment unclear and deserves further investigation. A tentative explanation could be an H-atom transfer between the radical of the antioxidant and γ-terpinene.[8] Compared with the other inhibitors, α-tocopherol and PMHC form rather stable and relatively unhindered phenoxyl radicals that do not decay quickly by reacting with ROO• and thus live enough to be regenerated by HOO• as shown in *Scheme 2.5B.* Interestingly, α-tocopherol is the main endogenous antioxidant present in sunflower oil thus, γ-terpinene alone is able to extend the induction time of this oil (entries 1 and 2).

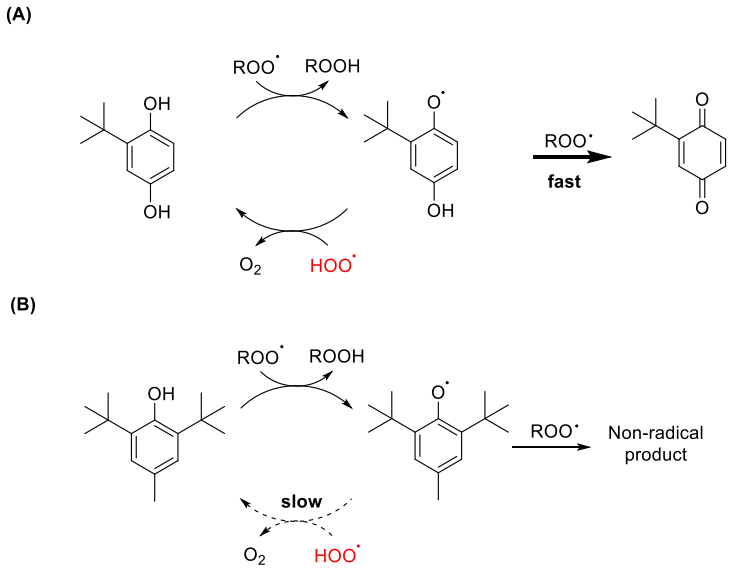

Scheme 2.8 *Explanation of the Lack of Synergy between γ-Terpinene and TBHQ or BHT*

2.5.3 Materials and Methods

Materials. All chemicals and solvents were commercially available (Merk, Sigma-Aldrich, Milan, Italy). γ-Terpinene was purified by percolating it twice on basic alumina microcolumns. (±)-α-Tocopherol, 2,2,5,7,8-pentamethyl-6-chromanol (PMHC), tert-butyl hydroquinone (TBHQ), 2,6-di-tert-butyl-4-methylphenol (BHT), catechol, 4-hydroxy-2,2,6,6-tetramethylpiperidine 1-oxyl (HO-TEMPO) and 4-acetamido-2,2,6,6-tetramethylpiperidine 1-oxyl (AcNH-TEMPO), $FeSO_4$ heptahydrate, tert-butyl hydroperoxide 70% in H_2O, KSCN, FeCl3, and 2,2 bipyridine were of the highest purity available and were used as received. Solvents were HPLC-grade and were used without further purification. High-linoleic sunflower oil (SO) was purchased from a local market. Stripped sunflower oil (SSO) was prepared as previously reported by percolation on basic alumina and by treatment with activated carbon.[10] The SO composition was determined by 1H NMR: polyunsaturated chains 59.4 mol %, monounsaturated chains 27.3 mol %, saturated chains 13.3%.[55]

Measure of O_2 Consumption. Oxygen consumption during the sunflower oil autoxidation was measured by a O_2-sensitive optical probe (Pyroscience GmbH, Aachen, Germany) in a sealed apparatus previously described.[56] Briefly, 2.00 g of oil containing variable amounts of γ-terpinene and/or of the antioxidants are introduced into a 10 or 50 mL round bottomed flask with a magnetic stir bar connected to a miniaturized water-cooled condenser to keep the temperature of the O_2 sensitive probe below 40 °C. The sample is kept under vigorous stirring in a silicone bath at 130 °C. The O_2 probe is calibrated in air before each experiment. The amount of consumed O_2 is calculated from the internal volume of the apparatus.

Determination of Hydroperoxides. Hydroperoxides were determined by the ferric thiocyanate assay using tert-butyl hydroperoxide as a reference. Equal amounts (250 μL) of a solution of $FeSO_4$ heptahydrate (5 mM) in 0.02 M HCl and of KSCN (3%) in MeOH were mixed to the oil or tert-butyl hydroperoxide sample dissolved in methanol (1 mL). After one minute, the absorption at 520 nm was read.[72]

Determination of Total Tocopherols. In a 10 mL volumetric flask, 100 mg of SO was mixed with 5 mL of toluene. Then, 3.5 mL of 2,2 bipyridine solution (0.07% (w/w)

in 95% aqueous ethanol) and 0.5 mL of $FeCl_3$ were added, mixed, and finally, the volume was raised to 10 mL with ethanol (95%). After a 1 min rest, the absorbance was read at 520 nm using a spectrophotometer.[73]

2.6 Conclusion

In this chapter, the development of a new analytical method capable of measuring oxygen consumption during isotherms at 130°C, through an optical O_2 probe, was reported here. This apparatus has allowed us, through the analysis of the curves obtained, to measure various parameters that describe the oxidation of the oil, and therefore to disentangle the role of the composition of the fatty acids from that of the antioxidants or other minor compounds. Furthermore, the addition of a fixed concentration of the antioxidant propyl gallate provided a semi-quantitative estimate of the radical generation rate. Using this information, it is possible to proceed with the subsequent studies. Screening of various phenolic antioxidants, having monophenolic, hydroquinone or catechol active moieties, showed that hydroquinones with an alkyl substituent show the best activity in terms of degree of inhibition of O_2 consumption and duration of the inhibition period. Using EPR spectroscopy, it can be shown that the radical stability of antioxidants plays a counterintuitive role in determining overall activity. Hydroquinones which form very unstable semiquinone radicals which rapidly disappear by donation of hydrogen atoms to another radical, therefore are unable to propagate the oxidative chain. On the other hand, tocopherols, which form relatively persistent radicals, are not very effective in countering oil peroxidation, because their radicals can extract an H atom from polyunsaturated lipids. However, the protective activity of α-tocopherol against autoxidation of sunflower oil at 130°C increases in a concentration-dependent manner when γ-terpinene is added, creating a synergistic effect. Experiments conducted on stripped sunflower oil have shown that the mechanism of synergy is based on the generation of HOO• radicals, which are formed when γ-terpinene oxidizes with unsaturated lipids. Our results suggest that the natural compound γ-terpinene can be used to enhance the antioxidant effect of α-tocopherol,

which is naturally present in many foods and edible oils and is used as an additive. The mixture of γ-terpinene and α-tocopherol may therefore represent a new antioxidant blend to be used in foods, to replace artificial antioxidants. Much effort should still be needed to fully elucidate the oxidation and inhibition mechanisms of lipid peroxidation, these results are important to develop new antioxidant strategies for the protection of oils with a high content of polyunsaturated fatty acids at high temperatures and possibly of foods containing lipids in general.

References

1. Singh, D. *et al.* A review on feedstocks, production processes, and yield for different generations of biodiesel. *Fuel* **262**, 116553 (2020).
2. Xin, J., Imahara, H. & Saka, S. Kinetics on the oxidation of biodiesel stabilized with antioxidant. *Fuel* **88**, 282–286 (2009).
3. Tavakoli, J. *et al.* Improving the Frying Performance and Oxidative Stability of Refined Soybean Oil by Tocotrienol-Rich Unsaponifiable Matters of Kolkhoung (*Pistacia khinjuk*) Hull Oil. *J Am Oil Chem Soc* **95**, 619–628 (2018).
4. Farhoosh, R. & Nyström, L. Antioxidant potency of gallic acid, methyl gallate and their combinations in sunflower oil triacylglycerols at high temperature. *Food Chem* **244**, 29–35 (2018).
5. Sazzad, B. S., Fazal, M. A., Haseeb, A. S. M. A. & Masjuki, H. H. Retardation of oxidation and material degradation in biodiesel: a review. *RSC Adv* **6**, 60244–60263 (2016).
6. Gertz, C. & Parkash Kochhar, S. A new method to determine oxidative stability of vegetable fats and oils at simulated frying temperature. *Oléagineux, Corps gras, Lipides* **8**, 82–88 (2001).
7. McCormick, R. L., Ratcliff, M., Moens, L. & Lawrence, R. Several factors affecting the stability of biodiesel in standard accelerated tests. *Fuel Processing Technology* **88**, 651–657 (2007).
8. Denisov, E. T. & Khudyakov, I. v. Mechanisms of action and reactivities of the free radicals of inhibitors. *Chem Rev* **87**, 1313–1357 (1987).
9. Jensen, R. K., Korcek, S., Zinbo, M. & Johnson, M. D. Initiation in hydrocarbon autoxidation at elevated temperatures. *Int J Chem Kinet* **22**, 1095–1107 (1990).
10. Baschieri, A., Pizzol, R., Guo, Y., Amorati, R. & Valgimigli, L. Calibration of Squalene, *p* -Cymene, and Sunflower Oil as Standard Oxidizable Substrates for Quantitative Antioxidant Testing. *J Agric Food Chem* **67**, 6902–6910 (2019).

11. Burton, G. W. & Ingold, K. U. Autoxidation of biological molecules. 1. Antioxidant activity of vitamin E and related chain-breaking phenolic antioxidants in vitro. *J Am Chem Soc* **103**, 6472–6477 (1981).
12. Dunn, R. O. Oxidative stability of soybean oil fatty acid methyl esters by oil stability index (OSI). *J Am Oil Chem Soc* **82**, 381–387 (2005).
13. Yaakob, Z., Narayanan, B. N., Padikkaparambil, S., Unni K., S. & Akbar P., M. A review on the oxidation stability of biodiesel. *Renewable and Sustainable Energy Reviews* **35**, 136–153 (2014).
14. Redondo-Cuevas, L., Castellano, G., Torrens, F. & Raikos, V. Revealing the relationship between vegetable oil composition and oxidative stability: A multifactorial approach. *Journal of Food Composition and Analysis* **66**, 221–229 (2018).
15. Supriyono, Sulistyo, H., Almeida, M. F. & Dias, J. M. Influence of synthetic antioxidants on the oxidation stability of biodiesel produced from acid raw Jatropha curcas oil. *Fuel Processing Technology* **132**, 133–138 (2015).
16. Yang, J., He, Q. S., Corscadden, K. & Caldwell, C. Improvement on oxidation and storage stability of biodiesel derived from an emerging feedstock camelina. *Fuel Processing Technology* **157**, 90–98 (2017).
17. Cedrowski, J., Litwinienko, G., Baschieri, A. & Amorati, R. Hydroperoxyl Radicals ($HOO^{\cdot}$): Vitamin E Regeneration and H-Bond Effects on the Hydrogen Atom Transfer. *Chemistry - A European Journal* **22**, 16441–16445 (2016).
18. Harrison, K. A., Haidasz, E. A., Griesser, M. & Pratt, D. A. Inhibition of hydrocarbon autoxidation by nitroxide-catalyzed cross-dismutation of hydroperoxyl and alkylperoxyl radicals. *Chem Sci* **9**, 6068–6079 (2018).
19. Korcek, S., Chenier, J. H. B., Howard, J. A. & Ingold, K. U. Absolute Rate Constants for Hydrocarbon Autoxidation. XXI. Activation Energies for Propagation and the Correlation of Propagation Rate Constants with Carbon–Hydrogen Bond Strengths. *Can J Chem* **50**, 2285–2297 (1972).
20. ICP OES. *Trace Metals in Organics*. (A Honeywell Company: Des Plaines, 2015).

21. Varatharajan, K. & Pushparani, D. S. Screening of antioxidant additives for biodiesel fuels. *Renewable and Sustainable Energy Reviews* **82**, 2017–2028 (2018).
22. Wang, J., Lu, Y., Zheng, T., Sang, S. & Lv, L. Scavenging of Acrolein by Food-Grade Antioxidant Propyl Gallate in a Model Reaction System and Cakes. *J Agric Food Chem* **67**, 8520–8526 (2019).
23. Wang, J., Lu, Y., Zheng, T., Sang, S. & Lv, L. Scavenging of Acrolein by Food-Grade Antioxidant Propyl Gallate in a Model Reaction System and Cakes. *J Agric Food Chem* **67**, 8520–8526 (2019).
24. Haidasz, E. A. *et al.* Acid Is Key to the Radical-Trapping Antioxidant Activity of Nitroxides. *J Am Chem Soc* **138**, 5290–5298 (2016).
25. Nieva-Echevarría, B., Goicoechea, E., Manzanos, M. J. & Guillén, M. D. A method based on 1H NMR spectral data useful to evaluate the hydrolysis level in complex lipid mixtures. *Food Research International* **66**, 379–387 (2014).
26. Knothe, G. Analyzing biodiesel: standards and other methods. *J Am Oil Chem Soc* **83**, 823–833 (2006).
27. Pullen, J. & Saeed, K. Experimental study of the factors affecting the oxidation stability of biodiesel FAME fuels. *Fuel Processing Technology* **125**, 223–235 (2014).
28. Mittelbach, M. & Gangl, S. Long storage stability of biodiesel made from rapeseed and used frying oil. *J Am Oil Chem Soc* **78**, 573–577 (2001).
29. Borges, A., de Freitas, V., Mateus, N., Fernandes, I. & Oliveira, J. Solid Lipid Nanoparticles as Carriers of Natural Phenolic Compounds. *Antioxidants* **9**, 998 (2020).
30. Baschieri, A. & Amorati, R. Methods to Determine Chain-Breaking Antioxidant Activity of Nanomaterials beyond DPPH•. A Review. *Antioxidants* **10**, 1551 (2021).
31. Piccinino, D. *et al.* Nano-Structured Lignin as Green Antioxidant and UV Shielding Ingredient for Sunscreen Applications. *Antioxidants* **10**, 274 (2021).

32. Roy, S. & Rhim, J.-W. New insight into melanin for food packaging and biotechnology applications. *Crit Rev Food Sci Nutr* **62**, 4629–4655 (2022).
33. Mollica, F., Lucernati, R. & Amorati, R. Expanding the spectrum of polydopamine antioxidant activity by nitroxide conjugation. *J Mater Chem B* **9**, 9980–9988 (2021).
34. Amorati, R. *et al.* Amphiphilic antioxidants from "cashew nut shell liquid" (CNSL) waste. *Org Biomol Chem* **9**, 1352 (2011).
35. Russo, E. *et al.* Valorization and Potential Antimicrobial Use of Olive Mill Wastewater (OMW) from Italian Olive Oil Production. *Antioxidants* **11**, 903 (2022).
36. Guo, Y. *et al.* Absolute Antioxidant Activity of Five Phenol-Rich Essential Oils. *Molecules* **26**, 5237 (2021).
37. Helberg, J. & Pratt, D. A. Autoxidation *vs.* antioxidants – the fight for forever. *Chem Soc Rev* **50**, 7343–7358 (2021).
38. Farhoosh, R., Niazmand, R., Rezaei, M. & Sarabi, M. Kinetic parameter determination of vegetable oil oxidation under Rancimat test conditions. *European Journal of Lipid Science and Technology* **110**, 587–592 (2008).
39. Dodos, G. S., Tsesmeli, C. E. & Zannikos, F. Evaluation of the antimicrobial activity of synthetic and natural phenolic type antioxidants in biodiesel fuel. *Fuel* **209**, 150–161 (2017).
40. Becker, R. & Knorr, A. An evaluation of antioxidants for vegetable oils at elevated temperatures. *Lubrication Science* **8**, 95–117 (1996).
41. Denisov, E. T. Reactivity of quinones as alkyl radical acceptors. *Kinetics and Catalysis* **47**, 662–671 (2006).
42. Guo, Y. *et al.* Hydrogen Atom Transfer from HOO · to *ortho* -Quinones Explains the Antioxidant Activity of Polydopamine. *Angewandte Chemie International Edition* **60**, 15220–15224 (2021).
43. Lucarini, M., Pedrielli, P., Pedulli, G. F., Cabiddu, S. & Fattuoni, C. Bond Dissociation Energies of O−H Bonds in Substituted Phenols from Equilibration Studies. *J Org Chem* **61**, 9259–9263 (1996).

44. Tuner, H. & Korkmaz, M. Radiostability of butylated hydroxytoluene (BHT): An ESR study. *Nucl Instrum Methods Phys Res B* **258**, 388–394 (2007).
45. Eloranta, J., Hämäläinen, E., Salo, E., Mäkelä, R. & Kekäläinen, U. Radicals Formed from alpha-Tocopherol Under Oxidizing and Reducing Conditions. An EPR and ENDOR Study. *Acta Chem Scand* **37a**, 383–391 (1983).
46. Duling, D. R. Simulation of Multiple Isotropic Spin-Trap EPR Spectra. *J Magn Reson B* **104**, 105–110 (1994).
47. Pullen, J. & Saeed, K. Experimental study of the factors affecting the oxidation stability of biodiesel FAME fuels. *Fuel Processing Technology* **125**, 223–235 (2014).
48. Lucarini, M., Pedrielli, P., Pedulli, G. F., Cabiddu, S. & Fattuoni, C. Bond Dissociation Energies of O−H Bonds in Substituted Phenols from Equilibration Studies. *J Org Chem* **61**, 9259–9263 (1996).
49. Li, J., Bi, Y., Yang, H. & Wang, D. Antioxidative Properties and Interconversion of *tert* -Butylhydroquinone and *tert* -Butylquinone in Soybean Oils. *J Agric Food Chem* **65**, 10598–10603 (2017).
50. Lucarini, M., Mugnaini, V. & Pedulli, G. F. Bond Dissociation Enthalpies of Polyphenols: The Importance of Cooperative Effects. *J Org Chem* **67**, 928–931 (2002).
51. Yanishlieva, N. v., Kamal-Eldin, A., Marinova, E. M. & Toneva, A. G. Kinetics of antioxidant action ofα- andγ-toco-pherols in sunflower and soybean triacylglycerols. *European Journal of Lipid Science and Technology* **104**, 262–270 (2002).
52. Bowry, V. W. & Stocker, R. Tocopherol-mediated peroxidation. The prooxidant effect of vitamin E on the radical-initiated oxidation of human low-density lipoprotein. *J Am Chem Soc* **115**, 6029–6044 (1993).
53. Roginsky, V., Barsukova, T., Loshadkin, D. & Pliss, E. Substituted p-hydroquinones as inhibitors of lipid peroxidation. *Chem Phys Lipids* **125**, 49–58 (2003).

54. Mollica, F., Gelabert, I. & Amorati, R. Synergic Antioxidant Effects of the Essential Oil Component γ-Terpinene on High-Temperature Oil Oxidation. *ACS Food Science & Technology* **2**, 180–186 (2022).
55. Guillén, M. D. & Ruiz, A. Rapid simultaneous determination by proton NMR of unsaturation and composition of acyl groups in vegetable oils. *European Journal of Lipid Science and Technology* **105**, 688–696 (2003).
56. Mollica, F. *et al.* Effect of Antioxidants on High-Temperature Stability of Renewable Bio-Oils Revealed by an Innovative Method for the Determination of Kinetic Parameters of Oxidative Reactions. *Antioxidants* **9**, 399 (2020).
57. Duling, D. R. Simulation of Multiple Isotropic Spin-Trap EPR Spectra. *J Magn Reson B* **104**, 105–110 (1994).
58. Eloranta, J., Hämäläinen, E., Salo, E., Mäkelä, R. & Kekäläinen, U. Radicals Formed from alpha-Tocopherol Under Oxidizing and Reducing Conditions. An EPR and ENDOR Study. *Acta Chem Scand* **37a**, 383–391 (1983).
59. Tuner, H. & Korkmaz, M. Radiostability of butylated hydroxytoluene (BHT): An ESR study. *Nucl Instrum Methods Phys Res B* **258**, 388–394 (2007).
60. Lucarini, M., Pedrielli, P., Pedulli, G. F., Cabiddu, S. & Fattuoni, C. Bond Dissociation Energies of O−H Bonds in Substituted Phenols from Equilibration Studies. *J Org Chem* **61**, 9259–9263 (1996).
61. Amorati, R., Foti, M. C. & Valgimigli, L. Antioxidant Activity of Essential Oils. *J Agric Food Chem* **61**, 10835–10847 (2013).
62. Baschieri, A., Ajvazi, M. D., Tonfack, J. L. F., Valgimigli, L. & Amorati, R. Explaining the antioxidant activity of some common non-phenolic components of essential oils. *Food Chem* **232**, 656–663 (2017).
63. Guo, Y., Baschieri, A., Amorati, R. & Valgimigli, L. Synergic antioxidant activity of γ-terpinene with phenols and polyphenols enabled by hydroperoxyl radicals. *Food Chem* **345**, 128468 (2021).
64. Li, G.-X. & Liu, Z.-Q. Unusual Antioxidant Behavior of α- and γ-Terpinene in Protecting Methyl Linoleate, DNA, and Erythrocyte. *J Agric Food Chem* **57**, 3943–3948 (2009).

65. Ruberto, G. & Baratta, M. T. Antioxidant activity of selected essential oil components in two lipid model systems. *Food Chem* **69**, 167–174 (2000).
66. Graßmann, J., Schneider, D., Weiser, D. & Elstner, E. Antioxidative Effects of Lemon Oil and its Components on Copper Induced Oxidation of Low Density Lipoprotein. *Arzneimittelforschung* **51**, 799–805 (2011).
67. Foti, M. C. & Ingold, K. U. Mechanism of Inhibition of Lipid Peroxidation by γ-Terpinene, an Unusual and Potentially Useful Hydrocarbon Antioxidant. *J Agric Food Chem* **51**, 2758–2765 (2003).
68. Mohanan, A., Nickerson, M. T. & Ghosh, S. Oxidative stability of flaxseed oil: Effect of hydrophilic, hydrophobic and intermediate polarity antioxidants. *Food Chem* **266**, 524–533 (2018).
69. Baschieri, A. *et al.* Extremely Fast Hydrogen Atom Transfer between Nitroxides and HOO · Radicals and Implication for Catalytic Coantioxidant Systems. *J Am Chem Soc* **140**, 10354–10362 (2018).
70. Garcés, R., Martínez-Force, E., Salas, J. J. & Venegas-Calerón, M. Current advances in sunflower oil and its applications. *Lipid Technol* **21**, 79–82 (2009).
71. Amorati, R., Pedulli, G. F., Pratt, D. A. & Valgimigli, L. TEMPO reacts with oxygen-centered radicals under acidic conditions. *Chemical Communications* **46**, 5139 (2010).
72. Mihaljević, B., Katušin-Ražem, B. & Ražem, D. The reevaluation of the ferric thiocyanate assay for lipid hydroperoxides with special considerations of the mechanistic aspects of the response. *Free Radic Biol Med* **21**, 53–63 (1996).
73. Wong, M. L., Timms, R. E. & Goh, E. M. Colorimetric determination of total tocopherols in palm oil, olein and stearin. *J Am Oil Chem Soc* **65**, 258 (1988).

CHAPTER III
EXPANDING THE SPECTRUM OF POLYDOPAMINE ANTIOXIDANT ACTIVITY BY NITROXIDE CONJUGATION

3.1 Preface

Polydopamine (PDA) materials are important due to their unique physicochemical properties and their potential as chemo-preventive agents for diseases connected with oxidative stress. Although PDA has been suggested to display antioxidant activity, its efficacy is controversial and its mechanism of action is still unclear. Herein, we report that accurately purified PDA nanoparticles in water at pH 7.4 are unable to quench alkyl peroxyls (ROO•), which are the radicals responsible for the propagation of lipid peroxidation, despite PDA reacting with the model DPPH• and $ABTS^{\bullet+}$ radicals. PDA nanoparticles prepared by copolymerization of dopamine with the dialkyl nitroxide 4-NH_2TEMPO show instead good antioxidant activity, thanks to the ROO• trapping ability of the nitroxide. Theoretical calculations performed on a quinone–catechol dimer, reproducing the structural motive of PDA, indicate a reactivity with ROO• like catechol. These results suggest that PDA nanoparticles have an ‘‘onion-like’’ structure, with a catechol-rich core, which can be reached only by DPPH• and $ABTS^{\bullet+}$, and a surface mainly represented by quinones. The importance of assessing the antioxidant activity by inhibited autoxidation studies is also discussed. This chapter is presented as it was published in the *Journal of Materials Chemistry B* (Mollica F.; Lucernati R.; Amorati R.; *J. Mater. Chem. B*, **2021**,9, 9980-9988).

3.2 Introduction

Melanins are a family of pigments formed by the oxidative polymerization of biologically-occurring phenols, including tyrosine, DOPA and dopamine (DA).[1,2] Polydopamine (PDA) has recently attracted enormous interest because of its excellent adhesion properties, redox activity and ability to easily form films and nanoparticles.[3] Although the exact molecular structure of PDA is still debated, there are pieces of evidence that it mainly consists of ortho-benzoquinone and catechol-containing units,

held together by both covalent and non-covalent interactions (*Scheme 3.1*).[4] The mechanism of the antioxidant activity of PDA has been the object of many studies, recently reviewed,[5] but it is far from being clarified.[5] PDA has been reported to trap free radicals such as HO•, NO•, 2,2-diphenyl-1-picrylhydrazyl (DPPH•) and the 2,20-azino-bis(3-ethylbenzothiazoline-6-sulfonic acid) radical cation ($ABTS^{\bullet+}$) and to display superoxide-dismutase activity.[5–7] Little is known about the reactivity of PDA toward peroxyl radicals which are the kinetically relevant oxidizing species that propagate lipid peroxidation (*Scheme 3.1*).[8–10] In a recent communication, we have shown that, in acetonitrile, PDA does not react with alkyl peroxyl radicals (ROO•) and thus it is unable to stop the lipid peroxidation of a model substrate. Instead, we could observe antioxidant activity only in the presence of both ROO• and HOO• radicals.[11] The role of the solvent in these reactions and the reason why PDA is reactive with DPPH• and $ABTS^{\bullet+}$ radicals but not with ROO• remains unclear. Moreover, as the antioxidant activity of PDA is expected to be influenced by the release of low molecular weight monomers or oligomers from the polymer, also the influence of PDA purification should be better clarified. Herein, we aim at expanding the knowledge on the antioxidant activity of PDA by measuring the reaction of PDA nanoparticles with biologically relevant ROO• radicals in water at *pH* 7.4 and by comparing the results to those obtained with DPPH• and $ABTS^{\bullet+}$ (*Scheme 3.1*) that are the two most popular radicals used in in vitro antioxidant activity assays. We also envisaged to increase the antioxidant activity of PDA by introducing a dialkyl nitroxide into the polymer, as this kind of strategy was shown to increase protection from the radiation of keratinocytes by PDA.[12] TEMPO (2,2,6,6-tetramethylpiperidinoxyl)-derived nitroxides in fact are very active ROO• quenchers in water and show catalytic activity, thanks to their ability to switch between the oxoammonium ($N{=}O^{+}$) and hydroxylamine (NOH) forms (*Figure 3.1a*).[13–15] We therefore linked 4-NH_2TEMPO (4-amino-2,2,6,6-tetramethylpiperidinoxyl radical) to PDA by an original copolymerization strategy (*Figure 3.1a*). The effect of the purification procedure on the radical trapping ability of PDA and the implication of these results on PDA antioxidant activity are discussed.

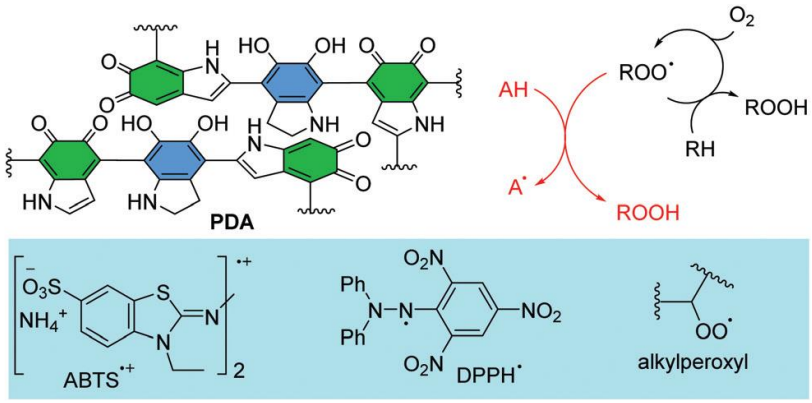

Scheme 3.1 *PDA structure, mechanism of action of radical trapping antioxidants and the structure of peroxyl and model radicals.*

3.3 Results

3.3.1 Synthesis and characterization

Polydopamine nanoparticles (PDAn) were synthetized by oxidative polymerization of DA in air, by mixing DA (as hydrochloride) and NH_4OH, following an already reported procedure (*Figure 3.1a*).[16,17] Polydopamine/4-NH_2TEMPO nanoparticles (PDAnT) were synthetized by oxidative DA polymerization in the presence of 4-NH_2TEMPO, after an accurate choice of the DA/4-NH_2TEMPO ratio. We found that 4-NH_2TEMPO caused fast oxidation of DA, yielding a polydisperse material, in agreement with previous reports on the effect of 2-phenyl-4,4,5,5-tetramethylimidazoline-1-oxyl 3-oxide (PTIO•) on DA polymerization.[18] The EPR analysis of the DA/4-NH_2TEMPO reaction showed that the signal of 4-NH_2TEMPO disappeared in a few minutes, then it appeared again after the addition of NH_4OH, suggesting that the nitroxide is first reduced to hydroxylamine by DA, then it is oxidized back to nitroxide by O_2 (*see Figure A3.1, Appendix).* Infrared (IR) and UV-vis spectra showed the typical features of polydopamine,[16] and transmission electron microscopy (TEM) and dynamic light scattering (DLS) analysis indicated that both materials were reasonably monodispersed. TEM diameters were 180 nm and 380 nm for PDAn and PDAnT, respectively, and were in agreement with DLS measurements (*Figure 3.1b and Figure A3.2-A3.4, Appendix*).

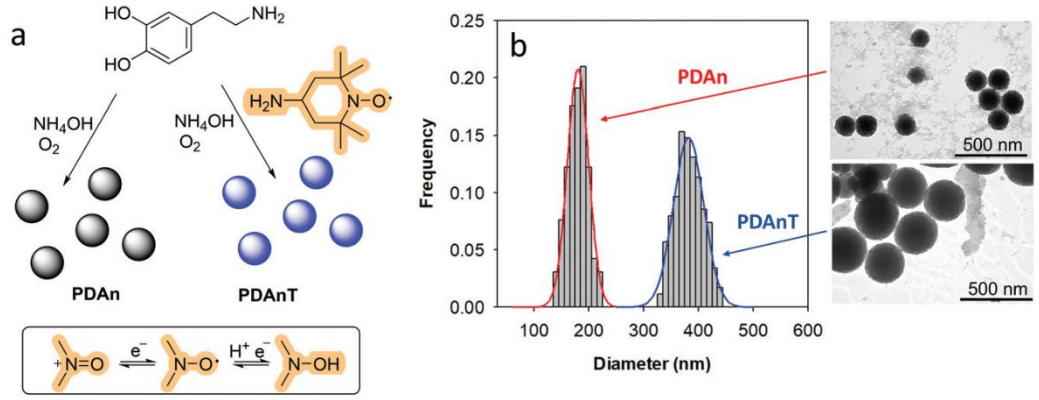

Figure 3.1 *(a) Synthesis of PDA nanoparticles and redox properties of nitroxides; (b) TEM images of PDAn and PDAnT.*

3.3.2 EPR characterization

The X-band electron paramagnetic resonance (EPR) spectra of PDAn showed a weak signal, attributed to a semiquinone radical formed by the comproportionation of catechol and quinone groups,[19] whose concentration was 6.6 μmol g^{-1}, in agreement with previous reports.[12,19] In the case of PDAnT, an intense spectrum typical of a nitroxide in the slow-motion regime, characterized by broadened lines with uneven heights,[15] was detected (*Figure 3.2*). This EPR spectrum was successfully interpreted by numerical fitting using Easy-Spin software (*see Figure 3.2*), revealing the presence of about 97% 4-NH_2TEMPO tightly bound to the nanoparticles and 3% of "fast moving" nitroxide (*see Figure A3.5–A3.7 for details, Appendix*).[20] The spin concentration in PDAnT was 190 μmol g^{-1}. The spectral features and the spin concentration of PDAnT were comparable to those reported by Gianneschi and co-workers for polydopamine nanoparticles bearing covalently bound TEMPO residues (reported spin densities ranged from 101 to 379 μmol g^{-1} depending on the preparation procedure).[12]

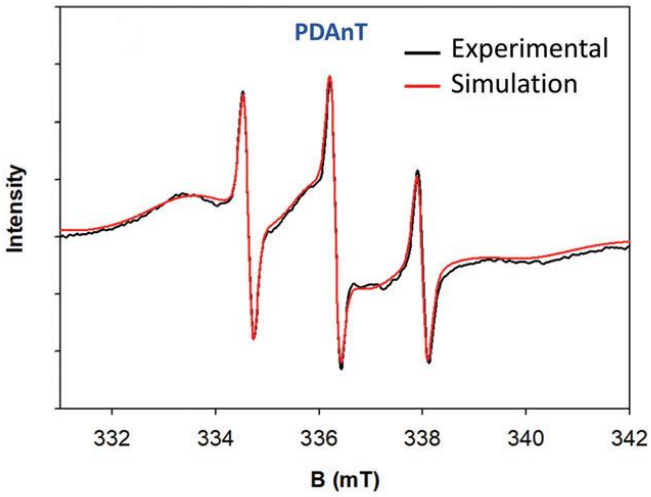

Figure 3.2 *Experimental and simulated EPR spectra of PDAnT in water (0.9 mg mL-1).*

3.3.3 Purification of PDA nanoparticles

All nanoparticles were purified by three centrifugation cycles at 11500g and one at 1500g to separate the bigger aggregates, followed by four overnight dialysis cycles in deionized water. Dialysis did not significantly change the dimensions and the spectral features of the nanoparticles *(see Figure A3.2-A3.3, Appendix*). The dialysate liquids were collected and concentrated under reduced pressure. UV-vis analysis, reported in *Figure 3.3a-b*, showed the presence of an absorption peak at 280 nm which was attributed to catechol impurities, given the similarity to the λ_{max} of DA (278 nm). The absorption between 400 and 500 nm suggested that also quinones were present. A more precise identification by electrospray ionization mass spectrometry (ESI-MS) was unsuccessful, although it excluded the presence of unreacted DA or of catechols emerging from DA cyclization (*i.e*. 5,6-di-hydroxyindole) and revealed the presence of signals presumably originating from the fragmentation of DA dimers or trimers (*see Figure A3.8, Appendix).*[4] In the assumption that the molar absorptivity of these impurities was the same as that of DA, their amounts in the samples ranged from 78 to 4 μM and diminished through the dialysis cycles (*see the insets of Figure 3.3a-b*). In the case of PDAnT, besides

the presence of catechol impurities, the UV-vis spectra also showed the occurrence of unreacted 4-NH_2TEMPO (*purple line in Figure 3.3b*).

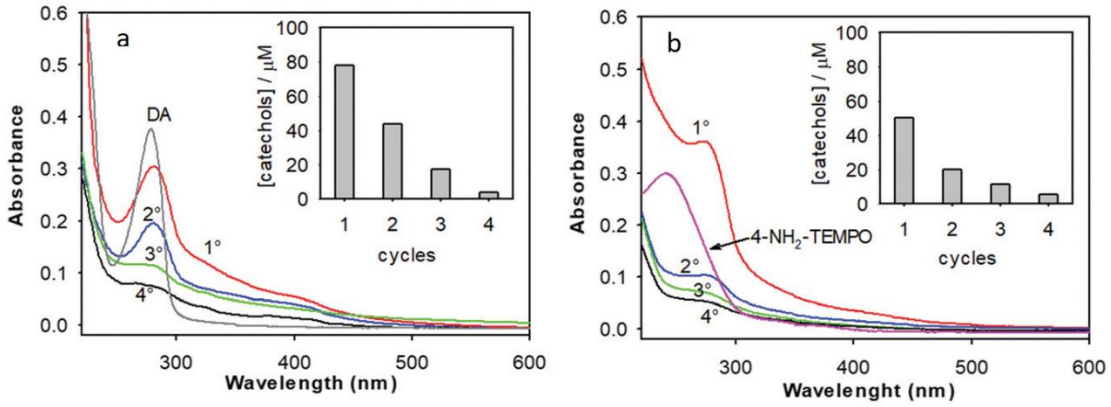

Figure 3.3 *UV-vis spectra of the dialysates after each dialysis cycle for PDAn (a) and PDAnT (b). the insets show the concentration of catechol impurities.*

The residual 4-NH_2TEMPO could be better quantified by EPR spectroscopy, and it showed a decrease from 45 to 0.8 µM after 4 dialysis cycles (*Figure 3.4)*. It should be emphasized that the spectrum of 4-NH_2TEMPO free in solution is markedly different from that of PDAnT, thus providing a clear proof of the linkage of the nitroxide to the nanoparticles and an easy measure of the degree of purification of the material.

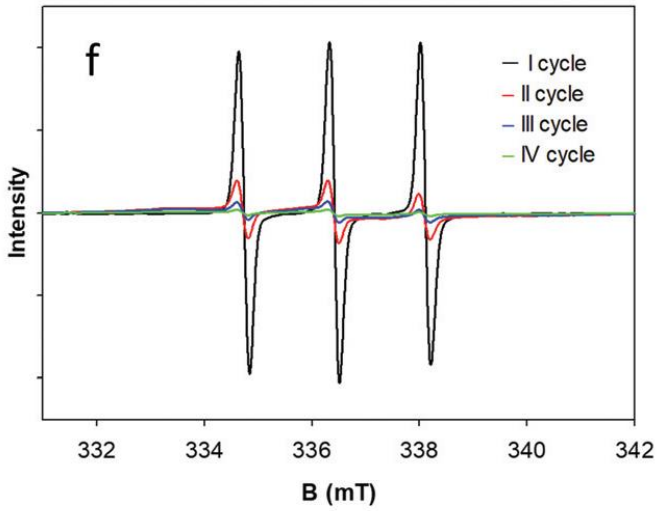

Figure 3.4 *EPR spectra of the dialysates of PDAnT.*

3.3.4 Reaction with peroxyl radicals

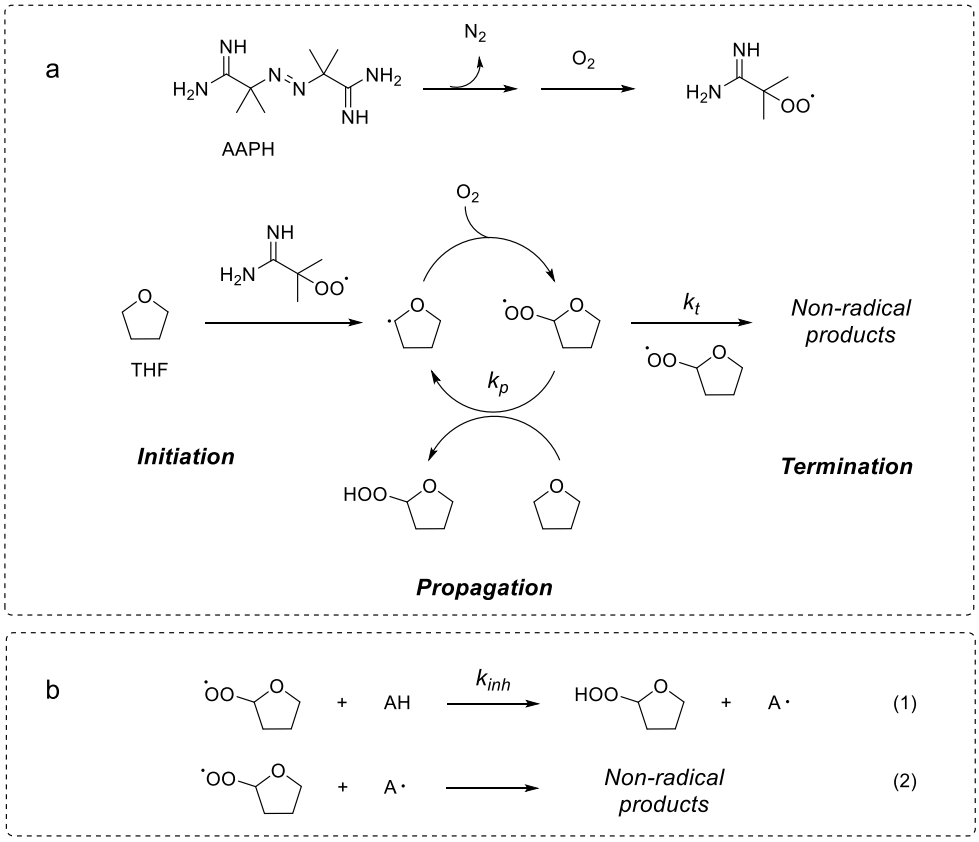

Scheme 3.2 *(a) Kinetic scheme of THF autoxidation. (b) Inhibition of autoxidation by a generic chain-breaking antioxidant, AH.*

The ability to trap alkylperoxyl (ROO•) radicals in water was measured by studying the inhibition of the autoxidation of tetrahydrofuran (THF)[21] as described in *Scheme 3.2a*. The reaction was initiated by the decomposition of the thermal azoinitiator 2,2ˈ-azobis(2-amidinopropane) dihydrochloride (AAPH) at 30 °C (*Scheme. 3.2a*) and the rate was determined by measuring the O_2 consumption with automatic gas-uptake recording apparatus.[21] In the absence of antioxidants, O_2 decreased linearly (*see the dashed line in Figure 3.5*), while in the presence of antioxidants the O_2 consumption was reduced, and an inhibition period was observed. The typical reactions of phenolic antioxidants with ROO• radicals are shown by equations 1 and 2 in *Scheme. 3.2b*. From the slope of O_2 consumption and the length of the inhibition period, the inhibition

constant k_{inh} and the number of radicals trapped by the antioxidant (stoichiometric coefficient, *n*) could be obtained.[22]

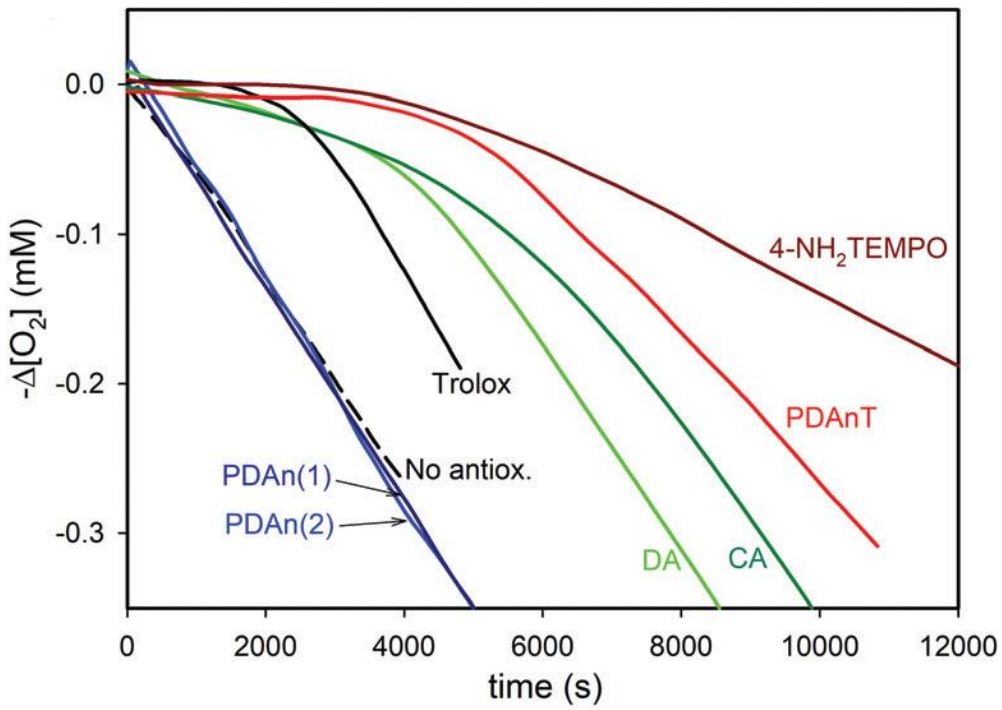

Figure 3.5 *Oxygen consumption during the autoxidation of THF (1.2 M) initiated by AAPH (50 mM) at 30 °C, pH 7.4, in the presence of PDAn purified by centrifugation (PDAn(1)) or by both centrifugation and dialysis (PDAn(2)) (20 μg mL^{-1}); Trolox (38 μM); DA (25 μM); CA (25 μM); PDAnT (22 μg mL^{-1}); and 4-NH$_2$TEMPO (25 μM).*

The results showed that DA and catechol (CA), used for comparison purposes, displayed a high antioxidant activity, whereas PDAn was unable to slow down the THF autoxidation. Interestingly, PDAn samples before and after the purification by dialysis were both inactive, indicating that the concentration of catechol impurities was too low to influence THF autoxidation. To better clarify the role of impurities, we performed the same experiment on a sample of PDAn purified only by one cycle of centrifugation. In this case, THF autoxidation was inhibited (*see Figure A3.9, Appendix*), thus confirming that insufficient purification leads to an overestimation of the antioxidant activity. The experiments performed with 4-NH$_2$TEMPO confirmed the previous

finding[15] that this nitroxide is an excellent quencher of ROO• and, gratifyingly, also PDAnT displayed a similar strong antioxidant activity. The antioxidant activity of nitroxides in water is due to the electron transfer from the R_2NO• moiety to ROO• to form the oxoammonium cation ($R_2N{=}O^+$) and ROO^-, which is protonated by the solvent to afford ROOH (*reaction 1 in Scheme 3.3a*). The nitroxide is then regenerated by the reaction of $R_2N{=}O^+$ with reductants (such as THF) to afford the hydroxylamine, which in turn reacts with ROO• and regenerates the nitroxide (*reactions 2 and 3, Scheme 3.3a*).[13–15] Except for PDAn, for all the investigated compounds a very strong inhibition of THF autoxidation was observed, implying that k_{inh} values were bigger than 5×10^5 M^{-1} s^{-1}. The stoichiometries of the antioxidants, obtained from the duration of the antioxidant effect, are reported in *Table 1*. The large stoichiometries of DA and CA compared to that of the reference antioxidant Trolox can be ascribed to the reactivity of the ortho-quinone with the solvent that regenerates the catechol moiety (*Scheme 3.3b*).[23,24] When considering that a catechol group is able to donate two H-atoms to two ROO•, the stoichiometry of about 6 suggests that the catechol group is regenerated twice. In the case of nitroxides, the stoichiometry >1 is instead due to the catalytic cycle shown in reactions 1-3.

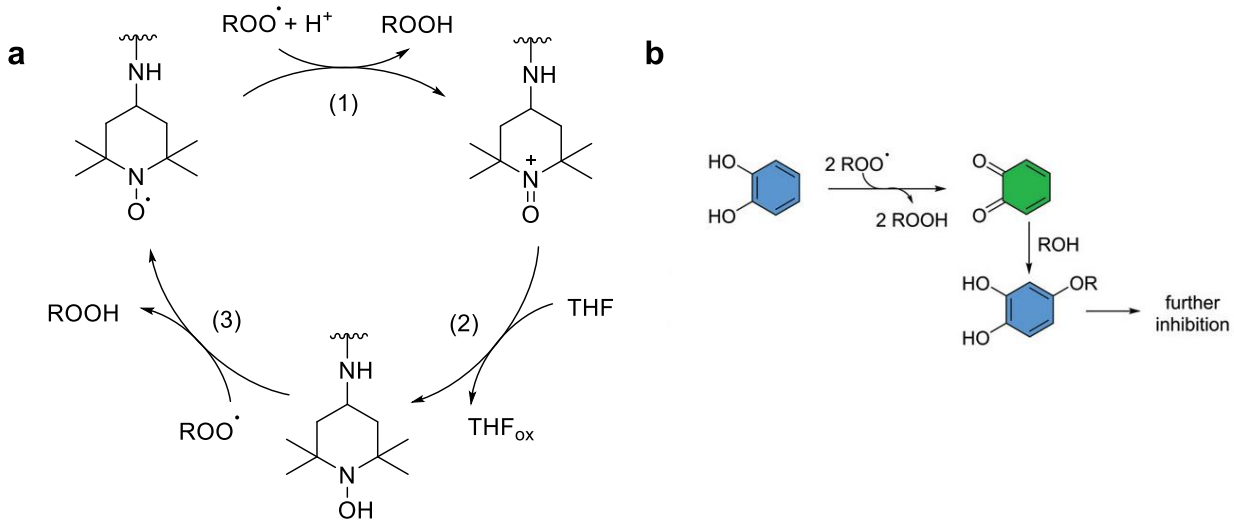

Scheme 3.3 *(a) Catalytic inhibition of autoxidation by nitroxides. (b) Solvent (ROH) addition to ortho-quinones derived from catechols increases the duration of inhibition.*

3.3.5 Reaction with stable radicals

The reactions of PDAn, PDAnT, DA and 4-NH_2TEMPO with the stable radicals DPPH• and $ABTS^{\bullet+}$ were investigated by EPR spectroscopy to avoid interference by the intense color of polydopamine. The typical results of time course experiments are reported in *Figure 3.6* and *Figure A3.10-A3.17* (*Appendix*), and the stoichiometry of radical trapping after 45 min is summarized in *Table 3.1*. The results clearly show that polydopamine-based nanoparticles react with the two radicals, although less efficiently than the monomer DA. In the case of the reaction with DPPH•, the reaction with DA occurred instantaneously during the mixing of the reactants, with a stoichiometry of 5.4 DPPH• radicals trapped by each DA molecule. Even when used at higher concentrations (on weight basis), the reactions of PDAn and PDAnT were slower than that of DA, and the stoichiometries (on weight basis) were much smaller (see Table 3.1). 4-NH_2TEMPO was completely inactive, in agreement with previous reports.[25]

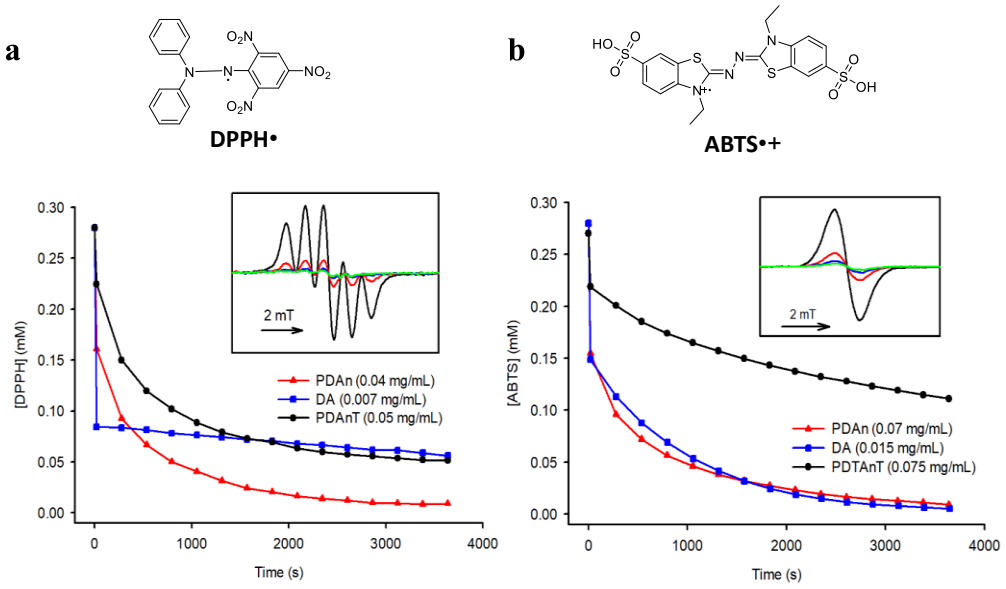

Figure 3.6 *Structures and reaction with DPPH•, solvent: ethanol (a), and with* $ABTS^{\bullet+}$*, solvent: water (b). The insets show the decay of EPR spectra of the two radicals (time interval: 15 min).*

Table 3.1 *Radical trapping stoichiometries measured in different assays. Results are expressed as mol (or mmol) of radicals quenched by a mol or by a mg of antioxidant.*

	mol_{rad} [a] mol_{antiox}^{-1}			μmol_{rad} [b] mg_{antiox}^{-1}	
	$ROO^{\bullet}$	$DPPH^{\bullet}$	$ABTS^{\bullet+}$	$DPPH^{\bullet}$	$ABTS^{\bullet+}$
Dopamine	5.2 ± 0.3	4.6 ± 0.8	2.6 ± 0.4	30 ± 6	17 ± 2
Catechol	6.1 ± 0.3	—	—	—	—
4-NH_2TEMPO	5.0 ± 0.3	≈0	≈0	≈0	≈0
PDAnT	2.0 ± 0.3[c]	—	—	5.1 ± 09	2.0 ± 0.4
PDAn	≈0	—	—	6.5 ± 0.2	4.3 ± 0.8

[a] Moles of radicals quenched by a mole of antioxidant. [b] μmoles of radicals quenched by a mg of antioxidant. [c] Refers to the nitroxide concentration, determined by EPR.

The different scavenging activity of DA against persistent radicals can be explained by considering the mechanisms that occur during the reaction. In a polar solution at a controlled pH, DA eliminates DPPH• pattern radicals quickly and effectively. At pH 7.4 the scavenging activity is related to the deprotonation of hydroxyl groups, with the participation of the rapid transfer of electrons from the phenolate anion to the DPPH• (SPLET mechanism) as well as much slower HAT in a single run. Conversely, the dominant mechanism in the ABTS assay is the HAT.

3.3.6 Reactivity of PDA models

To clarify the reasons for the lack of reactivity of PDAn with ROO•, this reaction was investigated by means of theoretical calculations. In general, the reaction of catechol derivatives with ROO• can follow different proton, hydrogen and electron transfer pathways which are summarized in *Scheme 3.4*.[26,27] Undissociated catechols (I) can react with ROO• by H-atom transfer (path A) to afford phenoxyl radical II that, at pH 7.4, dissociates to radical anion V (the pK_a of ortho-semiquinone is 5.0).[28] Deprotonation of catechols (path B) affords anion III, which can react with ROO• either via a H-atom transfer (path C) or via electron transfer (path D), followed by proton

exchange between the reactants. The B + D reaction sequence is reminiscent of the SPLET (sequential proton loss electron transfer) mechanism often invoked to explain the reactivity of phenols with radicals.26 The barrier of step A, the pK_a values (step B)[29] and the free energy variation for steps C and D were investigated by means of DFT calculations.[30]

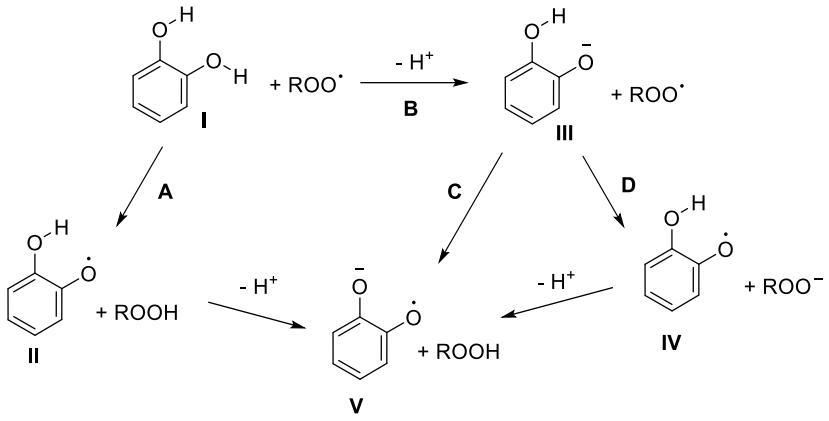

Scheme 3.4 *Reaction of catechol derivatives with ROO•*

	$\Delta G^{\ddagger}$ (A) kcal mol^{-1}	pK_a (B)	ΔG° (C) kcal mol^{-1}	ΔG° (D) kcal mol^{-1}
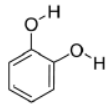 CA	11.3	9.1	−12.7	6.4
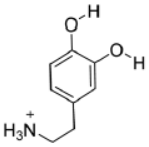 DA	12.3	8.7	−11.8	9.7
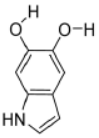 DHI	8.4	9.4	−14.8	0.15
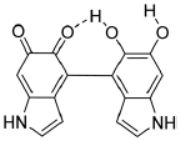 DHID	12.0	8.5	−13.2	3.5

Table 3.2 *Theoretical calculations of the reaction of catechol derivatives and ROO•*

This approach is aimed at obtaining a comparison between selected species relevant for polydopamine chemistry: DA, CA, 5,6-dihydroxyindole (DHI), and a partially oxidized 4-4' dimer of 5,6-dihydroxyindole (DHID), whose structure is reported in *Table 3.2* and *Figure 3.7*. The latter molecule was chosen as a simplified model of PDAn to simulate the polymer,[31] as it is the most stable among the DHI dimers containing both the quinone and the catechol moiety in close proximity.[32] The results reported in *Table 3.2* and *Figure 3.7* show that the direct reaction of ROO• with all the investigated catechols (path A) has an energy barrier of about 12 kcal mol^{-1}, except in the case of DHI whose $\Delta G^{\ddagger}$ is calculated as 8.4 kcal mol^{-1}. The lower barrier of DHI can be explained in terms of radical stabilization by the indole ring. Interestingly, DHID has a similar $\Delta G^{\ddagger}$ to CA, despite its reaction with CH3OO• being overall more exergonic (*see Figure 3.7*). This result can be explained in terms of radical delocalization on the ortho-quinone ring (see the blue surfaces in *Figure 3.7*), which is dependent on the dihedral angle between the aryl and the ortho-quinone rings (*angle ϕ in Figure 3.7*). The delocalization is highest when the two rings are on the same plane ($\phi = 0$) and is minimal for the perpendicular orientation. Therefore, the bigger ϕ in the transition state (TS) than in the products calculated for DHID suggests a smaller radical stabilization in the TS.

Regarding the acidity of the investigated compounds (step B), the pK_a of DHID is smaller than those of CA, DA and DHI, suggesting that the dimer can form the anion more easily than the other catechols.

Path C is significantly exergonic for all compounds, with DHID having a slightly smaller DG1 than CA and DA. The $DG^{\ddagger}$ values for step C could not be calculated because the reaction was barrierless.

The electron transfer step (path D) becomes endergonic or, only in the case of DHI, slightly exergonic, suggesting that the SPLET mechanism plays a negligible role in the reactivity of catechols with ROO• in water. Overall, all the calculated descriptors strongly support the idea that DHID is less reactive than DHI, but it has a comparable reactivity toward ROO• than that of the catechols CA and DA which in water are good antioxidants (*see Figure 3.5*).

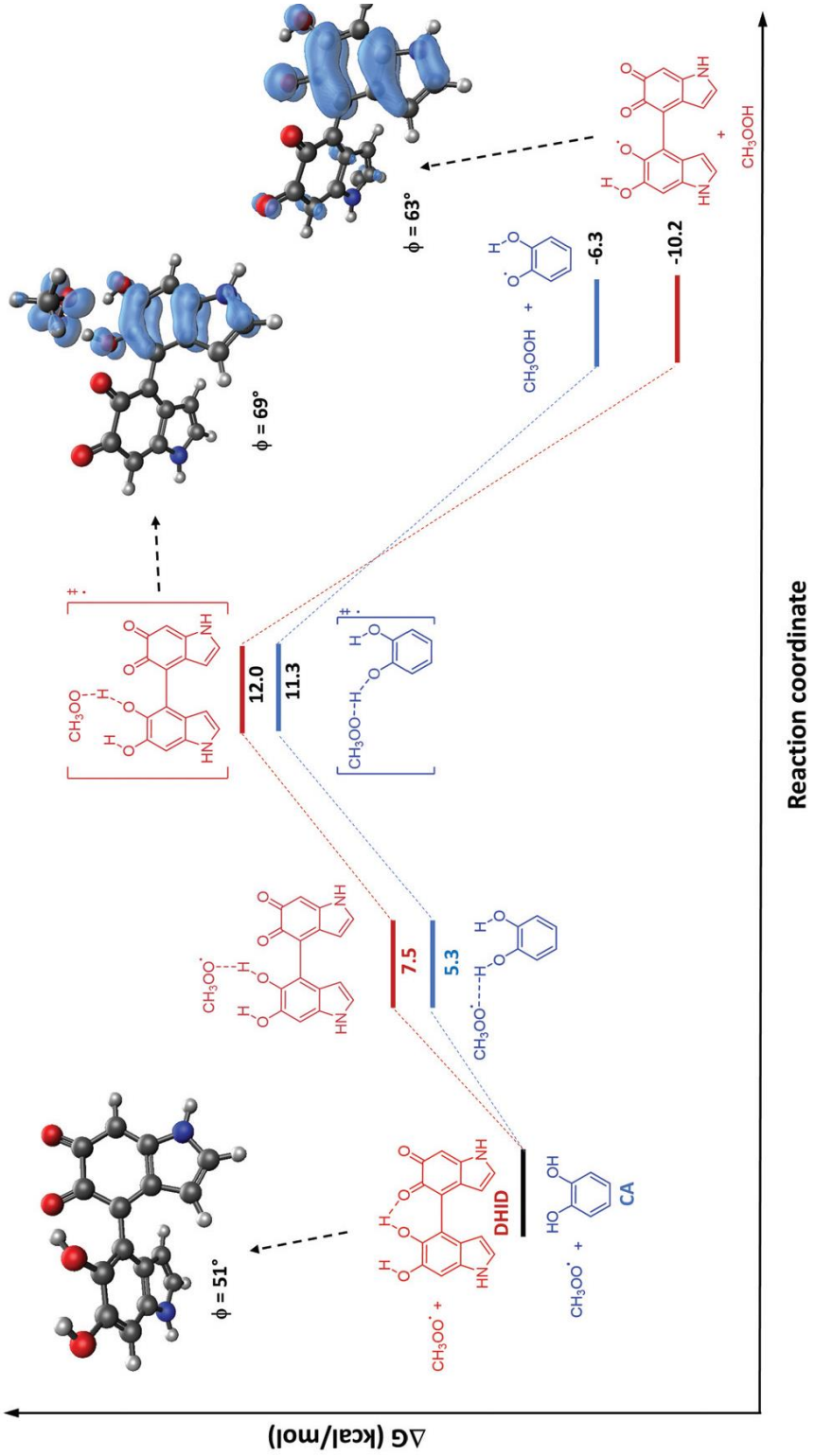

Figure 3.7 *Free energy profile for H-atom abstraction from the DHID, model of the catechol moieties in PDA, and CA by a peroxyl radical. The dihedral angle ϕ between the aryl and the ortho-quinone rings is reported. Blue surfaces represent the spin density. Free-energy changes are calculated in water at 25 °C.*

3.4 Discussion

3.4.1 PDA purification

The first point that needs to be clarified when addressing the antioxidant activity of PDA is the role of diffusible monomers and oligomers that may be absorbed into the material. It is well known that certain drugs and chemicals bind to natural and synthetic melanins and are retained in the pigments for long periods.[33] Drugs with aromatic and basic groups such as chloroquine, chlorpromazine and levofloxacin are tightly absorbed,[34] and thus the entrapment of DA and its monomeric and oligomeric derivatives into the growing PD nanoparticles is not unexpected. As DA and its derivatives such as DHI are highly antioxidant,[35] their presence must be kept into account when studying PDA. Herein, the purification of PDA nanoparticles was performed in two steps, consisting in three centrifuge cycles, followed by four overnight dialysis cycles. Moreover, at each dialysis cycle, the dialysate solutions were concentrated and analyzed by UV-vis spectrometry. These experiments clearly showed that diffusible molecules, containing catechol and quinone groups, were present in the samples and that their concentration decreased somewhat slowly despite the purification efforts (*see insets in Figure 3.3a-b*), suggesting a release from PDAn and PDAnT. We ascertained the role of diffusible catechols by performing all the tests of the antioxidant activity before and after the dialysis cycles and we found no difference between the two samples. Apparently, the concentration of the impurities present after the three centrifugation cycles was too low to contribute to the reaction with radicals. To better investigate this point, we also prepared a sample of PDAn purified only by a single centrifuge cycle, and we tested its ability to inhibit THF autoxidation. The result reported in *Figure A3.7 (Appendix)* showed a good antioxidant effect, thus indicating that insufficient purification may lead to false positive results. We believe that the same caution should be paid also when studying the antioxidant activity of phenolic polymers in general.

3.4.2 Intrinsic ROO• trapping activity of PDA

The study of the ability of PDAn to slow down the autoxidation of THF in water at pH 7.4 confirmed our previous results obtained in acetonitrile solution, indicating that PDAn does not possess any direct chain-breaking antioxidant activity. While this result seems in contrast with the many claims of antioxidant activity of PDA, it is in agreement with a study of Nau and co-workers who found that sepia melanin is a poor quencher of the excited states of benzophenone and of 2,3-diazabicyclo[2.2.2]oct-2-ene, and has a nearly negligible antioxidant efficacy on liposome oxidation.[36] The antioxidant activity of PDA was instead evident when the autoxidation was initiated by light because of its UV absorbing properties.[37] The lack of reactivity with ROO• radicals is puzzling when compared to the fact that PDA is able to quench both DPPH• and $ABTS^{\bullet+}$. A possible explanation may be the presence of strong H-bond complexes between the catechol moieties and the carbonyl groups in PDA, which might increase the dissociation energy of the O-H group and impair the reaction with ROO•.[38,39] However, this hypothesis should be discharged because theoretical calculations indicate that DHID, even if its catechol groups are H-bonded to the carbonyl, displays a reactivity with ROO• similar to DA or CA in water, suggesting that the catechols of PDA should trap ROO• radicals similarly to DA and CA. Therefore, to explain the lack of the antioxidant effect of PDAn, we hypothesis that the PDAn surface is constituted only by ortho-quinone groups, while catechol moieties are confined in the inner core. This two-layer structure can be justified because, during the synthesis of PDAn, any catechol group exposed on the surface would be deprotonated and oxidized by O_2. The radical quenching ability of PDAn can be rationalized by admitting that DPPH• and $ABTS^{\bullet+}$ are able to reach the inner part of the nanoparticle by a relatively slow diffusion process and are quenched by the catechol groups, as shown in *Scheme 3.3*.

In the case of ROO• radicals, this diffusion process must compete with the propagation of the oxidative chain, and thus the efficacy of radical trapping is much diminished. The presence of a quinone-rich outer shell also explains why PDAn is a good trap for reducing radicals such as HOO• and $O_2^{\bullet-}$ (*see Scheme 3.3*).[3,11,40] In this

case, the radicals reduce the ortho-quinone moieties to the corresponding semiquinones, which in turn possess radical trap- ping capabilities toward oxidizing ROO• radicals.

3.4.3 Antioxidant activity of PDAnT

The idea of linking nitroxides to PDA was first sought by Woehlk et al. with the aim to obtain a redox active functional surface.[41] To incorporate a TEMPO moiety in PDA, they synthetized a precursor consisting of 4-NH_2TEMPO covalently linked to 3,4-dihydroxy-L-phenylalanine (L-DOPA) by an amide bond. The same precursor was then adopted by Gianneschi and co-workers to obtain "radical enriched" PDA nanoparticles that displayed protective properties against reactive oxygen species in keratinocytes.[12] Herein, we achieved the same goal by using a straightforward one-pot strategy consisting in the oxidative co-polymerization of 4-NH_2TEMPO and DA under basic conditions. The link of TEMPO moieties to PDA is expected to be based on the nucleophilic attack of the amino group of 4-NH_2TEMPO to the ortho-quinone groups of PDAn, similarly to other amines which have been reported to be incorporated in the growing PDA polymer (*e.g.* tris(hydroxymethyl)aminomethane).[42] In the search for the best synthetic strategy, we attempted different approaches, such as 4-NH_2TEMPO addition to preformed PDAn under basic conditions or the use of the non-radical TEMPO precursor 4-amino-2,2,6,6-tetramethylpiperidine, but these efforts proved unsuccessful. The shape of the EPR spectrum of PDAnT obtained after a thorough purification clearly indicated that nitroxides are bound to the nanoparticles. Despite its simplicity, our method provided PDAnT with an EPR spectrum and a radical enrichment that were very similar to those reported by Gianneschi and co-workers.[12] Gratified by this result, we investigated the ROO• trapping ability of PDAnT as this piece of information is important to rationalize the biological activity of this and of analogous materials previously reported. The inhibition of THF autoxidation in water was very strong and like that observed in the case of the parent 4-NH_2TEMPO. The stoichiometry of radicals trapped by PDAnT suggests that, although a significant part of TEMPO moieties is available to

the reaction with ROO•, another portion (about 60%) is buried into the polymer and is therefore inactive.

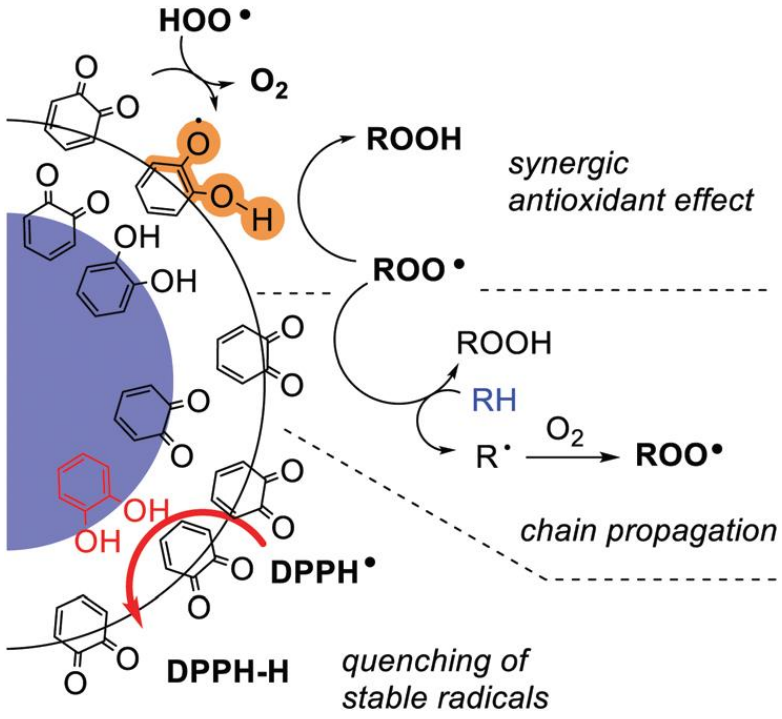

Scheme 3.3 Layered structure of polydopamine nanoparticles explaining the absence of direct reaction with ROO•, the synergic antioxidant effect in the presence of HOO• and ROO• radicals, and the reactivity toward stable radicals such as DPPH•. RH represents the oxidizable substrate, which competes with polydopamine for the ROO• radical.

3.5 Conclusion

In this work we have shown that polydopamine nanoparticles (PDAn) in water are not able to directly trap alkyl peroxyl radicals (ROO•) that are responsible for chain propagation in the autoxidation of organic substrates. Instead, PDAn can quench the DPPH• and $ABTS^{\bullet+}$ stable radicals.[43,44] Together with our previous results indicating that PDAn reacts with the reducing HOO• radicals, this demonstrates that the surface of PDAn is mainly constituted by ortho-quinones which are unable to trap ROO•

radicals but can interact with the reducing superoxide radical ($HOO•/O_2•^-$), resulting in an antioxidant effect. On the other hand, the slow reaction with DPPH• and $ABTS•^+$ can be explained by considering that catechol moieties are present in the inner core of PDAn, where they cannot be promptly accessed by ROO• and thus cannot compete with chain propagation. We have also shown that PDAn loaded with a stable nitroxide of the TEMPO family, PDAnT, are excellent antioxidants and show a high reactivity toward ROO•. As nitroxide-containing PDA nanoparticles have been shown to have low toxicity in cells,12 our findings further reinforce the idea that nitroxide-decorated PDA nanoparticles are promising platforms for the development of novel and more effective antioxidant materials for biomedical and food applications. Our results also provide evidence that DPPH• and $ABTS•^+$ should be used with caution to predict the reaction with ROO•, as these assays are prone to false- positive or false-negative results due to their structural difference with the biologically relevant alkylperoxyl radicals.[45]

Materials and methods

Materials. Analytical-grade solvents and commercially available reagents were of the highest purity commercially available and were used as received, unless otherwise stated. THF was purified by distillation and water was Millipore grade (resistivity Z18 MΩ). The radical ABTS$^{\bullet+}$ was prepared by mixing a 7 mM aqueous solution of 2,20-azino-bis(3-ethylbenzothiazoline-6-sulfonic) ammonium salt with a 2.45 mM potassium persulfate solution and stored overnight in the dark.[46] Its concentration was determined by EPR using 0.28 mM DPPH• solution as the standard.

Transmission electron microscopy (TEM) measurements. A Philips CM 100 TEM operating at 80 kV was used. For TEM investigations, a few drops of the NP solution in water were deposited on Formvar-coated copper grids and dried under high vacuum.

Dynamic light scattering (DLS) measurements. The determination of the hydrodynamic diameter distributions of NPs was carried out through dynamic light scattering measurements employing a Malvern Nano ZS instrument equipped with a 633 nm laser diode. Samples were housed in disposable poly- styrene cuvettes of a 1 cm optical path length using water as the solvent.

IR spectra. Infrared absorption spectra were directly recorded on solids using a Perkin-Elmer Spectrum 100 FT-IR spectrometer equipped with a universal ATR (attenuated total reflectance) accessory (contact crystal: diamond).

EPR spectroscopy studies. The electron paramagnetic resonance (EPR) spectra were collected at 35 °C with a MiniScope MS 5000 (Magnettech) in glass capillary tubes. The concentration of nitroxide bound to the nanoparticles was determined by comparing the double integral of its EPR spectrum to that of 4-NH_2TEMPO. Spectral simulation was performed using the software EasySpin with the graphical interface SimLabel as shown in Figure A3.5–A3. [20,47]

Synthesis

PDAn. The synthesis was carried out by oxidative polymerization of DA at basic pH.[16,17] Dopamine-HCl (130 mg, 11 mM) was solubilized in a mixture of deionized

water (51 mL) and ethanol (9 mL) and heated to 50 °C under stirring. Then 275 mL of 30% NH_4OH was added (0.24 M) and the solution turned from pale yellow to dark brown color in a few minutes. The reaction was kept under stirring for 24 hours at 50 °C. The obtained PDA nanoparticles (PDAn) were purified by three high-speed centrifugation cycles (11 500g for 15 minutes, washing the precipitate each time with deionized water), followed by one low-speed centrifugation cycle (1500g for 10 minutes) to eliminate the bigger aggregates. An aliquot of PDAn was further purified using a dialysis membrane (cut-off = 14 KDa) and 500 mL of deionized water for a total of four cycles. To monitor purification, at each dialysis cycle, 30 mL of dialysate water was collected and concentrated, and was analyzed by UV-Vis spectroscopy and ESI-MS (*see Figure A3.8 for details, Appendix*). Known volumes of PDAn at different levels of purification were lyophilized to obtain their concentrations, which were 0.78 mg mL^{-1} and 0.82 mg mL^{-1} for PDAn purified only by centrifugation or by centrifugation and dialysis, respectively. The nanoparticles were characterized by DLS, TEM, UV-Vis spectroscopy and ATR FT-IR spectroscopy as reported in *Figure 3.1b, 3.3* and *Figure A3.2 (Appendix).*

PDAnT. After several tests, the synthesis procedure was modified to slow down the polymerization, to obtain functionalized, monodisperse nanoparticles. In a flask dopamine-HCl (30 mg, 11 mM) was solubilized in deionized water (12 mL) and stirred and heated to 50 °C. In another vessel, $4NH_2$-TEMPO (18 mg, 7.5 mM), 30% NH_4OH (63 mL, 0.11 M), and ethanol (2 mL) were mixed and added slowly to the dopamine solution and left to react for 24 hours at 50 °C. The final product was purified and characterized as previously described for PDAn (*see Figure A3.3, Appendix*) and its concentration was 0.9 mg mL^{-1}.

Reaction with DPPH• and $ABTS^{\bullet+}$ radicals

A stock solution of the stable radical was mixed to different amounts of concentrated solution of the investigated phenols or nanoparticles. After mixing for about three

seconds, the reaction mixture was loaded in a 50 mL glass capillary tube and introduced into the EPR cavity thermostatted at 35 °C. Spectra were collected every 4 minutes.

Autoxidation studies

The kinetics of the reaction with alkylperoxyl radicals was studied by autoxidation experiments in differential oxygen-uptake apparatus based on a Validyne DP 15 pressure transducer built in our laboratory.[48] The samples consisted of AAPH (50 mM), THF (10% v/v, 1.2 M) and 0.1 M phosphate buffer (pH 7.4), at the temperature of 30 °C under vigorous stirring. By using the α-tocopherol hydrosoluble analogue Trolox as a reference antioxidant (having n = 2), the rate of radical initiation was calculated, using the relation $R_i = n[Antiox.]/\tau$, where τ is the duration of the inhibition period, as R_i = 3.0 x 10^{-8} Ms^{-1}. This equation also provided the stoichiometry *n* of the antioxidant.[46]

Theoretical calculations

Geometry optimization and frequencies were computed at the *B3LYP/6-311 + G(d,p)* level by using Gaussian 09.[49] The solvent was modelled using the standard self-consistent reaction field (PCM) procedure as implemented in the Gaussian 09 set of programs. Stationary points were confirmed by checking the absence of imaginary frequencies. The pK_a values were calculated by following the empirical relationship proposed by Galano et al.[29] by using Equation (1) where $\Delta G_{S(BA)}$ represents the difference in Gibbs free energy (in kcal mol^{-1}), in aqueous solution, between the acid (A) and its corresponding conjugated base (B).

$$pK_a = m\Delta G_{S(BA)} + C_0$$

The empirical parameters *m* and C_0 were 0.286 and -73.092, respectively, which have been optimized for the deprotonation of phenolic OH groups at the theory level of *B3LYP/6-311++g(d,p) SCRF = (SMD, solvent = water).*

References

1. Cao, W. *et al.* Unraveling the Structure and Function of Melanin through Synthesis. *J Am Chem Soc* **143**, 2622–2637 (2021).
2. d'Ischia, M., Napolitano, A., Pezzella, A., Meredith, P. & Buehler, M. Melanin Biopolymers: Tailoring Chemical Complexity for Materials Design. *Angewandte Chemie International Edition* **59**, 11196–11205 (2020).
3. Cheng, W. *et al.* Versatile Polydopamine Platforms: Synthesis and Promising Applications for Surface Modification and Advanced Nanomedicine. *ACS Nano* **13**, 8537–8565 (2019).
4. Lyu, Q., Hsueh, N. & Chai, C. L. L. Unravelling the polydopamine mystery: is the end in sight? *Polym Chem* **10**, 5771–5777 (2019).
5. Hu, J. *et al.* Polydopamine free radical scavengers. *Biomater Sci* **8**, 4940–4950 (2020).
6. Panzella, L. *et al.* Atypical Structural and π-Electron Features of a Melanin Polymer That Lead to Superior Free-Radical-Scavenging Properties. *Angewandte Chemie International Edition* **52**, 12684–12687 (2013).
7. el Yakhlifi, S. *et al.* Oxidant-dependent antioxidant activity of polydopamine films: The chemistry-morphology interplay. *Colloids Surf A Physicochem Eng Asp* **614**, 126134 (2021).
8. Foti, M. C. Use and Abuse of the DPPH˙ Radical. *J Agric Food Chem* **63**, 8765–8776 (2015).
9. Amorati, R. & Valgimigli, L. Advantages and limitations of common testing methods for antioxidants. *Free Radic Res* **49**, 633–649 (2015).
10. Shah, R., Farmer, L. A., Zilka, O., van Kessel, A. T. M. & Pratt, D. A. Beyond DPPH: Use of Fluorescence-Enabled Inhibited Autoxidation to Predict Oxidative Cell Death Rescue. *Cell Chem Biol* **26**, 1594-1607.e7 (2019).
11. Guo, Y. *et al.* Hydrogen Atom Transfer from HOO · to *ortho* -Quinones Explains the Antioxidant Activity of Polydopamine. *Angewandte Chemie International Edition* **60**, 15220–15224 (2021).

12. Cao, W. *et al.* Radical-Enriched Artificial Melanin. *Chemistry of Materials* **32**, 5759–5767 (2020).
13. Griesser, M. *et al.* The Catalytic Reaction of Nitroxides with Peroxyl Radicals and Its Relevance to Their Cytoprotective Properties. *J Am Chem Soc* **140**, 3798–3808 (2018).
14. Baschieri, A. *et al.* Extremely Fast Hydrogen Atom Transfer between Nitroxides and HOO · Radicals and Implication for Catalytic Coantioxidant Systems. *J Am Chem Soc* **140**, 10354–10362 (2018).
15. Genovese, D. *et al.* Nitroxides as Building Blocks for Nanoantioxidants. *ACS Appl Mater Interfaces* **13**, 31996–32004 (2021).
16. Huang, Y. *et al.* Mimicking Melanosomes: Polydopamine Nanoparticles as Artificial Microparasols. *ACS Cent Sci* **3**, 564–569 (2017).
17. Jiang, X., Wang, Y. & Li, M. Selecting water-alcohol mixed solvent for synthesis of polydopamine nano-spheres using solubility parameter. *Sci Rep* **4**, 6070 (2014).
18. Wang, X. *et al.* Size control synthesis of melanin-like polydopamine nanoparticles by tuning radicals. *Polym Chem* **10**, 4194–4200 (2019).
19. Tadyszak, K., Mrówczyński, R. & Carmieli, R. Electron Spin Relaxation Studies of Polydopamine Radicals. *J Phys Chem B* **125**, 841–849 (2021).
20. Stoll, S. & Schweiger, A. EasySpin, a comprehensive software package for spectral simulation and analysis in EPR. *Journal of Magnetic Resonance* **178**, 42–55 (2006).
21. Amorati, R., Baschieri, A., Morroni, G., Gambino, R. & Valgimigli, L. Peroxyl Radical Reactions in Water Solution: A Gym for Proton-Coupled Electron-Transfer Theories. *Chemistry - A European Journal* **22**, 7924–7934 (2016).
22. Shah, R., Poon, J.-F., Haidasz, E. A. & Pratt, D. A. Temperature-Dependent Effects of Alkyl Substitution on Diarylamine Antioxidant Reactivity. *J Org Chem* **86**, 6538–6550 (2021).
23. Saito, S., Gao, H. & Kawabata, J. DPPH (= 2,2-Diphenyl-1-picrylhydrazyl = 2,2-Diphenyl-1-(2,4,6-trinitrophenyl)hydrazyl) Radical-Scavenging Reaction of

Protocatechuic Acid Esters (= 3,4-Dihydroxybenzoates) in Alcohols: Formation of Bis-alcohol Adduct. *Helv Chim Acta* **89**, 821–831 (2006).

24. Guernelli, S., Cariola, A., Baschieri, A., Amorati, R. & lo Meo, P. Nanosponges for the protection and release of the natural phenolic antioxidants quercetin, curcumin and phenethyl caffeate. *Mater Adv* **1**, 2501–2508 (2020).
25. Pichla, M., Bartosz, G., Pieńkowska, N. & Sadowska-Bartosz, I. Possible artefacts of antioxidant assays performed in the presence of nitroxides and nitroxide-containing nanoparticles. *Anal Biochem* **597**, 113698 (2020).
26. Litwinienko, G. & Ingold, K. U. Solvent Effects on the Rates and Mechanisms of Reaction of Phenols with Free Radicals. *Acc Chem Res* **40**, 222–230 (2007).
27. Amorati, R. P. G. F. C. L. Z. L. L. L. Solvent and pH Effects on the Antioxidant Activity of Caffeic and Other Phenolic Acids. *J Agric Food Chem* **54**, 2932–2937 (2006).
28. Warren, J. J., Tronic, T. A. & Mayer, J. M. Thermochemistry of Proton-Coupled Electron Transfer Reagents and its Implications. *Chem Rev* **110**, 6961–7001 (2010).
29. Galano, A. *et al.* Empirically Fitted Parameters for Calculating p K_a Values with Small Deviations from Experiments Using a Simple Computational Strategy. *J Chem Inf Model* **56**, 1714–1724 (2016).
30. Baschieri, A., Pulvirenti, L., Muccilli, V., Amorati, R. & Tringali, C. Chain-breaking antioxidant activity of hydroxylated and methoxylated magnolol derivatives: the role of H-bonds. *Org Biomol Chem* **15**, 6177–6184 (2017).
31. Liebscher, J. *et al.* Structure of Polydopamine: A Never-Ending Story? *Langmuir* **29**, 10539–10548 (2013).
32. He Chen, S. Z. Z. Z. M. L. Q. Z. Application of Dopamine Functional Materials in Water Pollution Control. *Progress in Chemistry* **31**, 571–579 (2019).
33. Karlsson, O. & Lindquist, N. G. Melanin and neuromelanin binding of drugs and chemicals: toxicological implications. *Arch Toxicol* **90**, 1883–1891 (2016).

34. Jakubiak, P., Lack, F., Thun, J., Urtti, A. & Alvarez-Sánchez, R. Influence of Melanin Characteristics on Drug Binding Properties. *Mol Pharm* **16**, 2549–2556 (2019).
35. Memoli, S. *et al.* Diffusible melanin-related metabolites are potent inhibitors of lipid peroxidation. *Biochimica et Biophysica Acta (BBA) - Lipids and Lipid Metabolism* **1346**, 61–68 (1997).
36. Zhang, X., Erb, C., Flammer, J. & Nau, W. M. Absolute Rate Constants for the Quenching of Reactive Excited States by Melanin and Related 5,6-Dihydroxyindole Metabolites: Implications for Their Antioxidant Activity. *Photochem Photobiol* **71**, 524–533 (2007).
37. Ezzahir, A. The influence of melanins on the photoperoxidation of lipids. *J Photochem Photobiol B* **3**, 341–349 (1989).
38. Woll, M. G., Fisk, J. D., LePlae, P. R. & Gellman, S. H. Stereoselective Synthesis of 3-Substituted 2-Aminocyclopentanecarboxylic Acid Derivatives and Their Incorporation into Short 12-Helical β-Peptides That Fold in Water. *J Am Chem Soc* **124**, 12447–12452 (2002).
39. Amorati, R., Menichetti, S., Viglianisi, C. & Foti, M. C. Proton–electron transfer pathways in the reactions of peroxyl and dpph˙ radicals with hydrogen-bonded phenols. *Chemical Communications* **48**, 11904 (2012).
40. Baschieri, A., Amorati, R., Valgimigli, L. & Sambri, L. 1-Methyl-1,4-cyclohexadiene as a Traceless Reducing Agent for the Synthesis of Catechols and Hydroquinones. *J Org Chem* **84**, 13655–13664 (2019).
41. Woehlk, H. *et al.* Engineering Nitroxide Functional Surfaces Using Bioinspired Adhesion. *Langmuir* **34**, 3264–3274 (2018).
42. della Vecchia, N. F. *et al.* Tris Buffer Modulates Polydopamine Growth, Aggregation, and Paramagnetic Properties. *Langmuir* **30**, 9811–9818 (2014).
43. Liu, H. *et al.* Role of polydopamine's redox-activity on its pro-oxidant, radical-scavenging, and antimicrobial activities. *Acta Biomater* **88**, 181–196 (2019).

44. Jing, Y. *et al.* Ultrathin two-dimensional polydopamine nanosheets for multiple free radical scavenging and wound healing. *Chemical Communications* **56**, 10875–10878 (2020).
45. Baschieri, A. & Amorati, R. Methods to Determine Chain-Breaking Antioxidant Activity of Nanomaterials beyond DPPH•. A Review. *Antioxidants* **10**, 1551 (2021).
46. Re, R. *et al.* Antioxidant activity applying an improved ABTS radical cation decolorization assay. *Free Radic Biol Med* **26**, 1231–1237 (1999).
47. Etienne, E., le Breton, N., Martinho, M., Mileo, E. & Belle, V. SimLabel: a graphical user interface to simulate continuous wave EPR spectra from site-directed spin labeling experiments. *Magnetic Resonance in Chemistry* **55**, 714–719 (2017).
48. Baschieri, A. *et al.* Enhanced Antioxidant Activity under Biomimetic Settings of Ascorbic Acid Included in Halloysite Nanotubes. *Antioxidants* **8**, 30 (2019).
49. Frisch, M. J. et al. *Gaussian 09, Revision D.01*. (2009).

Appendix

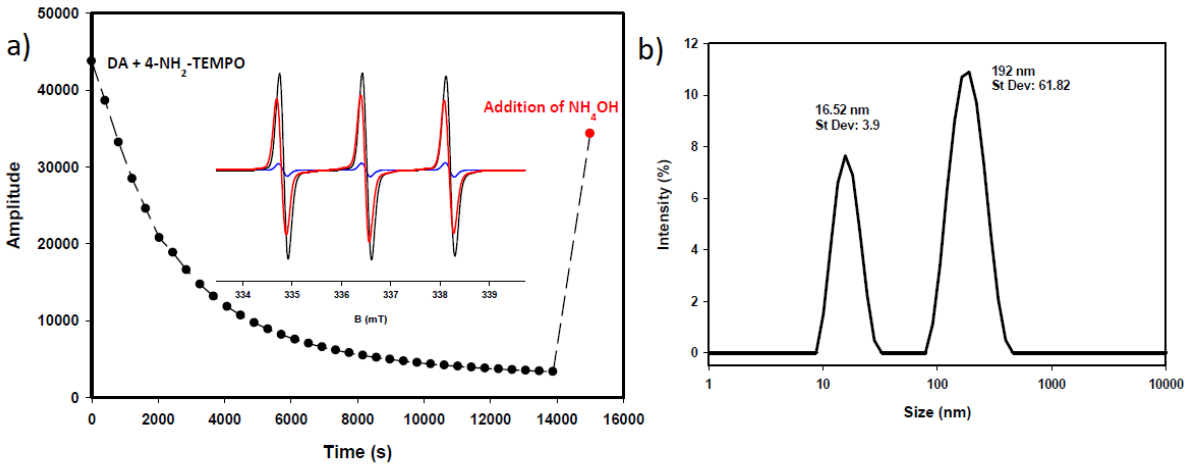

Figure A3.1. *(a) EPR signal measured after mixing dopamine and 4-NH_2TEMPO. The red dot represents the signal after NH_4OH addition. (b) DLS spectrum of polydisperse particles obtained by the sequential mixing of 4-NH_2TEMPO and NH_4OH.*

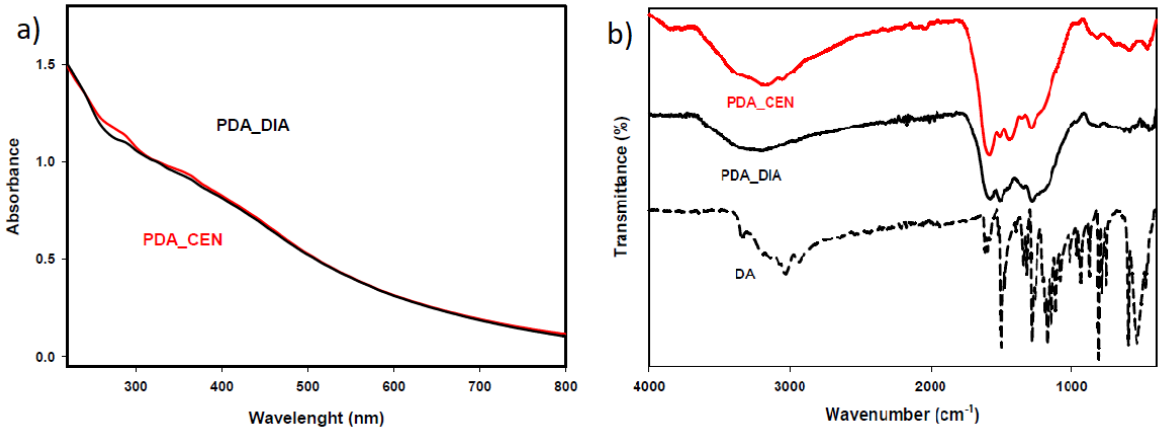

Figure A3.2. *Chemical and morphological characterization of PDAn purified only by centrifugation (PDA_CEN) or by centrifugation and dialysis (PDA_DIA). a) UV-vis spectrum in water of (–) PDA_CEN and (–) PDA_DIA (30μg/mL); b) FTIR-ATR spectra on solid samples of (–) PDA_CEN, (–) PDA_DIA and (- - -) DA.*

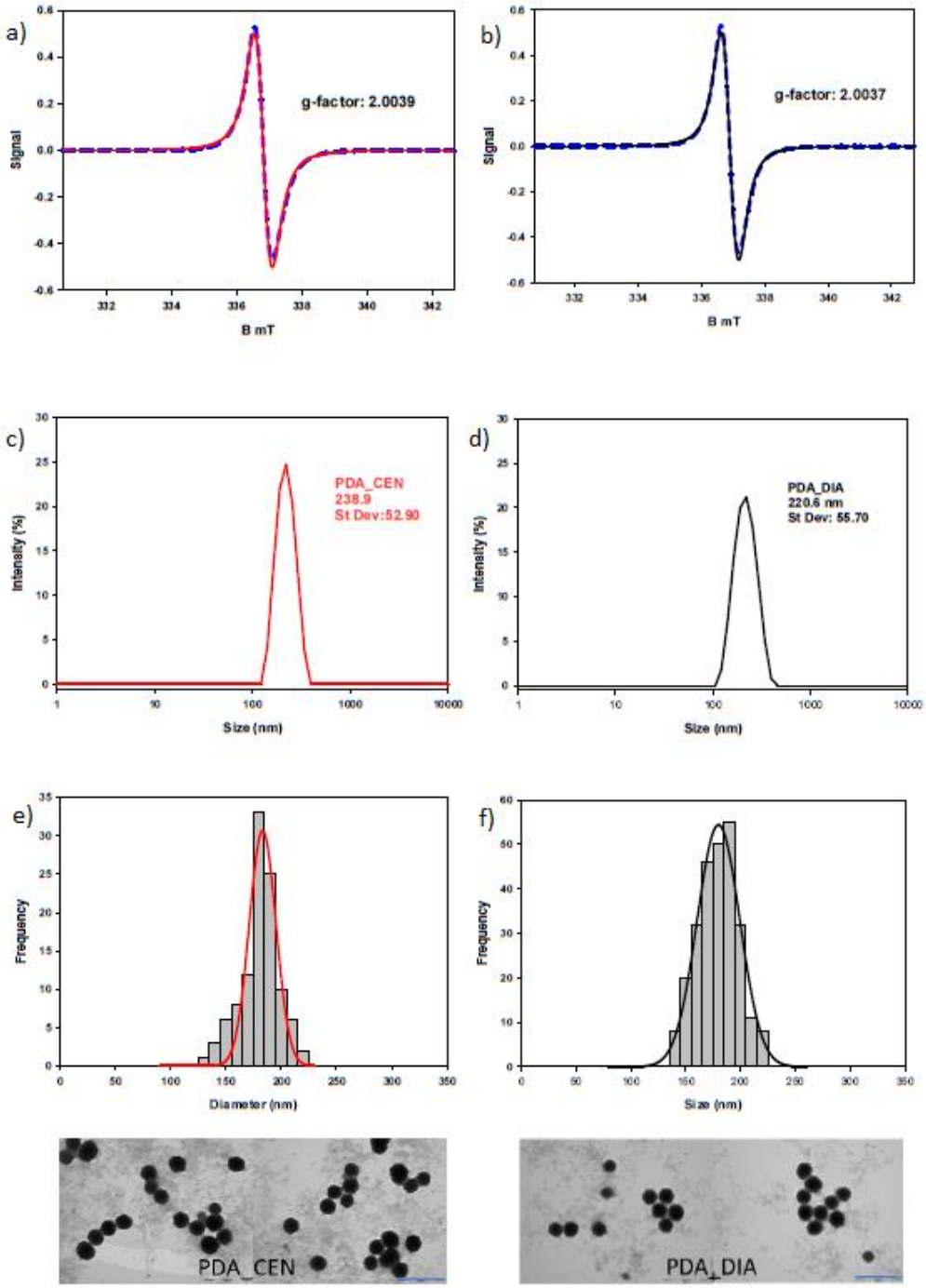

Figure A3.3*. Chemical and morphological characterization of PDAn purified only by centrifugation PDA_CEN or by centrifugation and dialysis (PDA_DIA). Experimental (- - -) and simulated EPR spectra on solid samples of (–) PDA_CEN (a) and (–) PDA_DIA (b); DLS spectra (c, d); E,) Gaussian distribution and TEM images of (–) PDA_CEN (e) and (–) PDA_DIA (f). The blue bar is equivalent to 500 nm.*

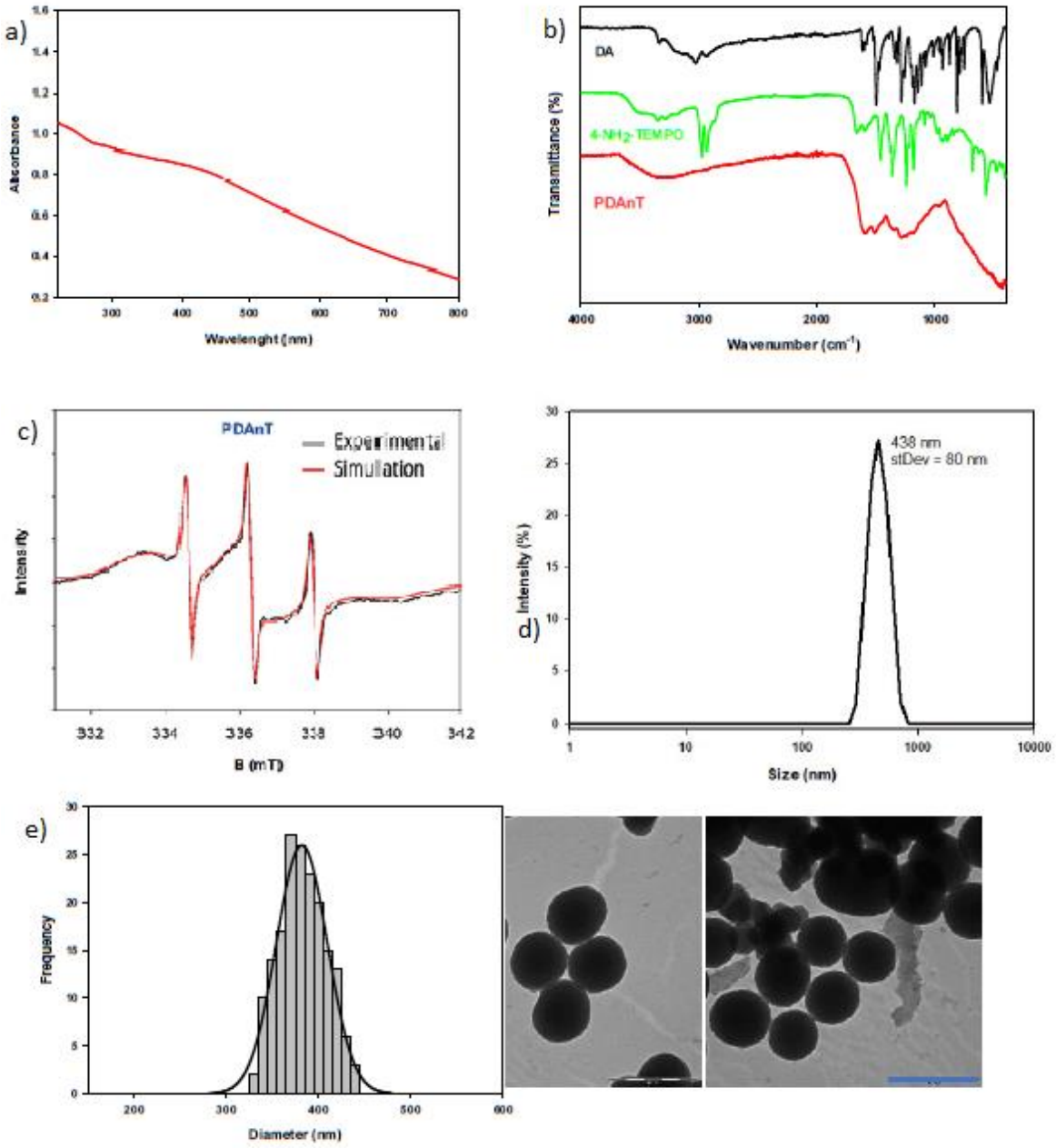

Figure A3.4. *Chemical and morphological characterization of functionalized polydopamine nanoparticles. a) UV-vis spectrum in water of (–) PDAnT (30μg/mL); b) FTIR-ATR spectra on solid samples of (–) DA (Dopamine-HCl), (–) 4-NH_2-TEMPO and (–) PDAnT; c) experimental (- - -) and simulated (–) EPR spectrum of PDAnT in water (0.9mg/mL); d) DLS spectra and e) Gaussian distribution and TEM images (Bar=500 nm).*

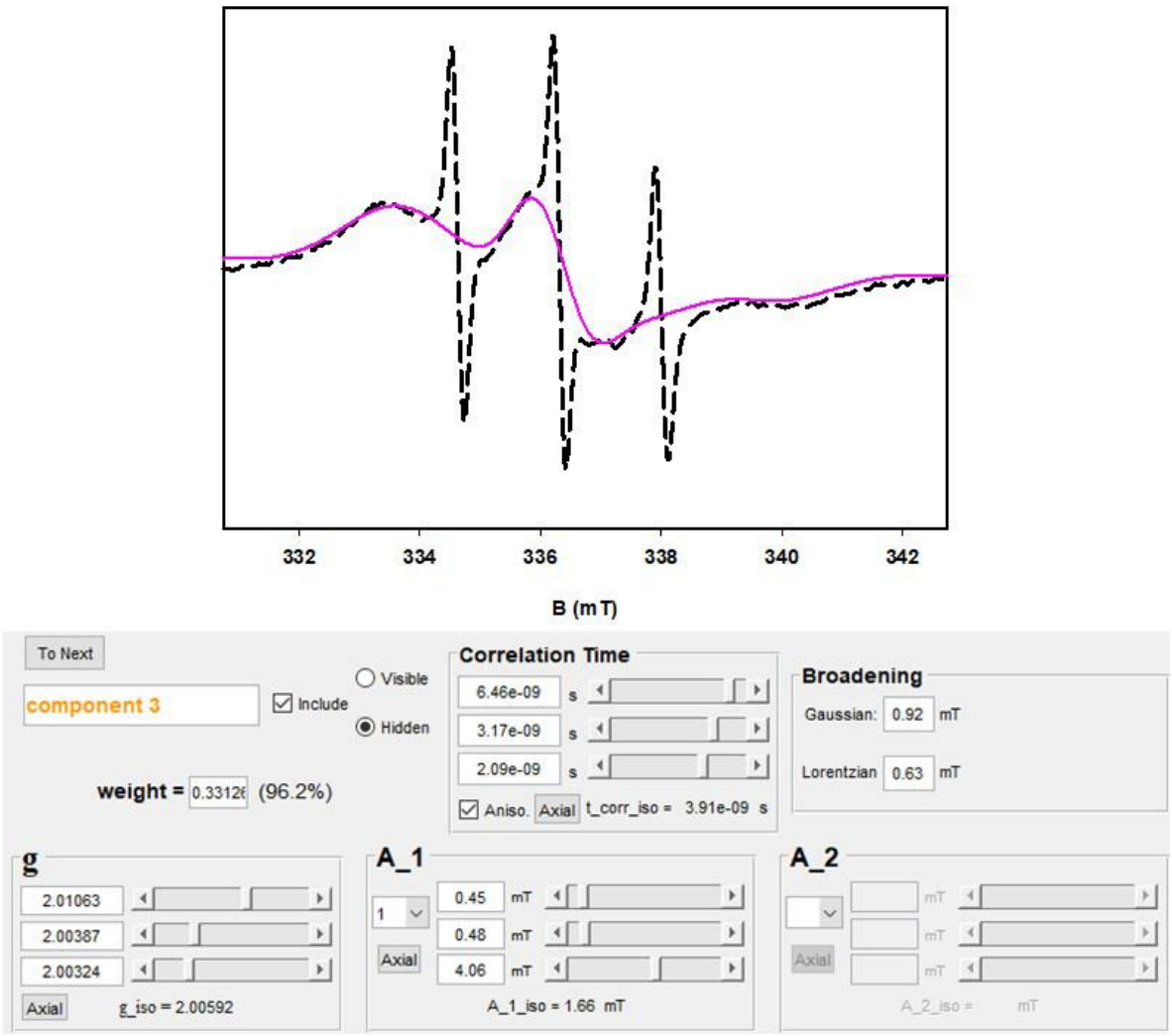

Figure A3.5*. Simulation of the EPR spectrum of PDnT. Slow component, accounting for 96,2% of the signal.*

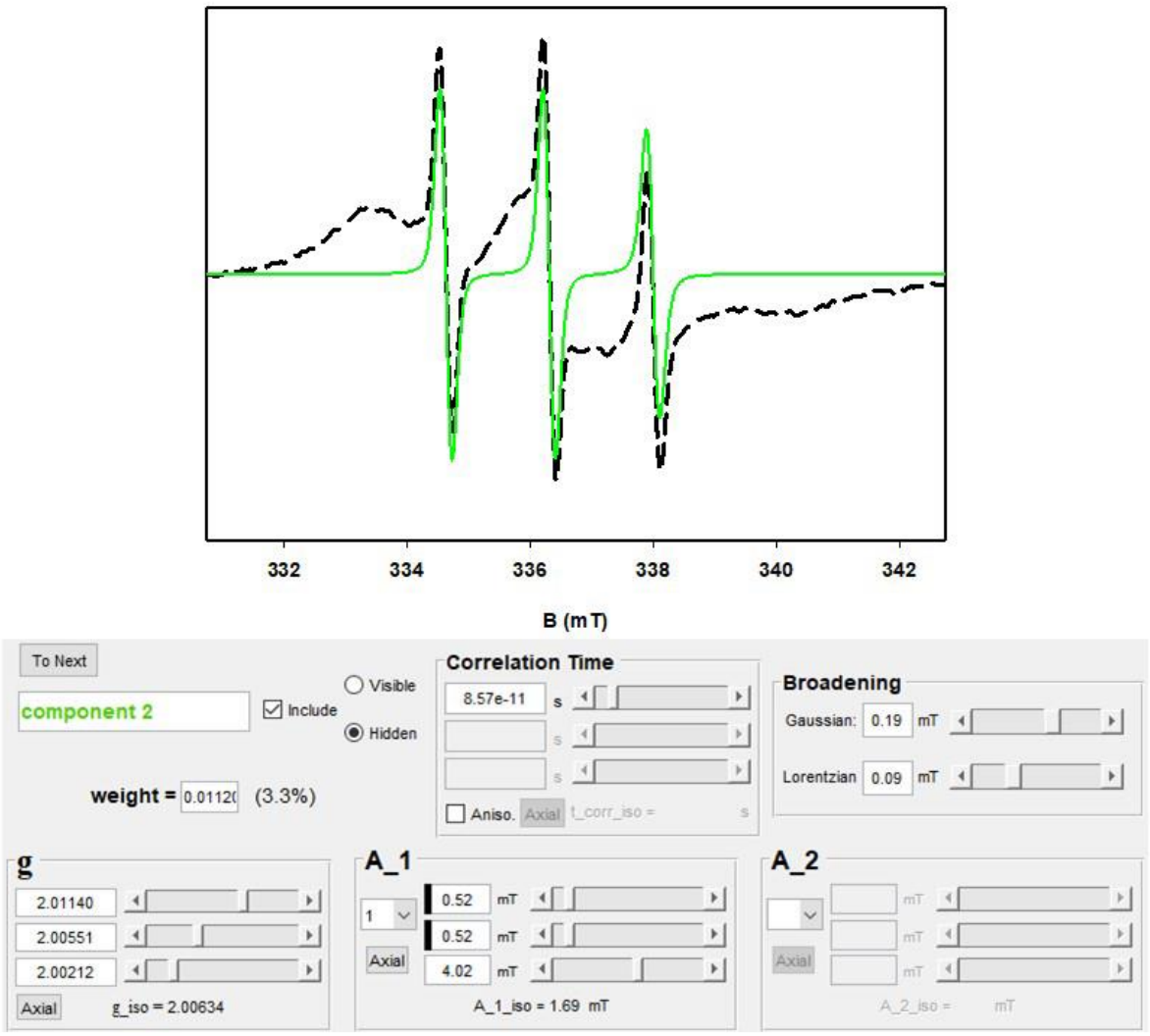

Figure A3.6*. Simulation of the EPR spectrum of PDTnT. Fast component, accounting for 3.3% of the signal.*

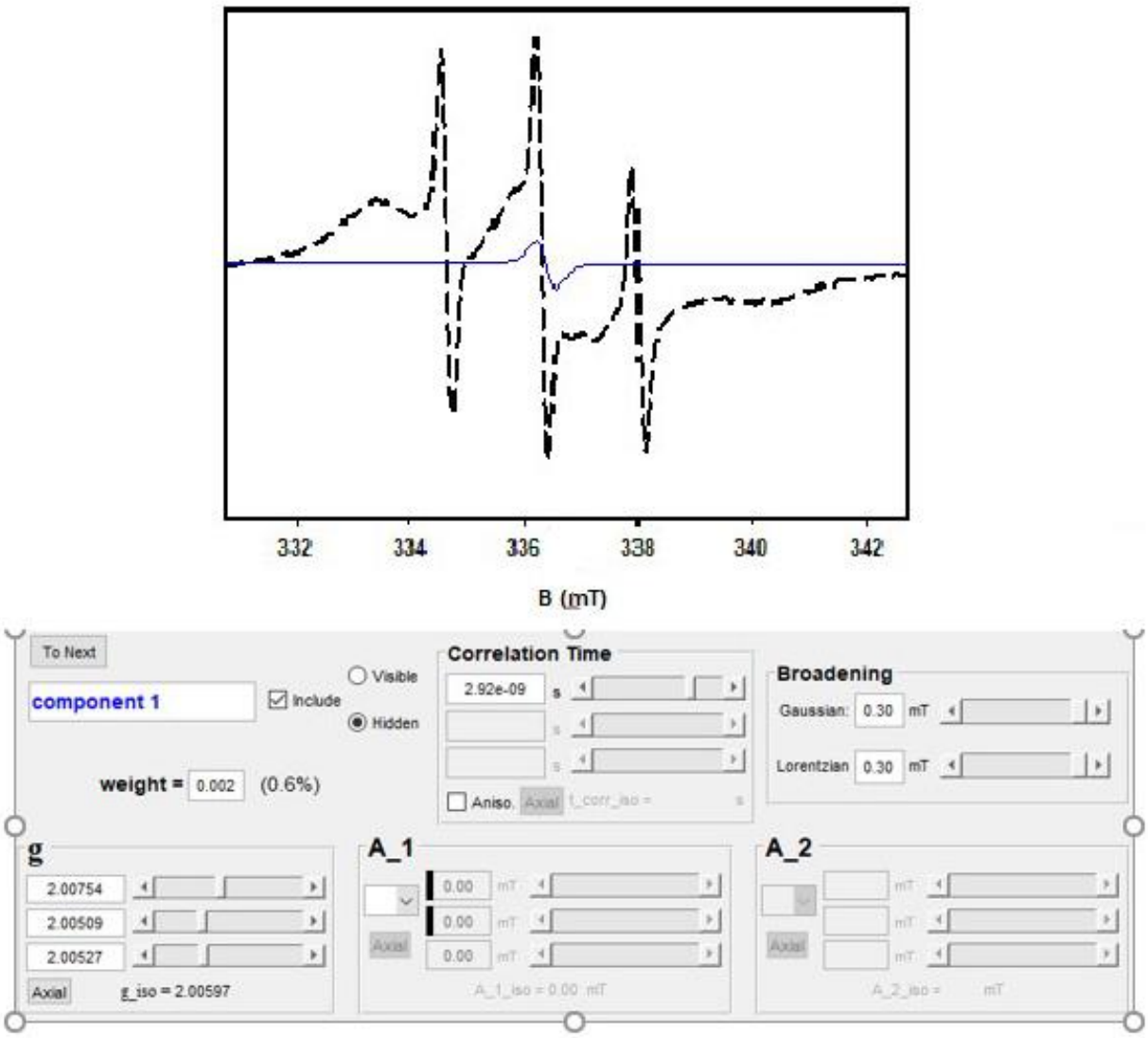

Figure S3.7*. Simulation of the EPR spectrum of PDTnT. Slow component, accounting for 0.6% of the signal.*

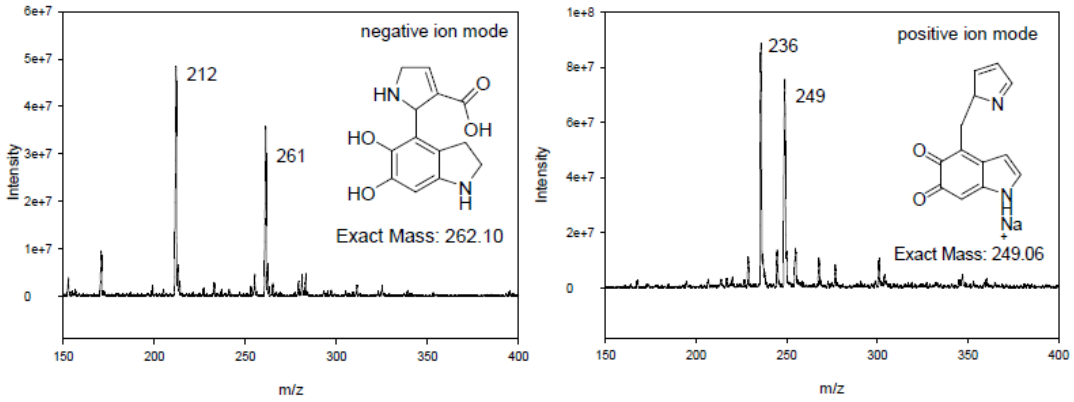

***Figure A3.8**. ESI-MS spectra of dialysate. Direct infusion, ESI type, desolvation gas (N2), 242 L/h; cone gas (skimmer), 33 L/h; desolvation temperature, 120 °C, source block temperature, 80 °C; capillary voltage, 3.00 kV; cone voltage, 22 V; hexapole extractor, 3 V. The tentative identification of some peaks is reported, based on the structures reported in reference* [4].

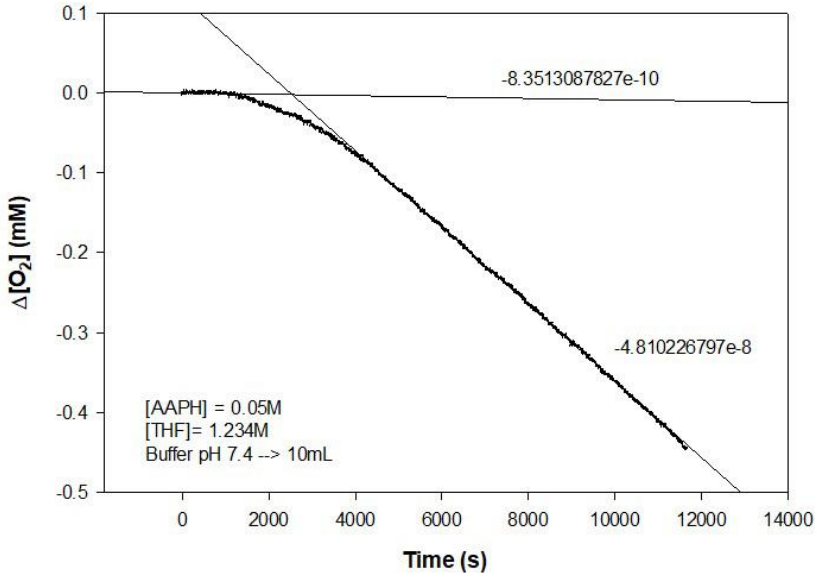

***Figure A3.9**. O_2 consumption measured during the autoxidation of THF initiated by AAPH at 30 °C in the presence of PDAn purified by only one centrifugation.*

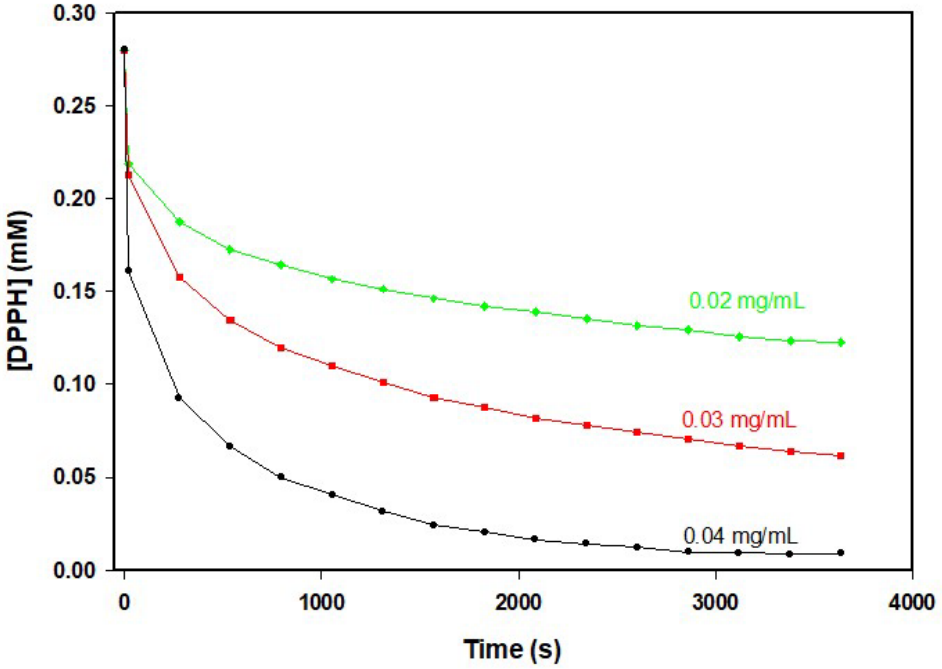

***Figure A3.10**. Reaction between DPPH• (0.28 mM) and PDAn (see concentration on each plot) purified by centrifugation and dialysis, in ethanol, studied by EPR spectroscopy.*

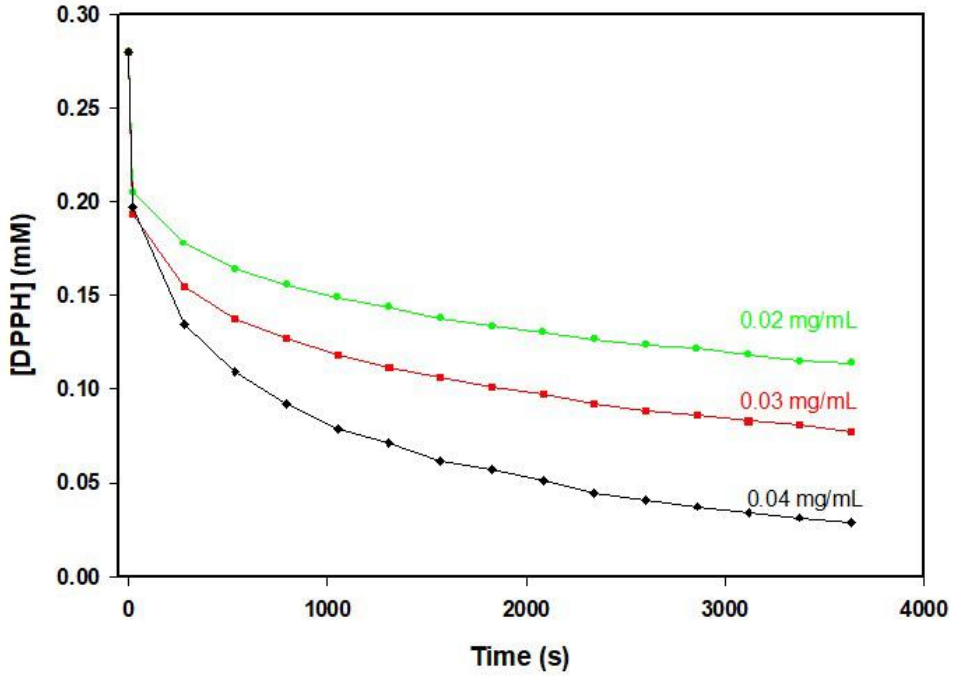

***Figure A3.11.** Reaction between DPPH• (0.28 mM) and PDAn (see concentration on each plot) purified bycentrifugation, in ethanol, studied by EPR spectroscopy.*

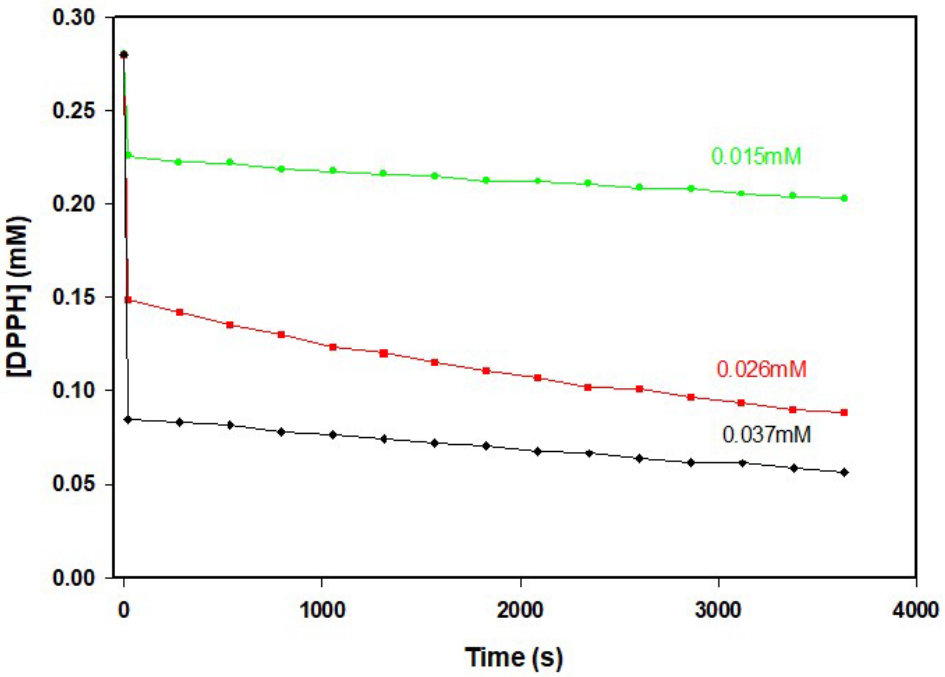

Figure A3.12. *Reaction between DPPH• (0.28 mM) and DA (see concentration on each plot), in ethanol,studied by EPR spectroscopy.*

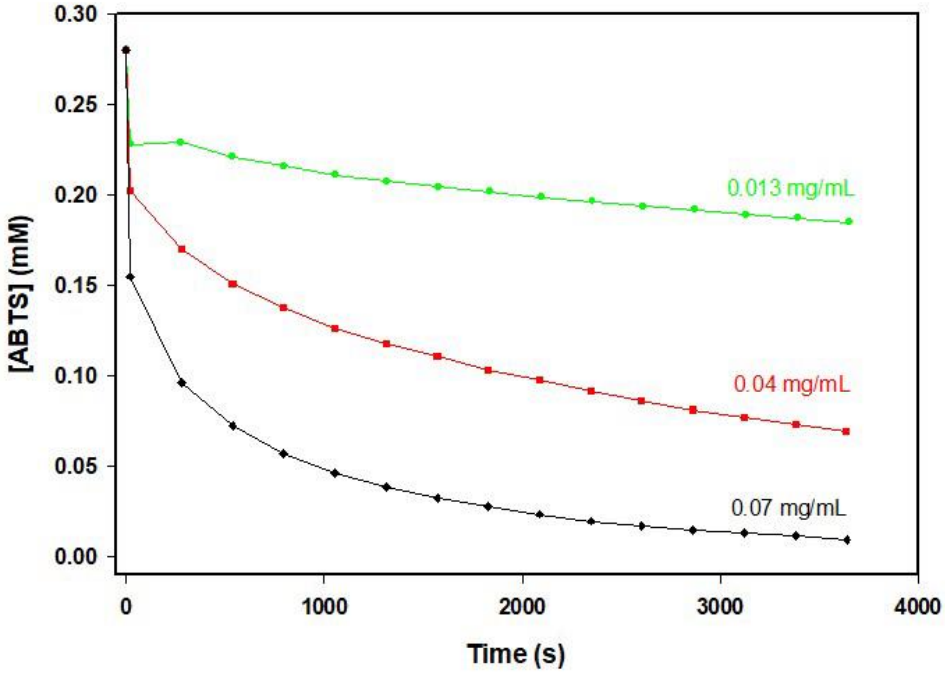

Figure A3.13. *Reaction between DPPH• (0.28 mM) and PDAnT (see concentration on each plot), in ethanol,studied by EPR spectroscopy.*

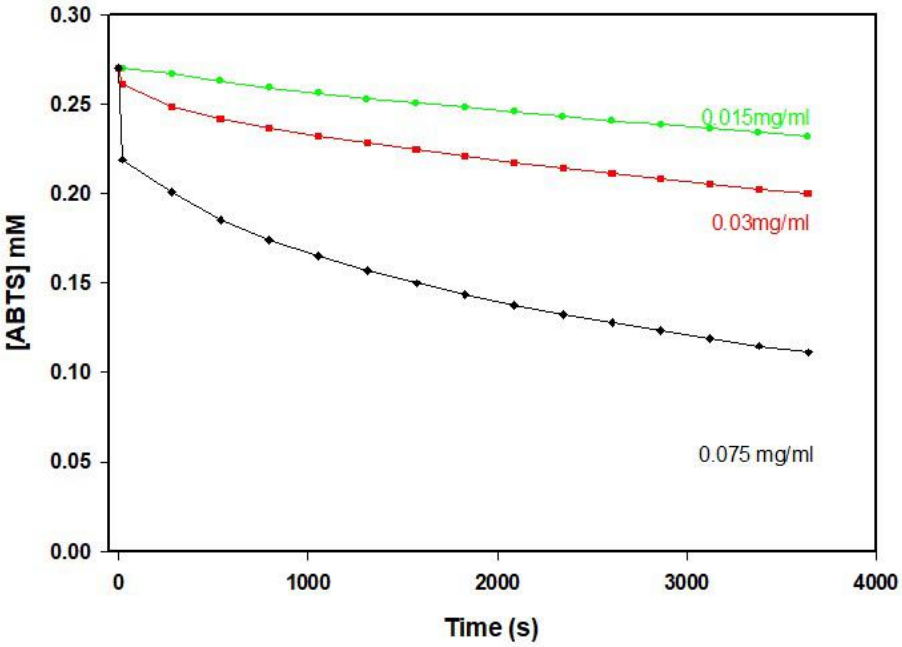

Figure A3.14. *Reaction between ABTS+• (0.27 mM) and PDAnT (see concentration on each plot), in water,studied by EPR spectroscopy.*

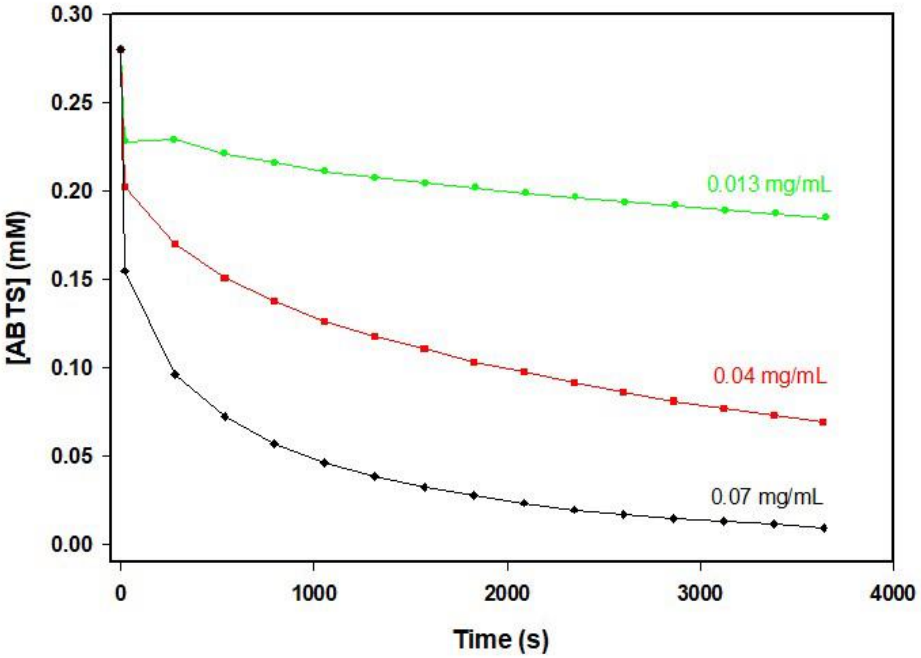

Figure A3.15. *Reaction between ABTS+• (0.28 mM) and PDAn (see concentration on each plot) purified bycentrifugation and dialysis, in water, studied by EPR spectroscopy.*

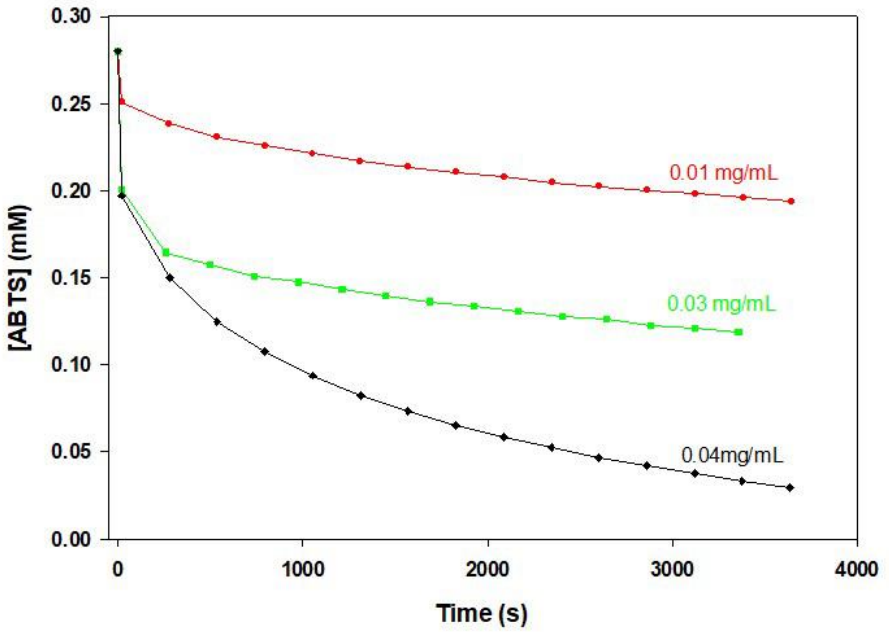

Figure A3.16. *Reaction between ABTS+• (0.28 mM) and PDAn (see concentration on each plot) purified bycentrifugation, in water, studied by EPR spectroscopy.*

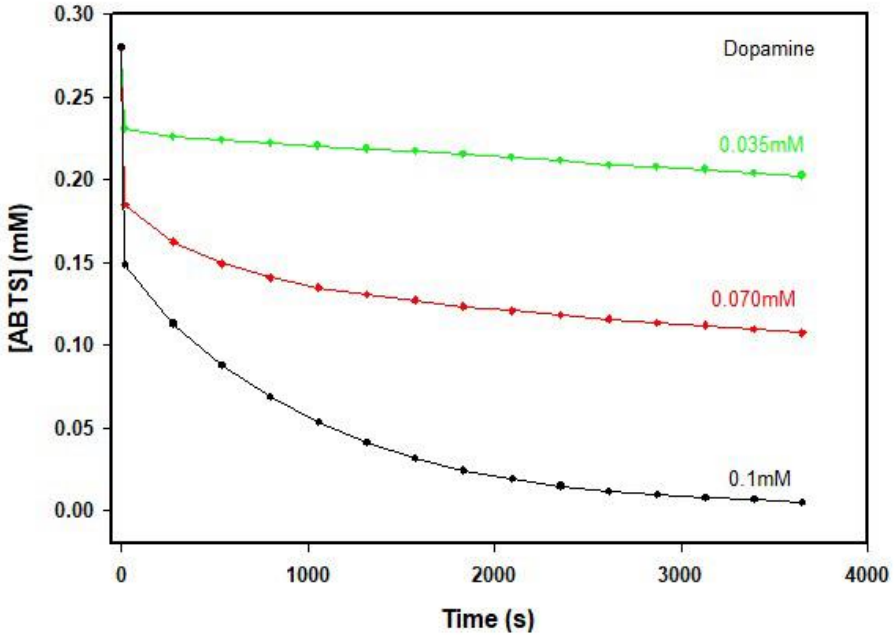

Figure A3.17. *Reaction between ABTS+• (0.28 mM) and DA (see concentration on each plot), in water,studied by EPR spectroscopy.*

CHAPTER IV
PRO-AROMATIC NATURAL TERPENES AS UNUSUAL ANTIOXIDANTS WITH POTENT FERROPTOSIS INHIBITION ACTIVITY

4.1 Preface

Ferroptosis is a cell-death mechanism based on extensive peroxidation of unsaturated lipids of cellular membranes, implicated in neurodegenerative diseases. We show herein that the essential oil component γ-terpinene, a natural monoterpene with a unique highly-oxidizable 1,4-cyclohexadiene skeleton, strongly inhibits peroxidation of unsaturated lipid in model heterogeneous systems (micelles and liposomes) by forming $HOO^{\bullet}$ radicals that diffuse outside from the lipid core, blocking radical chain propagation. This mechanism is particularly effective at physiological pH, as $HOO^{\bullet}$ is deprotonated to weakly oxidizing superoxide ($O_2^{\bullet-}$). In addition, γ-terpinene shows a very potent protective activity against ferroptosis, being effective in the nanomolar range in human neuroblastoma cell model (SH-SY5Y), paving the way to the development of novel drugs and to the rational explanation of the pharmacological activity of aromatic plants. The content of this chapter was submitted in the *Angewandte Chemie* (Mollica, F.; Guernelli, S.; Bergamini, C.; Rizzardi, N.; Baschieri, A.; Amorati, R.)

4.2 Introduction

Ferroptosis is a recently discovered cell-death mechanism implicated in severe diseases such as neurodegeneration and ischemia-reperfusion injury.[1] The molecular basis of ferroptosis consists of iron accumulation in the cytoplasm, coupled to the impairment of lipid hydroperoxide detoxification by glutathione peroxidase-4 (GPX4), a selenoprotein that catalyzes the reduction of lipid hydroperoxides to their corresponding alcohols by glutathione (GSH). The simultaneous presence of hydroperoxides and labile iron causes an uncontrolled generation of free radicals that initiates the peroxidation of the phospholipid bilayer, ultimately leading to the loss of

membrane integrity and cell death.[2] Chemical strategies to promote or suppress ferroptosis are receiving enormous attention, respectively, for enhancing the efficacy of cancer therapy, or to tackle neurodegenerative diseases.[3] Recently, it has been shown that many potent inhibitors of ferroptosis are also effective radical trapping antioxidants (RTA) being able to suppress the peroxidation radical chain that is re-sponsible for the membrane impairment.[4] The Pratt group showed that, unexpectedly, the most effective RTA have the ability of being regenerated by superoxide ($O_2^{\bullet-}$/HOO•),[5] that reduces the radicals of the antioxidants back to their active form.[6] Experiments performed with a controlled superoxide source also demonstrated the positive role of a moderate concentration of superoxide on cell survival in the presence of RTA.[5] From a mechanistic point of view, the RTA investigated so far act by donating a labile H-atom to the chain-propagating alkylperoxyl radical (ROO•) forming a stabilized radical (RTA-H•) unable to further propagate the oxidative chain *(Eq. 4.1),* and eventually being able of being regenerated by O2•⁻/HOO• *(Eq 4.2).*[5,6]

$$LOO^{\bullet} + RTA \xrightarrow{k_{inh}} LOOH + RTA_{-H}{}^{\bullet} \qquad \text{Eq 4.1}$$

$$RTA_{-H}{}^{\bullet} + HOO^{\bullet} \xrightarrow{k_p} RTA + O_2 \qquad \text{Eq 4.2}$$

Given the importance of inhibiting ferroptosis, we wandered if this goal could be achieved by a completely different mechanism consisting of converting the lipophilic LOO• radicals, that are essentially localized in membrane interior,[7] into small and hydrophilic hydroperoxyl (HOO•) radicals, that move to the water phase forming the relatively harmless $O_2^{\bullet-}$,[8] thereby interrupting the radical chain inside the lipidic particle (*Scheme 4.1*).

A similar "radical exporting" mechanism was put forward by Ingold et al. when comparing the antioxidant activity of α-tocopherol and reduced CoQ (ubiquinol) in low-density lipoprotein.[9] In this regard, 1,4-cyclohexadienes, a class of pro-aromatic organic compounds not usually regarded as RTA,[10–14] could have anti-ferroptotic activity because they react relatively quickly with LOO• ($k_H \approx 2 \times 10^3$ $M^{-1}s^{-1}$)[15–17]

forming, upon reaction with O_2, an alkylperoxyl radical that breaks down to HOO• and an aromatic product by a 1,4-intramolecular H-atom transfer ($k_{1,4\text{-}HAT} = 4\times10^4\ M^{-1}s^{-1}$)[18] *(see Scheme 4.1)*. To verify this hypothesis, we used the natural compound γ–terpinene (γ-T, *see Scheme 4.1*), a lipophilic monoterpene, found in the volatile components of many plants used in human diet, like lemon and oregano, that possesses the desired 1,4-cyclohexadiene skeleton. Notably, after the reaction, γ-T is converted to para-cymene (Cy) that is another safe essential oil component.[11,12]

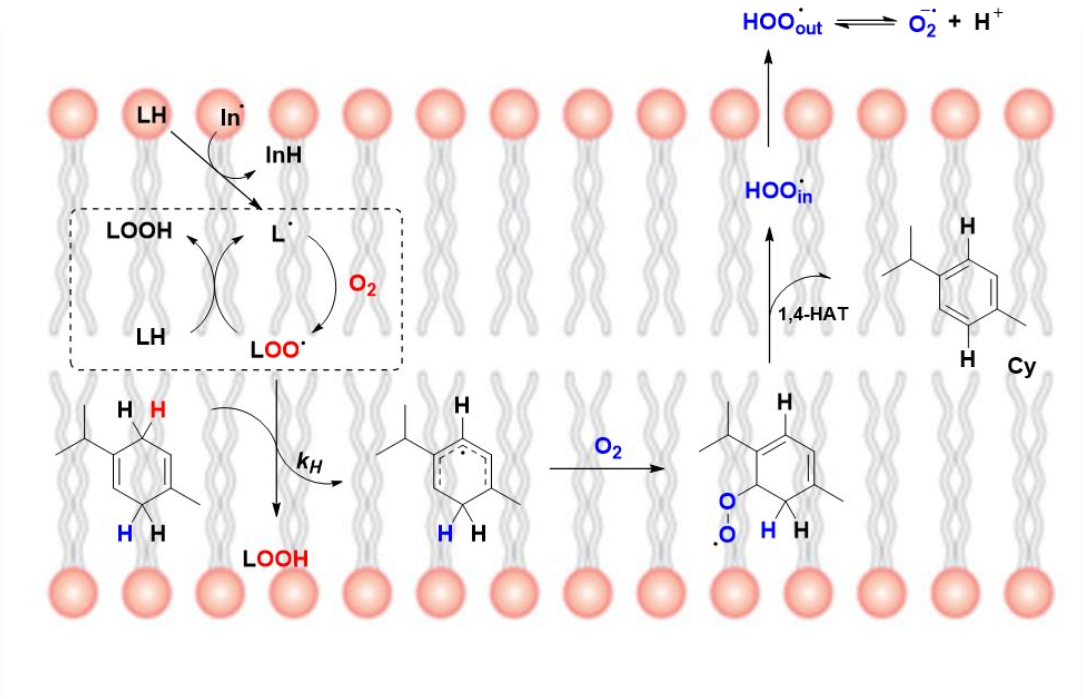

Scheme 4.1 *"Radical exporting" mechanism explaining the inhibition of lipid peroxidation by γ-terpinene.*

4.3 Results and Discussion

Firstly, we studied the ability of γ-T to inhibit the autoxidation of methyl linoleate (MeLH) in Triton-X100 micelles at pH 7.4, that is above the HOO• pKa (4.69).[8] The reaction was initiated by the hydrosoluble azoinitiator 2,2'-azobis(2-amidinopropane) dihydrochloride (AAPH) at 30 °C and was followed by measuring by UV-vis spectroscopy the disappearance of the lipophilic oxidation probe STY-BODIPY (λ=564

nm, ε=94000 $M^{-1}cm^{-1}$) which co-oxidizes with MeLH (*Figure 4.1*).[5] In the absence of antioxidants, the consumption of STY-BODIPY was fast and linear, indicating the onset of the autoxidation of MeLH. The addition of small amounts (.ca 50 μM) of γ-T caused an approximately tenfold reduction of the probe consumption and at pH 7.4 an antioxidant effect at all concentrations. [19,20] These results indicate that γ-T can react with ROO• forming HOO• that goes out from the micelle, thereby stopping the propagation of the oxidative chain. At pH 7.4, HOO• deprotonates to $O_2^{\bullet-}$, that is unable to abstract a H-atom from MeLH or γ-T.

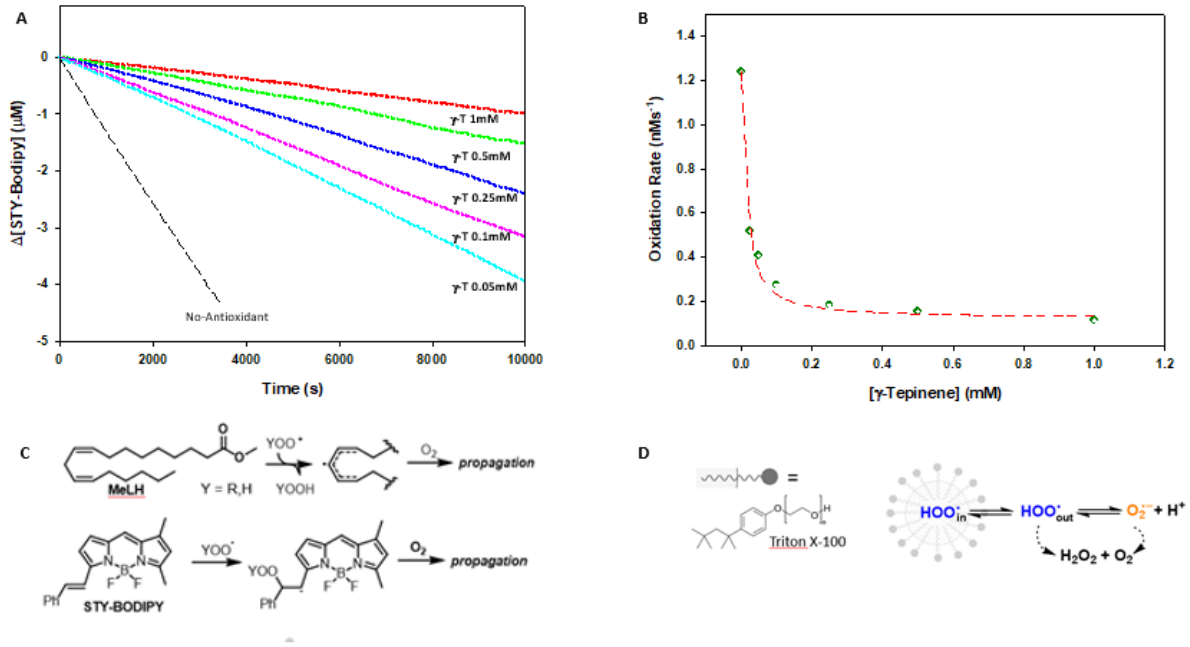

***Figure 4.1 A**) Consumption of STY-BODIPY (10 μM) during the autoxidation of MeLH (2.7 mM) in Triton X-100 micelles (8.0 mM) initiated by AAPH (10 mM) at 30 °C, in buffered water at pH 7.4. **B**) measured rate of STY-BODIPY consumption as function of the concentration of γ-T, dashed lines represent the trend expected from a co-oxidation kinetic model. **C)** Oxidation mechanism of MeLH and STY-BODIPY. **D**) Mechanism of radical exportation from the micellar inside to the water phase, and subsequent decay of the superoxide radicals.*

The inability of deprotonated superoxide $O_2^{\bullet-}$ to propagate the oxidative chain was verified by studying the peroxidation of 1,4-cyclohexadiene (1,4-CHD) in acetonitrile in the presence of bases of variable strength. The reaction was initiated by the

decomposition of azo-bis(isobutyronitrile) (AIBN) at 30 °C and its rate was determined by measuring the O_2 uptake by a gas-uptake re-cording apparatus (*Figure 4.2 A-B*).[6] The results show that the O_2 consumption rate was reduced proportionally to the base strength, as measured by the pK_a of their conjugated acids in MeCN and water: pyridine < tert-octylamine < piperidine ≈ Me4piperidine < Bu4NOH. This result can be interpreted as deriving from the deprotonation of the chain carrying HOO• radicals to $O_2^{\bullet -}$, that are not able to abstract a H-atom form 1,4-CHD.

To demonstrate the relevance of the HOO• radical exportation in membranes, we investigated the effect of γ-T on the peroxidation of unilamellar phosphatidylcholine liposomes (PCL) from egg yolk, containing approximately 15% of oxidizable polyunsaturated fatty acids (including linoleate and arachidonic acid).[21] The reaction was initiated by AAPH at 37 °C and was monitored by measuring the dissolved O_2 by an optical oximetric probe.[22] The results reported in *Figure 4.2D-E* clearly show that γ-T has an antioxidant effect near to that of α-tocopherol (α-TOH), one of the most important physiological defense against lipid peroxidation in living organisms,[23] implying that they have similar reactivity toward LOO•, i.e. k_{inh} (α-TOH) ≈ k_H (γ-T). Interestingly, the k_{inh} of α-TOH decreases dramatically passing from a homogeneous apolar solvent to liposomes (3.2×10^6 $M^{-1}s^{-1}$ in PhCl vs. 4.3×10^3 $M^{-1}s^{-1}$ in PCL)[24,25] as effect of the strong H-bonds between the OH group and the phosphate groups (*Figure 4.2F*).[25] On the contrary, the k_H (γ-T) that can be estimated from the experiments in liposomes is similar to that measured for 1,4-CHD in apolar solvents ($k_H = 3.8 \times 10^3$ $M^{-1}s^{-1}$ in CCl4),[15] implying that γ-T, thanks to its hydrocarbon nature, is located in the lipophilic portion of the membrane, where LOO• are mainly found (*see Figure 4.2F*).[7] The antioxidant effect of γ-T also implies that the HOO• radical can escape from the membrane before it reacts with the bis-allylic functions of polyunsaturated fatty acids. If considering that HOO• has a reactivity in H-atom abstractions similar to LOO•,[6] it would react with bis-allylic groups with a $k \approx 62$ $M^{-1}s^{-1}$ (at 30 °C)[15] that, in PCL, having a bis-allylic group concentration ∼0.54 M,[21] implies that the life time of HOO• is (62 $M^{-1}s^{-1} \times 0.54$ M)$^{-1}$ = 0.03 s.[26] The time required for the diffusion outside the bilayer (t),

can be estimated to be as low as 5×10^{-8} s by equation 3,[26] where D is the diffusion coefficient of HOO• ($D = 2\times10^{-5}$ cm^2 s^{-1})[27] and the diffusion distance (d) is half the thickness of the bilayer (~22 nm).[28]

$$d = 2.26(D\,t)^{1/2} \qquad \text{Eq 4.3}$$

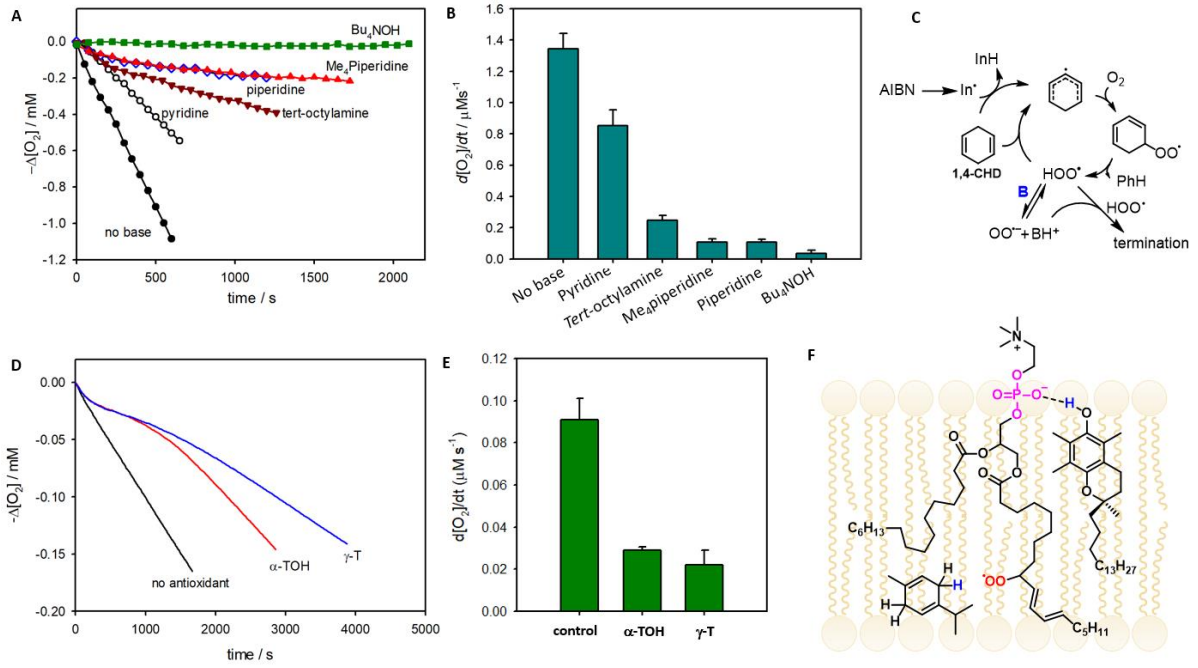

Figure 4.2. ***A - B)*** *Oxygen consumption (A) and rates of O_2 consumption (B) recorded during the autoxidation of 1,4-CHD (0.26M) in MeCN initiated by AIBN (25 mM) at 30 °C in the presence of bases (0.1 mM).* ***C)*** *Mechanism of the effect of bases (B) on 1,4-CHD autoxidation.* ***D – E)*** *Oxygen consumption (D) and rates of O_2 consumption (E) measured during the autoxidation of PCL (3.3 mM) initiated by AAPH (10 mM) at 37 °C in the presence of the antioxidants (10 μM).* ***F)*** *Different localization in PCL bilayer of α-TOH and γ-T.*

The protecting effect of γ-T on PCL peroxidation led us to investigate whether the HOO• radical exportation mechanism exerted by the molecule could protect cells from ferroptosis. To this end, we pre-treated neuroblastoma cells (SH-SY5Y), an in vitro model widely used in the study of mechanisms underlying ferroptosis in neurological

diseases,[29,30] with different concentrations of γ-T and induced ferroptosis using RSL3, a glutathione peroxidase 4 (GPX4) inhibitor.[31,32]

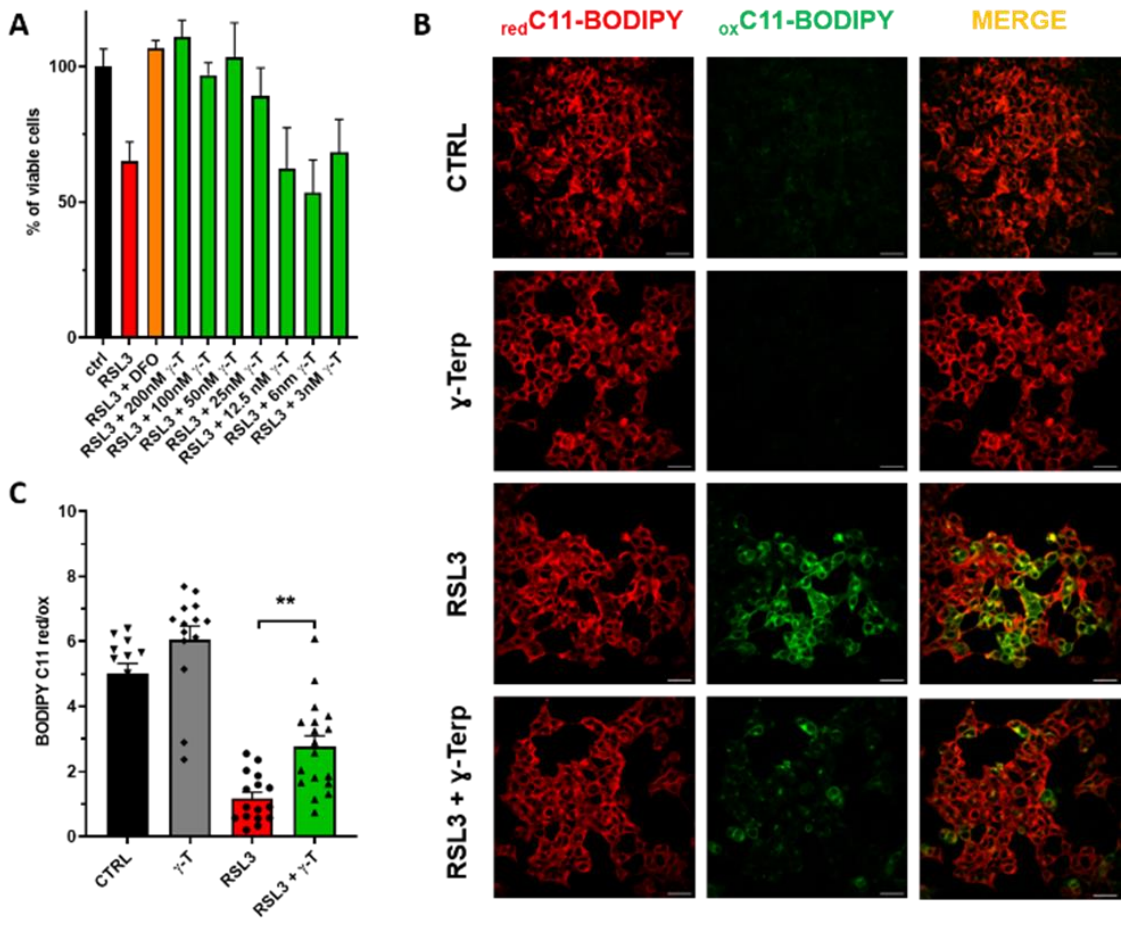

Figure 4.3 A) *Cell viability determined by resazurin assay. SH-SY5Y cells were pretreated with different concentrations of γ-terpinene (γ-T) for 1 hour and then incubated for 6 hours with 300nM RSL3. Pretreatment with 50μM deferoxamine (DFO) was used as a positive control. Data are reported as mean± s.e.m (n=6).* ***B)*** *Representative confocal images of live SH-SY5Y cells stained with the lipid peroxidation sensor BODIPY C11. Cells were pretreated with 50nM γ-T and then incubated for 6hours with 300nM of the ferroptosis inducer RSL3. Oxidation of the probe results in a shift of fluorescence emission from red to green. Scale bar represents 30μm.* ***C)*** *Fluorescence intensity ratio of reduced/oxidized BODIPY C11 emission. Data are reported as mean±s.e.m. (one-way ANOVA, ** p=0.014).*

The data shown in *Figure 4.3A* show that the pretreatment with γ-T is effective in counteracting ferroptotic cell death, with an estimated EC_{50} value of 20 nM. In addition, to further investigate the protective effect of γ-T on cell membrane redox status, we stained the cells with C11-BODIPY581/591 (Life Technologies, D3861).[33] C11-BODIPY localizes in cell membranes where it can be oxidized by peroxyl radicals; its oxidation is therefore an indirect manifestation of membrane lipid peroxidation and results in a shift of the fluorescence emission peak from ∼590 (red) nm to ∼510 nm (green). SH-SY5Y cells pretreated with vehicle and then treated with RSL3 (500nM, 6h) exhibited probe oxidation. Pretreatment with 60nM γ-T reduced probe oxidation upon subsequent RSL3 treatment (*Figure 4.3B*). *Figure 4.3C* shows the quantification of the reduced/oxidized probe signal, showing that pretreatment with γ-T significantly protects against RSL3-induced peroxidation.

4.4 Conclusion

In conclusion, our study has shown that the not toxic and naturally available γ-T presents a remarkable antioxidant activity in heterogeneous systems (micelles and liposomes) and is an outstanding inhibitor of ferroptosis. The reactivity principles enunciated herein are applicable to molecules bearing an opportunely substituted 1,4-cyclohexadiene skeleton (i.e. with two bis allylic H-atoms in 3 and 6 positions), and possibly to other easily oxidizable compounds, able to form HOO• by 1,4-HAT, including reduced CoQ and vitamin K.[9,18,34] The extraordinarily potent anti-ferroptotic activity of γ-T opens unprecedented possibilities to use this relatively nontoxic natural molecule as promising drug for neurodegenerative diseases. The high lipophilicity and low molecular weight could possibly provide high absorption and easy crossing of the blood brain barrier.[35] In addition, the widespread presence of γ-T as minor component of many essential oils could provide an explanation for the pharmacological activity of ex-tracts of aromatic plants of traditional medicine.[36,37]

4.5 Materials and methods

Materials and Instruments. All solvents (H_2O, DMSO) were of the highest grade commercially available (≥99.9% HPLC grade, Sigma-Aldrich) and used as received. γ-Terpinene (γ-T; >97%, Sigma-Aldrich), was percolated on alumina and silica before each experiment to remove impurities and traces of stabilizer. Chemicals were purchased from Sigma-Aldrich and TCI, and were used without any additional purification: 2,2'-Azobis(2-amidinopropane) dihydrochloride (AAPH; 97%, Sigma-Aldrich), Triton X-100 (*t*-Octylphenoxypolyethoxyethanol, for molecular biology, Sigma-Aldrich), Methyl linoleate (MeLH; 98%, TCI), L-α-Phosphatidylcholine (from egg yolk, Type XI-E, 100 mg/mL in chloroform, ≥99%, solution, Sigma-Aldrich), (±)-6-hydroxy-2,5,7,8-tetramethylchromane-2-carboxylic acid (Trolox; 97%, Sigma-Aldrich), α-Tocopherol (95.5%, Sigma-Aldrich).

The STY-BODIPY was synthesized according to literature procedure[1].

UV–visible measurements were performed using a Cary 1E (Varian) spectrometer coupled to Cary Temperature Control (Varian). Dynamic light scattering (DLS) measurements were conducted using a Zetasizer Nano ZS90 (Malvern Instruments). The concentration of O_2 was measured using an optical oxygen meter FireStingO_2 (PyroScience GmbH).

Autoxidation kinetics in micelles.

Micellar suspension of MeLH preparation. In a scintillation vial, 22 μL of methyl linoleate (MeLH) and 10 mL of 17.6 mM Triton X-100, were mixed by a vortex stirrer for 3 min. Next, 10 mL of phosphate buffer solution 0.1 M (pH 7.4) was added, and the mixture was stirred again for 3 min. The final concentration of MeLH and Triton X-100 in the micellar system was 3.3 mM for lipid and 8.8 mM for surfactant.[2]

Inhibited Co-autoxidation of MeLH in micellar system. A 3 mL quartz cuvette was loaded with 1.8 mL of micellar suspension of MeLH, 10 μL of 2 mM STY-BODIPY in DMSO and 200 μL of 100 mM AAPH in phosphate buffer solution. The solution was thoroughly mixed. The cuvette was placed into the thermostatted sample holder of a

UV−vis spectrophotometer and allowed to equilibrate to 30 °C. The absorbance at 564 nm was monitored for 10−20 min to ensure that the reaction was proceeding at a constant rate, after which a small aliquot in DMSO solution of the test antioxidant was added.

Autoxidation of Egg-Yolk phosphatidylcholine liposomes

Egg-Yolk PC Liposomes Preparation. 150 μL of a solution 100 mg/mL in chloroform of egg yolk phosphatidylcholine was added in a round-bottom flask and the solvent was then evaporated under argon and the lipids were vacuum-dried 1h to yield a thin film. The lipid film was hydrated with 1 mL of a 10 mM phosphate buffered saline (PBS) solution containing 150 mM NaCl (pH 7.4), yielding a 20 mM lipid suspension. The lipid suspension was then extruded 21 times using a mini extruder equipped with a polycarbonate membrane with 100 nm pores.[2]

Inhibited Autoxidation of Egg-Yolk PC Liposomes. To a 1 mL graduated flask were added 165 μL of liposome suspension of 20 mM in PBS, 100 μL of 100 mM AAPH in PBS solution and made up to the mark with PBS solution and mixed. Next, 600 ul of the mixture was transferred to a vial and used to measure O_2 consumption during autoxidation using a FireStingO2 optical oxygen meter (PyroScience GmbH) at 37 ° C. The rate of O_2 consumption was monitored for 10-15 minutes until it was ensured that the reaction was proceeding at a constant rate, after which 10 μL of a 600 μM solution in DMSO of the test antioxidant was added.

Autoxidation of 1,4-cyclohexadiene in acetonitrile

Autoxidation experiments were performed by measuring the oxygen consumption in a two-channel gas uptake apparatus, immersed in a thermostatted bath, based on Validyne DP15 pressure transducer developed in our laboratory.[3]

All the autoxidation experiments were initiated by the thermal decomposition of AIBN at 30 ◦C, in acetonitrile (ACN). In a typical experiment, an air-saturated solution of the oxidizable substrate 1,4-cyclohexadiene (0.26 M) containing AIBN (0.025 M) in ACN is equilibrated at 30 ◦C with an identical reference solution containing an excess of

2,2,5,7,8-pentamethyl-6-hydroxychromane (125 mM) so to block any radical chain in the reference during the experiment. After reaching a constant O_2 consumption, a stock solution of base in ACN is injected in the sample flask. Final concentration 0.1 mM.

Table S2. Different organic bases, pK_a of their conjugated acids in MeCN and water.

Base	**pK_a in ACN**	**pK_a in H_2O**
pyridine	12.53[a]	5.25[a]
tert-octylamine	≈ 18[b]	10.7[c]
piperidine	19.35 [b]	11.3[d]
2,2,6,6-tetramethylpiperidine	19.7[e]	11.8 [d]
tetrabutylammonium hydroxide		>13[f]

[a] from reference [38]; for common primary amines [39]; [c] from reference [40]; [d] from reference[41]; [e] estimated from [42]; [f] from reference[43]

Cell line and culture conditions*

SH-SY5Y cells (American Type Culture Collection, Manassas, VA, USA) were cultured in DMEM (EuroClone, Pero, Italy) supplemented with 10% (v/v) fetal bovine serum, 100 U/ml penicillin, and 100 µg/ml streptomycin (MilliporeSigma, Burlington, MA, USA). Cells were grown in a humidified incubator with 95% air and 5% CO2 at 37°C.

Cell viability assay*

Cell viability was assessed by resazurin-based assay following.[44,45]

Briefly, SH-SY5Y cells were seeded in 96-well plates at 2×10^4 cells/well density (Optiplate, Perkin Elmer). After 24 hours to allow adhesion, cells were treated with different concentrations of γ-terpinene for 1 hour dissolved in complete medium. After this time, cells were washed with Hanks balanced buffer solution (HBSS) and exposed to 300nM of RSL3 dissolved in complete medium for 6 hours. Then, cells were washed again with HBSS and incubated with resazurin (4mg/ml, 100µL per well) dissolved in

complete medium for 3 hours. The fluorescence emission was recorded using a plate reader (EnSpire, Perkin Elmer) at λ_{exc} 560nm, λ_{em} 590nm.

Lipid peroxidation assay*

The determination of lipid peroxidation induced by RSL3 treatment in SH-SY5Y cells was performed using the lipid peroxidation sensor dye BODIPY® 581/591 C11 (ThermoFisher Scientific) following the method reported in Pap et al.[46]

Briefly, cells were seeded in a 8-well chambered coverslip (µ-Slide 8 Well, (Ibidi, Germany) following manufacturer instructions. After 24 hours to allow adhesion, cells were pre-treated with 50nM γ-terpinene for 1hour. Then cells were washed with HBSS, stained with 1µM BODIPY® 581/591 C11 and exposed to 300nM RSL3 dissolved in complete medium for 6 hours. After this time, cells were washed with HBSS and images were acquired using a Nikon C1si confocal microscope (Nikon, Tokyo, Japan). Green and red fluorescence intensities were quantified using ImageJ software standard tools.

*These experiments were performed by Prof. Christian Bergamini and Nicola Rizzardi from Department of Pharmacy and Biotechnology (Unibo)

References

1. Stockwell, B. R. Ferroptosis turns 10: Emerging mechanisms, physiological functions, and therapeutic applications. *Cell* **185**, 2401–2421 (2022).
2. Conrad, M. & Pratt, D. A. The chemical basis of ferroptosis. *Nat Chem Biol* **15**, 1137–1147 (2019).
3. Conrad, M., Lorenz, S. M. & Proneth, B. Targeting Ferroptosis: New Hope for As-Yet-Incurable Diseases. *Trends Mol Med* **27**, 113–122 (2021).
4. Zilka, O. *et al.* On the Mechanism of Cytoprotection by Ferrostatin-1 and Liproxstatin-1 and the Role of Lipid Peroxidation in Ferroptotic Cell Death. *ACS Cent Sci* **3**, 232–243 (2017).
5. Poon, J.-F., Zilka, O. & Pratt, D. A. Potent Ferroptosis Inhibitors Can Catalyze the Cross-Dismutation of Phospholipid-Derived Peroxyl Radicals and Hydroperoxyl Radicals. *J Am Chem Soc* **142**, 14331–14342 (2020).
6. Cedrowski, J., Litwinienko, G., Baschieri, A. & Amorati, R. Hydroperoxyl Radicals ($HOO^{\cdot}$): Vitamin E Regeneration and H-Bond Effects on the Hydrogen Atom Transfer. *Chemistry - A European Journal* **22**, 16441–16445 (2016).
7. Garrec, J., Monari, A., Assfeld, X., Mir, L. M. & Tarek, M. Lipid Peroxidation in Membranes: The Peroxyl Radical Does Not “Float”. *J Phys Chem Lett* **5**, 1653–1658 (2014).
8. Sawyer, D. T. & Valentine, J. S. How Super Is Superoxide? *Acc. Chem. Res.* **14**, 393–400 (1981).
9. Ingold, K. U., Bowry, V. W., Stocker, R. & Walling, C. Autoxidation of lipids and antioxidation by alpha-tocopherol and ubiquinol in homogeneous solution and in aqueous dispersions of lipids: unrecognized consequences of lipid particle size as exemplified by oxidation of human low density lipoprotein. *Proceedings of the National Academy of Sciences* **90**, 45–49 (1993).
10. Bhunia, A. & Studer, A. Recent advances in radical chemistry proceeding through pro-aromatic radicals. *Chem* **7**, 2060–2100 (2021).

11. Foti, M. C. & Ingold, K. U. Mechanism of Inhibition of Lipid Peroxidation by γ-Terpinene, an Unusual and Potentially Useful Hydrocarbon Antioxidant. *J Agric Food Chem* **51**, 2758–2765 (2003).
12. Guo, Y., Baschieri, A., Amorati, R. & Valgimigli, L. Synergic antioxidant activity of γ-terpinene with phenols and polyphenols enabled by hydroperoxyl radicals. *Food Chem* **345**, 128468 (2021).
13. Mollica, F., Gelabert, I. & Amorati, R. Synergic Antioxidant Effects of the Essential Oil Component γ-Terpinene on High-Temperature Oil Oxidation. *ACS Food Science & Technology* **2**, 180–186 (2022).
14. Li, G.-X. & Liu, Z.-Q. Unusual Antioxidant Behavior of α- and γ-Terpinene in Protecting Methyl Linoleate, DNA, and Erythrocyte. *J Agric Food Chem* **57**, 3943–3948 (2009).
15. Howard, J. A. & Ingold, K. U. Absolute rate constants for hydrocarbon autoxidation. VI. Alkyl aromatic and olefinic hydrocarbons. *Can J Chem* **45**, 793–802 (1967).
16. Sortino, S., Petralia, S. & Foti, M. C. Absolute rate constants and transient intermediates in the free-radical-induced peroxidation of γ-terpinene, an unusual hydrocarbon antioxidant. *New J. Chem.* **27**, 1563–1567 (2003).
17. Harrison, K. A., Haidasz, E. A., Griesser, M. & Pratt, D. A. Inhibition of hydrocarbon autoxidation by nitroxide-catalyzed cross-dismutation of hydroperoxyl and alkylperoxyl radicals. *Chem Sci* **9**, 6068–6079 (2018).
18. Guo, Y. & Amorati, R. The underrecognized role of the hydrop-eroxyl (HOO•) radical in chain propagation of lipids and its implication in antioxidant activity. in *Lipid oxidation in food and biological systems* (2022).
19. Baschieri, A., Ajvazi, M. D., Tonfack, J. L. F., Valgimigli, L. & Amorati, R. Explaining the antioxidant activity of some common non-phenolic components of essential oils. *Food Chem* **232**, 656–663 (2017).
20. Howard, J. A. & Yamada, T. Absolute rate constants for hydrocarbon autoxidation. 31. Autoxidation of cumene in the presence of tertiary amines. *J Am Chem Soc* **103**, 7102–7106 (1981).

21. Blesso, C. Egg Phospholipids and Cardiovascular Health. *Nutrients* **7**, 2731–2747 (2015).
22. Genovese, D. *et al.* Nitroxides as Building Blocks for Nanoantioxidants. *ACS Appl Mater Interfaces* **13**, 31996–32004 (2021).
23. Angeli, J. P. F., Shah, R., Pratt, D. A. & Conrad, M. Ferroptosis Inhibition: Mechanisms and Opportunities. *Trends Pharmacol Sci* **38**, 489–498 (2017).
24. Burton, G. W. *et al.* Autoxidation of biological molecules. 4. Maximizing the antioxidant activity of phenols. *J Am Chem Soc* **107**, 7053–7065 (1985).
25. Shah, R., Farmer, L. A., Zilka, O., van Kessel, A. T. M. & Pratt, D. A. Beyond DPPH: Use of Fluorescence-Enabled Inhibited Autoxidation to Predict Oxidative Cell Death Rescue. *Cell Chem Biol* **26**, 1594-1607.e7 (2019).
26. Roots, R. & Okada, S. Estimation of Life Times and Diffusion Distances of Radicals Involved in X-Ray-Induced DNA Strand Breaks or Killing of Mammalian Cells. *Radiat Res* **64**, 306 (1975).
27. UEHARA, S. & NIKJOO, H. Monte Carlo Simulation of Water Radiolysis for Low-energy Charged Particles. *J Radiat Res* **47**, 69–81 (2006).
28. Balgavý, P. *et al.* Bilayer thickness and lipid interface area in unilamellar extruded 1,2-diacylphosphatidylcholine liposomes: a small-angle neutron scattering study. *Biochimica et Biophysica Acta (BBA) - Biomembranes* **1512**, 40–52 (2001).
29. Slanzi, A., Iannoto, G., Rossi, B., Zenaro, E. & Constantin, G. In vitro Models of Neurodegenerative Diseases. *Front Cell Dev Biol* **8**, (2020).
30. Ou, M. *et al.* Role and mechanism of ferroptosis in neurological diseases. *Mol Metab* **61**, 101502 (2022).
31. Rizzardi, N. *et al.* Coenzyme Q10 Phytosome Formulation Improves CoQ10 Bioavailability and Mitochondrial Functionality in Cultured Cells. *Antioxidants* **10**, 927 (2021).
32. Yang, W. S. *et al.* Regulation of Ferroptotic Cancer Cell Death by GPX4. *Cell* **156**, 317–331 (2014).

33. Drummen, G. P. C., van Liebergen, L. C. M., Op den Kamp, J. A. F. & Post, J. A. C11-BODIPY581/591, an oxidation-sensitive fluorescent lipid peroxidation probe: (micro)spectroscopic characterization and validation of methodology. *Free Radic Biol Med* **33**, 473–490 (2002).
34. Mishima, E. *et al.* A non-canonical vitamin K cycle is a potent ferroptosis suppressor. *Nature* **608**, 778–783 (2022).
35. Abbott, N. J., Patabendige, A. A. K., Dolman, D. E. M., Yusof, S. R. & Begley, D. J. Structure and function of the blood–brain barrier. *Neurobiol Dis* **37**, 13–25 (2010).
36. Cioanca, O., Hritcu, L., Mihasan, M. & Hancianu, M. Cognitive-enhancing and antioxidant activities of inhaled coriander volatile oil in amyloid β(1–42) rat model of Alzheimer's disease. *Physiol Behav* **120**, 193–202 (2013).
37. Corasaniti, M. T. *et al.* Cell signaling pathways in the mechanisms of neuroprotection afforded by bergamot essential oil against NMDA-induced cell death *in vitro*. *Br J Pharmacol* **151**, 518–529 (2007).
38. Kaljurand, I. *et al.* Extension of the Self-Consistent Spectrophotometric Basicity Scale in Acetonitrile to a Full Span of 28 p K_a Units: Unification of Different Basicity Scales. *J Org Chem* **70**, 1019–1028 (2005).
39. Tshepelevitsh, S. *et al.* On the Basicity of Organic Bases in Different Media. *European J Org Chem* **2019**, 6735–6748 (2019).
40. Droge, S. T. J., Hermens, J. L. M., Rabone, J., Gutsell, S. & Hodges, G. Phospholipophilicity of $C_x H_y N^+$ amines: chromatographic descriptors and molecular simulations for understanding partitioning into membranes. *Environ Sci Process Impacts* **18**, 1011–1023 (2016).
41. Yang, D., Zuccarello, G. & Mattes, B. R. Physical Stabilization or Chemical Degradation of Concentrated Solutions of Polyaniline Emeraldine Base Containing Secondary Amine Additives. *Macromolecules* **35**, 5304–5313 (2002).
42. Rossini, E., Bochevarov, A. D. & Knapp, E. W. Empirical Conversion of p K_a Values between Different Solvents and Interpretation of the Parameters:

Application to Water, Acetonitrile, Dimethyl Sulfoxide, and Methanol. *ACS Omega* **3**, 1653–1662 (2018).

43. Jin, S., Sanii, R., Song, B.-Q. & Zaworotko, M. J. Crystal Engineering of Ionic Cocrystals Sustained by the Phenol–Phenolate Supramolecular Heterosynthon. *Cryst Growth Des* **22**, 4582–4591 (2022).
44. Gilbert, D. F. & Friedrich, O. *Cell Viability Assays: Methods and Protocols, Methods in Molecular Biology*. vol. 1601 (Springer Science+Business Media LLC , 2017).
45. Präbst, K., Engelhardt, H., Ringgeler, S. & Hübner, H. Basic Colorimetric Proliferation Assays: MTT, WST, and Resazurin. in 1–17 (2017). doi:10.1007/978-1-4939-6960-9_1.
46. Pap, E. H. W. *et al.* Ratio-fluorescence microscopy of lipid oxidation in living cells using C11-BODIPY $^{581/591}$. *FEBS Lett* **453**, 278–282 (1999).